WIND TURBINE GENERATOR INTERFERENCE TO ELECTROMAGNETIC SYSTEMS

FINAL REPORT

April 1978 - March 1979

August 1979

Contract No. EY-76-S-02-2846.A003

by: D.L. Sengupta and T.B.A. Senior

Prepared for:

Department of Energy
Division of Solar Technology
Wind Systems Branch
Washington, D.C. 20545

14438-3-F = RL-2274

WIND TURBINE GENERATOR INTERFERENCE TO ELECTROMAGNETIC SYSTEMS

by

D.L. Sengupta and T.B.A. Senior
The University of Michigan
Radiation Laboratory
Ann Arbor, Michigan 48109

Final Report

April 78 - March 1979

August 1979

Contract No. EY-76-S-02-2846.A003

Prepared for

Department of Energy
Division of Solar Technology
Wind Systems Branch
Washington, D.C. 20545

NOTICE

TABLE OF CONTENTS

Acknowledgement			i
Executive Summary			ii
Abstract			vi
Chapter 1		INTRODUCTION	1
	1.1	Background	1
	1.2	Present Study	3
Chapter 2		MODULATION OF CIRCULARLY POLARIZED ELECTROMAGNETIC SIGNALS BY A SLOWLY ROTATING METAL PLATE	5
	2.1	Scattering of Horizontally Polarized Waves	6
	2.2	Scattering of Vertically Polarized Waves	11
	2.3	Scattering of Circularly Polarized Waves	12
		2.3.1 Discussion	14
	2.4	Reception of Direct and Scattered Waves	16
	2.5	Some Experimental Results	21
	2.6	General Discussion	24
Chapter 3		SOME PRACTICAL ASPECTS OF THE TV INTERFERENCE PROBLEM	26
Chapter 4		SCATTERING FROM VERTICAL AXIS MACHINES	45
	4.1	Scattering Formulas	46
	4.2	Measured Data	49
	4.3	Remarks	59
Chapter 5		TV INTERFERENCE STUDIES	61
	5.1	Scale Model Windmills	61
	5.2	Laboratory Microwave TV System	62
	5.3	Initial Testing of the System: Inside the Laboratory	76

5.4 Initial Testing of The System: Outside the Laboratory 78

5.5 TV Interference Tests and Results 83

5.5.1 Recording of the Received Signal 83

5.5.2 Geometry 84

5.5.3 Giromill Test Results 86

5.5.4 The Darrieus Test Results 95

5.5.5 MOD-0 Windmill Test Results 99

5.5.6 Discussion 102

5.6 Conclusions 106

Chapter 6 WINDMILL INTERFERENCE TO A LORAN-C SYSTEM 108

6.1 The Loran-C System 109

6.1.1 Parameters Associated with Transmitting Stations 109

6.1.2 Transmitted Signals 111

6.1.3 Loran-C Pulse 112

6.2 Received Signal in the Presence of a Windmill 114

6.2.1 Phase Comparison of Direct and Scattered Signals 115

6.3 Amplitude Comparison of Direct and Scattered Signals 120

6.3.1 Direct Signal 121

6.3.2 Scattered Signal 124

6.3.3 Ratio of the Scattered and Direct Signals 126

6.3.4 Numerical Results: Forbidden Regions 128

6.4 Mutual Interaction Between a Windmill and Loran-C Transmitting Antenna 129

6.5 Conclusions 133

References 134

Appendix 136

ACKNOWLEDGMENT

It is a pleasure to acknowledge the assistance of our colleagues in the performance of this study. We are particularly grateful to Mr. J.E. Ferris who was responsible for all aspects of the experimental program; Prof. H. Weil who carried out the initial analysis of the reception of circularly polarized electromagnetic waves in the presence of a slowly rotating rectangular metal plate; Mr. F. Jahanshahi, who helped with the analysis of interference to a Loran-C System, and Mr. P.R. Jedrzejewski who performed much of the experimental work. We also appreciate many helpful discussions with Dr. V.V. Liepa during the design phase of the laboratory microwave TV system. We are indebted to Mrs. Diane Connolly for her expert and patient typing of the manuscript.

EXECUTIVE SUMMARY

A number of problems associated with wind turbine (WT) interference to the electromagnetic environment were investigated. These studies, and the significant findings thereof, are summarized below.

The scattering of circularly polarized electromagnetic waves by a slowly rotating rectangular metal plate, and the reception of such incident and scattered waves by an arbitrarily polarized receiving antenna, were investigated theoretically and experimentally. It was found that with a circularly polarized incident field, the scattered field is in general elliptically polarized. In the forward and specular directions the scattered wave becomes circularly polarized with a sense of polarization similar and opposite, respectively, to that of the incident field. Consequently, a similarly polarized receiving antenna, with polarization matched to receive the direct or incident circularly polarized signal, will discriminate against the specularly scattered interfering signal. This implies that the video distortion to TV reception within the backward interference region of a WT is less with circularly polarized signals than with conventional horizontally polarized signals, all other conditions being equal.

Our previous analyses based on the 'worst case' assumptions, i.e., the WT blades oriented such that the maximum scattered signals are directed to a receiving point with the receiving antenna isotropic, shows that the interference zone of a large WT can be quite large at the upper UHF TV Channel frequencies. However, directional receiving antennas are used in many practical situations; also the interference zone is merely the region where video distortion could possibly occur, and gives no information about the probability of its occurrence. In order to assess the practical

severity of the TV interference problem, the use of a directional receiving antenna and various statistical (and other) factors governing the occurrence of interference have been theoretically examined. It is found that the availability and correct orientation of a directional antenna will decrease the maximum interfering distance as well as the actual possibility of interference throughout the backward portion of the interference zone. For example, within the backward interference region of a MOD-0A WT, the maximum interfering distance on TV Channel 52 is about 1.1 km when using an isotropic receiving antenna; with a directional antenna receiving the direct signal through its main beam maximum and the WT-scattered signal through the backlobe maximum which is 15 dB down (i.e., $\sim$0.2 times the mainbeam maximum), the corresponding distance is about 0.2 km. A method has been developed to estimate the percent viewing time during which unacceptable video distortion may occur during TV reception within the interference zone of a WT by taking into account the relevant statistical parameters, wind speed, direction, etc. For example, for a receiver located in the backward region of, and at a distance 0.5 km from, the MOD-0A WT on Block Island, the probability of experiencing significant interference on Channel 53 is 9 percent when using an isotropic receiving antenna, but only 2 percent with a properly oriented directional antenna having a back-to-front ratio 0.2. In practice, therefore, the interference problem could be much less severe than is suggested by the basic interference zone obtained under the deterministic assumptions, but it is still true that this zone defines the region where interference could occur. In fact, were a directional antenna operated incorrectly, i.e., pointed at the WT, interference could exist even beyond the zone.

A variety of scattering measurements were carried out in a microwave anechoic chamber using 1/40 scale models of the MOD-OA WT, the Darrieus and the Giromill to determine their electromagnetic scattering characteristics. It was found that the scattering cross-section of a scale model MOD-OA WT is about 5 dB greater than for the Darrieus, and 5 dB less than that for the Giromill.

A laboratory microwave TV system has been developed to study the TV interference effects produced by the rotating scale models of a variety of WTs. The exact TV Channel frequency at which these effects are applicable for a given full scale WT is determined by the scale factor of the model and the frequency of the microwave signal used. The system consists of a commercial TV signal generator providing some test program (video pattern and audio information). The modulated RF output is up-converted in frequency to 4 GHz and radiated by a suitable antenna in an outside environment. The direct (primary) signal and the one scattered by the rotating blades of a scale model WT are then received and down-converted to a frequency acceptable to a TV receiver, enabling us to observe the interference under a variety of controlled conditions. In particular, the modulation waveform, modulation index and the video distortion (if any) produced by a given WT can be determined. The system has been used at the frequency 4.07 GHz ($\lambda \simeq 7.6$ cm) to investigate the interference produced by 1/10 scale models of the Giromill and Darrieus, and by $\sim$1/40 scale model of MOD-OA WT. The results can therefore be used to obtain the interference effects caused by the two full-scale vertical axis machines at about TV Channel 14, and by the full scale horizontal axis machine at about TV Channel 6. The modulation waveforms produced by the scale model Giromill and Darrieus are different from those

of the scale model MOD-0A WT, the latter being similar to those obtained at Plum Brook using the full-scale MOD-0A WT. With the Giromill and Darrieus models, the threshold type of video distortion was observed in the backward interference region for a modulation index of about 0.27; with the MOD-0A model the corresponding modulation index was about 0.17. From the results of the threshold measurements it appears that the interference produced by the Giromill and the MOD-0A would be of the same order of magnitude while that of the Darrieus would be much less.

The possible interference to the performance of a Loran-C system caused by a large horizontal axis WT has been investigated theoretically. Since the physical dimensions of even the MOD-1 machine are very small compared to the extremely large wavelength (λ = 3 km) of Loran-C signals, the maximum signal scattered from the WT was found to be about 100 dB lower than the direct signal at the receiver even when the WT is located as close as 100 m to the Loran-C transmitter or receiver. It is unlikely that the Loran-C receiver performance would be degraded by such low level interfering signals. The mutual interaction effects of the WT on the performance of a Loran-C transmitting antenna were found to be insignificant for a WT located as close as $\lambda/12$ ($\simeq$250 m) from the transmitter. From the results obtained, it appears that a WT located at distances $\gtrsim \lambda/12$ (= 250 m) from any Loran-C transmitter or receiver will not have a significant effect on the Loran-C performance.

ABSTRACT

Selected problems associated with wind turbine generator interference to the electromagnetic environment have been investigated theoretically and experimentally.

A study of the reception of circularly polarized electromagnetic waves in the presence of a slowly rotating rectangular metal plate indicates that a similarly polarized receiving antenna discriminates against the scattered signals in the backward scattering region. This implies that the video distortion to TV reception within the backward interference zone of a windmill will be less with circularly polarized signals than with conventional horizontally polarized signals, all other conditions being equal.

A method has been developed to estimate the percent viewing time during which unacceptable video distortion may occur during TV reception within the interference zone of a WTG, by taking into account the relevant statistical parameters, e.g., wind speed, direction, etc.

The electromagnetic scattering characteristics of small scale models of the Darrieus and Giromill have been measured in a microwave anechoic chamber.

A laboratory microwave TV system has been developed for studying the TV interference produced by a variety of windmills. Some representative results are given for the Giromill, Darrieus and MOD-0 machines.

Possible interference to the performance of a Loran-C system caused by large horizontal axis windmills has been investigated theoretically and it has been found that under normal conditions no degradation in performance is likely to occur due to the siting of a WTG near a Loran-C transmitter.

CHAPTER 1

INTRODUCTION

This is the final report of a third year's study of the effects of wind turbine generators (WTG) or windmills on the electromagnetic environment. Since the present research has been a continuation of a sustained research program, it is appropriate to begin by a brief summary of our previous studies.

1.1 Background

Over the past two years the interference produced by horizontal axis wind turbine generators or windmills to a number of electromagnetic systems has been identified and quantified [1-3]. The work was originally motivated by the possibility of interference to TV reception. Analyses of blade scattering quickly established that the rotating blades of the WTG could serve to pulse amplitude modulate the total field received in its vicinity, and an examination of the basic detection process in a TV receiver showed that the extraneous modulation could cause video (but not audio) distortion. This led to an intense study [2] of TV interference using field tests with the NASA/ERDA 100 KW WTG at Plum Brook, Ohio, scale model measurements, and laboratory simulations. One outcome was the establishing of a threshold for the modulation index representing the largest value for which the video distortion was judged acceptable for small periods of viewing; and the dependence of this threshold on the ambient signal level, the TV channel number and the test receiver used was explored. Examples of the interference at different modulation levels were recorded on a video tape furnished to the sponsor. Knowing the threshold and the equivalent scattering area of the particular

windmill blade, it is then possible to define an interference zone about a WTG for each of the TV channels available in its vicinity, the zone being that where the video distortion could be unacceptable. Using analyses and computations of the propagation and scattering phenomena, a simple technique was developed [3] for computing the interference zones for large horizontal axis WTG's such as the MOD-0, MOD-0A, and MOD-1 machines.

In addition to the TV work, the possibility of windmill interference to other electromagnetic systems has been examined. In the case of FM broadcasts, laboratory simulations have shown that interference is detectable only at very high modulation levels or where the ambient signal is itself low, and for all practical purposes the interference will be negligible except possibly within a few tens of meters of the WTG. Studies [2] of the interference to two specific air navigation systems, VOR and DVOR, have indicated that no significant degradation in the performance of these systems will occur if the WTG is sited according to the standard guidelines (for stationary objects) established by the FAA. We have also analyzed the performance of two typical microwave communication link systems whose repeater stations could be located in the vicinity of a WTG. It was found that the blade rotation produces a frequency smearing of the received baseband signal energy, but the maximum smear is much less than the total FDM bandwidth of the channel. Using then the threshold value for the interference-to-signal (RF carrier) level allowed by the telephone companies, the concept of a forbidden zone around the link receiver was developed, the zone being that where the placement of a windmill could cause unacceptable interference, and illustrative examples were given in [2].

1.2 Present Study

In spite of the wide ranging nature of the above-mentioned investigations, there are other systems and/or circumstances where WTG-generated interference could be a problem, and the objective of the present study has been to treat some of these.

The use of circular polarization for television transmission has been suggested in order to eliminate the reception of extraneous multipath signals due to single reflections. This could significantly affect the interference caused by a windmill. The implications of the use of circularly polarized signals to WTG-generated interference are discussed in Chapter 2 by investigating the reception of circularly polarized signals in the presence of a slowly rotating rectangular metal plate.

In all our previous calculations of the zones [3] of interference about a WTG, such parameters as the windmill pointing direction and the blade pitch angle were chosen to maximize interference for a given TV channel and receiver location, and in addition the receiving antenna was assumed omnidirectional. As a result, the interference zone is the region of possible TV video disruption, but gives no information about the probability of disruption actually occurring. Chapter 3 describes a method to arrive at a statistical measure, e.g., percent time viewed when the interference is unacceptable, by taking into account the statistical nature of the pertinent parameters.

Large horizontal axis windmills have been the focus of our previous studies. The vertical axis windmills, in particular the Darrieus and Giromill, are very different structures from the horizontal axis machines, and it is not obvious what their electromagnetic scattering is. Chapter 4 presents the results of a variety of scattering measurements carried out in a microwave anechoic chamber using small scale models of the Darrieus and Giromill.

Chapter 5 describes a laboratory microwave TV system which we have developed to enable us to observe and quantify the interference effects produced by a variety of windmills under controlled conditions without having to rely on outside signal sources. Some representative results for the Darrieus, Giromill and MOD-0 machines obtained using it are also presented.

Chapter 6 discusses theoretically the possible interference by a large WTG to a Loran-C system.

Because of the large number of quantities to be represented, it has been necessary to use some symbols to represent different quantities in different places. In every instance the symbol has been defined where introduced to avoid misrepresentation of its meaning. For easy reference, a list of selected symbols and acronyms used is given in the Appendix.

CHAPTER 2

MODULATION OF CIRCULARLY POLARIZED ELECTROMAGNETIC SIGNALS BY A SLOWLY ROTATING METAL PLATE

At the present time, virtually all TV transmitters in the U.S. are horizontally polarized, and the receiving antennas are designed to receive this polarization (the lack of any valid basis for this choice is evidenced by the fact that throughout Europe the transmissions are vertically polarized). Nevertheless, there is a move to change over to circular polarization because of the improved reception in urban areas. Such a change could affect the interference that a windmill produces, and it is therefore desirable to explore its impact. To this end, we present here an approximate theory for determining the scattered field (hence the modulation introduced) when a circularly polarized plane electromagnetic wave is incident on a rotating rectangular metal plate. As is well known, a circularly polarized electromagnetic wave may be obtained by a proper combination of two orthogonally-oriented linearly polarized waves. Thus, we shall obtain the desired fields by combining the appropriate scattered fields obtained with horizontally and vertically polarized waves illuminating the rotating plate. The horizontally polarized case has been investigated in [2,4], and the results obtained therein will be used as the basis for the present analysis. The implications of the results obtained on the reception of circularly polarized signals in the presence of a rotating plate are then discussed. Finally, results of some limited measurements confirming the general theoretical findings are given.

2.1 Scattering of Horizontally Polarized Waves

As mentioned earlier, this case has been investigated in [2,4] and we give here the appropriate expressions without detailed derivation. The fundamental assumption involved in the analysis is that all relevant velocities involved are much less than the velocity of light, and that the rotation frequency of the plate is much less than the frequency of the incident wave.

At time t = 0 a rectangular metal plate of dimensions L_1 and L_2 is assumed located in the plane $\phi = \phi_s$ with its axis A-A' aligned along the z-axis of a rectangular coordinate system whose origin is at 0, as shown in Fig. 2-1. The center of the plate is at 0 which is also the origin of a spherical coordinate system. The axis A-A' of the plate is now rotated in the x-z plane (i.e., around the y-axis) with an angular frequency Ω such that at time t its position is as shown in Fig. 2-2, where

$$\theta_s = \Omega t \quad . \tag{2.1}$$

The azimuth angle ϕ_s (in Fig. 2-1) of the plate is also the angle between the unit normal $\hat{n}$ to the plate and the normal to the plane of rotation (i.e., the y-axis) and will be referred to as the skew angle of the plate.

The plate is illuminated by a plane electromagnetic wave incident from the direction (θ_0,ϕ_0) with the electric field vector polarized in the horizontal (x-y plane) such that:

$$\vec{E}_1^i = E_0[\hat{x} \sin \phi_0 - \hat{y} \cos \phi_0] \exp[ik(x \sin \theta_0 \cos \phi_0 + y \sin \theta_0 \sin \phi_0 + z \cos \theta_0], \tag{2.2}$$

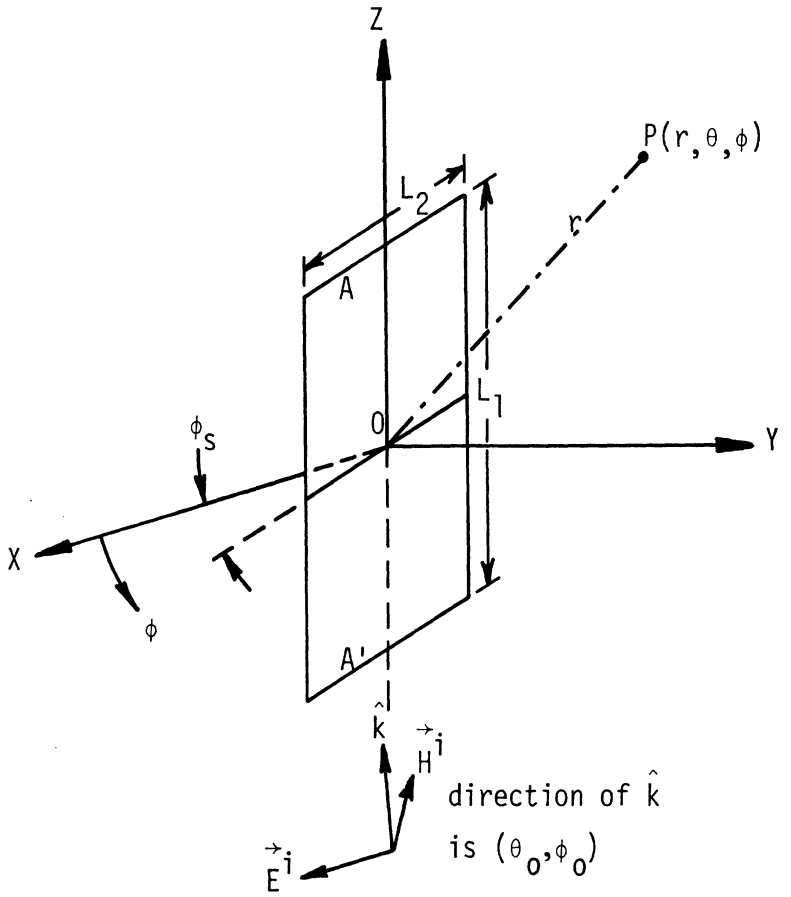

Fig. 2-1: Skewed rectangular plate at time t = 0. The skew angle is ϕ_s.

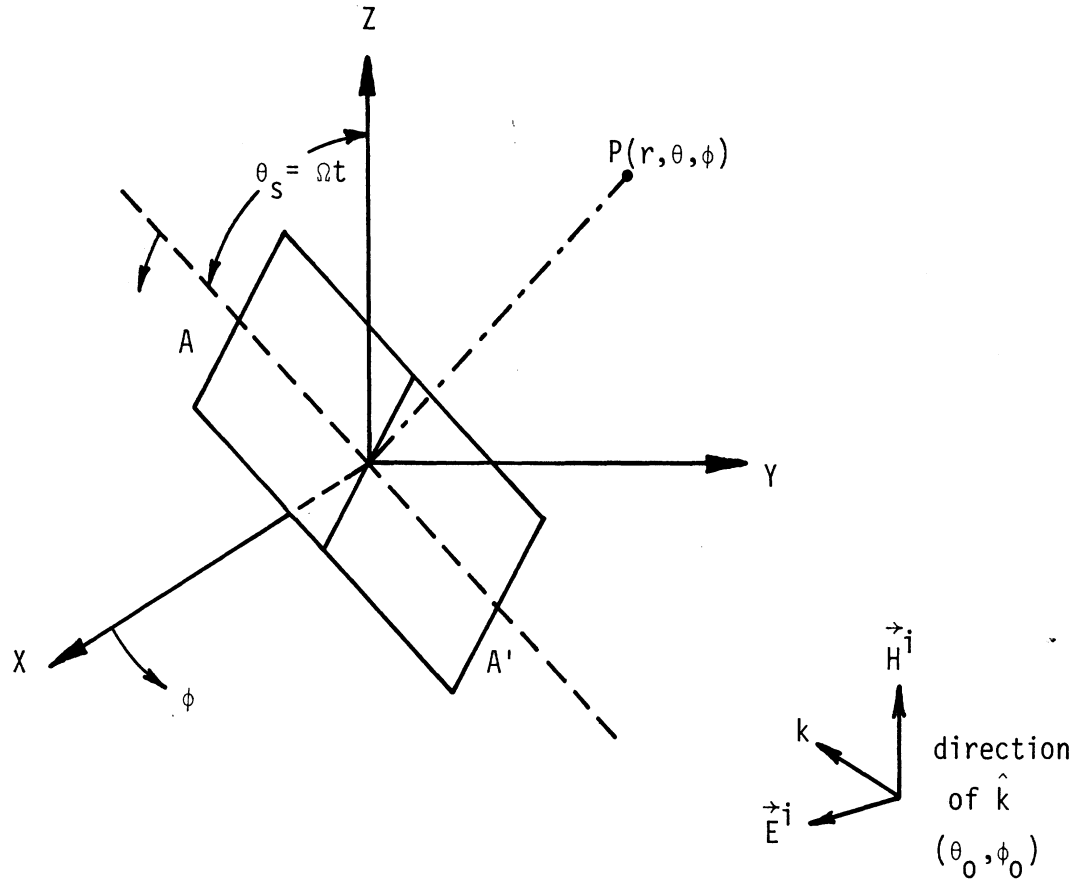

Fig. 2-2: Rotating skewed rectangular plate, with the incident field direction and the receiver location shown. The line AA' is rotating in the x-z plane.

$$\vec{H}_1^i = H_0[-\hat{x}\cos\theta_0\cos\phi_0 - \hat{y}\cos\theta_0\sin\phi_0 + \hat{z}\sin\theta_0] \qquad (2.3)$$

$$\exp[ik(x\sin\theta_0\cos\phi_0 + y\sin\theta_0\sin\phi_0 + z\cos\theta_0)],$$

where

E_0, $H_0 = E_0/Z$ are the amplitudes of the electric and magnetic field vectors, respectively,

Z is the intrinsic impedance of the medium,

$k = 2\pi/\lambda$ is the propagation constant in the medium,

$\hat{x},\hat{y},\hat{z}$ are the unit vectors in the x, y, and z directions, respectively, and a time dependence $\exp(i\omega t)$ is suppressed.

According to the physical optics approximation, the surface current density at an arbitrary point on the illuminated side of the plate is

$$\vec{J}_s = 2\,\hat{n} \times \vec{H}_1^i|_s \qquad (2.4)$$

where $\vec{H}_1^i|_s$ is the incident magnetic field at the point on the plate, with $\vec{J}_s = 0$ on the shadow side. In terms of the polar coordinates θ_s and ϕ_s, the unit normal $\hat{n}$ can be written as [2],

$$\hat{n} = -\hat{x}\cos\theta_s\sin\phi_s + \hat{y}\cos\phi_s + \hat{z}\sin\theta_s\sin\phi_s\ . \qquad (2.5)$$

Using (2.2) - (2.5), the current density $\hat{J}_s$ is

$$\vec{J}_s = 2\,H_0\vec{J} = 2\,H_0\,(\hat{x}j_x + \hat{y}j_y + \hat{z}j_z), \qquad (2.6)$$

where

$$\left.\begin{aligned} j_x &= \sin\theta_0\cos\phi_s + \cos\theta_0\sin\phi_0\sin\theta_s\sin\phi_s \\ j_y &= \sin\theta_0\cos\theta_s\sin\phi_s - \cos\theta_0\cos\phi_0\sin\theta_s\sin\phi_s \\ j_z &= \cos\theta_0\sin\phi_0\cos\theta_s\sin\phi_s + \cos\theta_0\cos\phi_0\cos\phi_s \end{aligned}\right\} \qquad (2.7)$$

With the above current distribution, the components of the far zone scattered electric fields are obtained as [2,4]:

$$E_\theta = -iE_o \frac{\exp(-ikr)}{kr} [j_x \cos\theta \cos\phi + j_y \cos\theta \sin\phi - j_z \sin\theta] C(\Omega t), \tag{2.8}$$

$$E_\phi = -iE_o \frac{\exp(-ikr)}{kr} [-j_x \sin\phi + j_y \cos\phi] C(\Omega t), \tag{2.9}$$

where

$$C(\Omega t) = 2\pi \frac{L_1 L_2}{\lambda^2} \operatorname{sinc}\left(\frac{L_1 B}{\lambda}\right) \operatorname{sinc}\left(\frac{L_2 A}{\lambda}\right) \tag{2.10}$$

with

$$\left.\begin{aligned} A &= (p\cos\theta_s - q\sin\theta_s)\cos\phi_s + u\sin\phi_s \\ B &= p\sin\theta_s + q\cos\theta_s \\ p &= \operatorname{sinc}\theta_o \cos\phi_o + \sin\theta\cos\phi \\ q &= \cos\theta_o + \cos\theta \\ u &= \sin\theta_o \sin\phi_o + \sin\theta\sin\phi \\ \operatorname{sinc}[x] &= \frac{\sin\pi x}{\pi x} \end{aligned}\right\} \tag{2.11}$$

In particular, for the special case $\theta = \theta_o = \pi/2$, the field components are

$$E_\theta \equiv 0$$

$$E_\phi = -iE_o \frac{\exp(-ikr)}{kr} [-\cos\phi_s \sin\phi + \sin\phi_s \cos\phi \cos\Omega t] C(\Omega t) \tag{2.12}$$

with

$$C(\Omega t) = \frac{2\pi L_1 L_2}{\lambda^2} \operatorname{sinc}\left[\frac{L_1}{\lambda}(\cos\phi_0 + \cos\phi)\sin\Omega t\right]$$

$$\cdot \operatorname{sinc}\left[\frac{L_2}{\lambda}\{(\cos\phi_0 + \cos\phi)\cos\Omega t\cos\phi_s$$

$$+ (\sin\phi_0 + \sin\phi)\sin\phi_s\}\right], \qquad (2.13)$$

where we have explicitly included the time dependence produced by the rotation of the plate.

Note that, in accordance with the notation used in [2,4], the product of the last two factors in (2.8) and (2.9) may be identified as the modulation function associated with the respective component of the field. For example, the modulation function $f_{m\phi}(t)$ associated with the horizontal component E_ϕ is, from (2.9),

$$f_{m\phi}(t) = [-\sin\phi\{\sin\theta_0\cos\phi_s + \cos\theta_0\sin\phi_0\sin\theta_s\sin\phi_s\}$$

$$+ \cos\phi\{\sin\theta_0\sin\phi_s\cos\Omega t - \cos\theta_0\cos\phi_0\sin\phi_s\sin\Omega t\}]C(\Omega t) \qquad (2.14)$$

$$C(\Omega t) = \frac{2L_1L_2}{\lambda^2}\operatorname{sinc}\left[\frac{L_1}{\lambda}(p\sin\Omega t + q\cos\Omega t)\right]$$

$$\cdot \operatorname{sinc}\left[\frac{L_2}{\lambda}\{(p\cos\Omega t - q\sin\Omega t)\cos\phi_s + u\sin\phi_s\}\right] \qquad (2.15)$$

where p, q, u are given by (2.11).

Discussion of the modulation function under various conditions may be found in [2,4] and will not be repeated here.

2.2 Scattering of Vertically Polarized Waves

In this case the magnetic field vector of the incident wave lies in the horizontal plane. We therefore assume the incident field vectors to be

$$\vec{E}_2^i = E_0 \left[-\hat{x} \cos\theta_0 \cos\phi_0 - \hat{y} \cos\theta_0 \sin\phi_0 + \hat{z} \sin\theta_0\right]$$

$$\cdot \exp ik(x \sin\theta_0 \cos\phi_0 + y \sin\theta_0 \sin\phi_0 + z \cos\theta_0)], \quad (2.16)$$

$$\vec{H}_2^i = H_0 \left[-\hat{x} \sin\phi_0 + \hat{y} \cos\phi_0\right] \exp [ik(x \sin\theta_0 \cos\phi_0 + y \sin\theta_0 \sin\phi_0$$

$$+ z \cos\theta_0)] \ . \quad (2.17)$$

The surface current density $\vec{J}_s$ can be written in the form (2.6) with the components

$$\left.\begin{aligned} j_x &= - \cos\phi_0 \sin\theta_s \sin\phi_s \\ j_y &= - \sin\phi_0 \sin\theta_s \sin\phi_s \\ j_z &= -\cos\phi_0 \cos\theta_s \sin\phi_s + \sin\phi_0 \cos\phi_s \end{aligned}\right\} \quad (2.18)$$

The far zone scattered electric fields are again given by (2.8) and (2.9) with j_x, j_y, j_z given by (2.18). In particular, the scattered electric field components for $\theta = \theta_0 = \pi/2$ are

$$E_\theta = -iE_0 \frac{\exp(-ikr)}{kr} [\cos\phi_0 \sin\phi_s \cos\Omega t - \sin\phi_0 \cos\phi_s] C(\Omega t) \quad (2.19)$$

$$E_\phi = -iE_0 \frac{\exp(-ikr)}{kr} [\cos\phi_0 \sin\phi \sin\phi_s \sin\Omega t - \sin\phi_0 \cos\phi \sin\phi_s \sin\Omega t] C(\Omega t)$$

$$(2.20)$$

with $C(\Omega t)$ as shown in (2.13). Note that in the present case the cross-polarized component E_ϕ is non-zero even for $\theta = \theta_0 = \pi/2$.

2.3 Scattering of Circularly Polarized Waves

Let the incident electric and magnetic fields be

$$\left.\begin{aligned} \sqrt{2}\,\vec{E}^{i} &= E_1^i - iE_2^i \\ \sqrt{2}\,\vec{H}^{i} &= H_1^i - i\,H_2^i \end{aligned}\right\} \qquad (2.21)$$

where $(\vec{E}_1^i, \vec{H}_1^i)$ and $(\vec{E}_2^i, \vec{H}_2^i)$ are given by (2.2), (2.3), and (2.16) - (2.17), respectively. In (2.21) the normalizing factor $\sqrt{2}$ is used so that the power carried by the incident wave $(\vec{E}^i, \vec{H}^i)$ equals that carried by the individual wave $(\vec{E}_1^i, \vec{H}_1^i)$ or $(\vec{E}_2^i, \vec{H}_2^i)$. The complete expression for the incident electric field can be written as

$$\vec{E}^{i} = \frac{E_o}{\sqrt{2}}(-\hat{\phi} + i\hat{\theta})\exp(i\omega t + kr), \qquad (2.22)$$

where $\hat{\theta}$, $\hat{\phi}$ are the unit vectors in the θ- and ϕ- directions, and the wave is propagating along the negative r direction. It is easy to see from (2.22) that the incident electric field is circularly polarized, and that the sense of polarization is "counter-clockwise, wave approaching," i.e., right circular according to the IRE definition [5]. This kind of wave may be transmitted and received by a right-handed helical beam antenna [6].

For the incident field (2.21) it is possible to obtain the scattered fields by combining the results in Sections 2.2 and 2.3. In particular, for the case $\theta = \theta_o = \pi/2$, the scattered electric fields are

$$E_\theta = \frac{E_o}{\sqrt{2}} \frac{\exp(-ikr)}{kr} F_\theta\, C(\Omega t), \qquad (2.23)$$

$$E_\phi = \frac{E_o}{\sqrt{2}} \frac{\exp(-ikr)}{kr} F_\phi\, C(\Omega t), \qquad (2.24)$$

where

$$F_\theta = -i(\sin \phi_0 \cos \phi_s - \cos \phi_0 \sin \phi_s \cos \Omega t)$$

$$F_\phi = (\sin \phi \cos \phi_s - \cos \phi \sin \phi_s \cos \Omega t) \qquad (2.25)$$

$$+ i(\cos \phi_0 \sin \phi - \sin \phi_0 \cos \phi) \sin \phi_s \sin \Omega t, \qquad (2.26)$$

with $C(\Omega t)$ given by (2.13) and the time dependence $\exp(i\omega t)$ suppressed Equations (2.23) - (2.26) indicate that, in general, the scattered field is elliptically polarized.

2.3.1 Discussion

The general expressions for the scattered fields obtained with circularly polarized incident waves are too complicated to yield useful information except by numerical evaluation. In the present section we discuss some special cases which may be of interest.

(i) Stationary Plate

In this case, $\theta_s = \Omega t \equiv 0$, and we obtain from (2.25) - (2.26) and (2.13):

$$F_\theta = -i \sin (\phi_0 - \phi_s)$$

$$F_\phi = \sin (\phi - \phi_s) \qquad (2.27)$$

$$C(\Omega t) = C(0) = \frac{2\pi L_1 L_2}{\lambda^2} \operatorname{sinc} \left[\frac{L_2}{\lambda} \{\cos(\phi_0 - \phi_s) + \cos(\phi - \phi_s)\} \right]. \qquad (2.28)$$

In conjunction with (2.23) and (2.24), (2.27) indicates that the field is generally elliptically polarized. In the specular direction $\phi = \pi - \phi_0 + 2\phi_s$, we obtain from (2.27)

$$\left.\begin{aligned} F_\theta &= -\,i \sin(\phi_o - \phi_s) \\ F_\phi &= \sin(\phi_o - \phi_s) \end{aligned}\right\} \qquad (2.29)$$

which indicates that the field is circularly polarized and the sense of polarization is counter-clockwise, wave receding, i.e., left-circular, which is opposite to the sense of the incident polarization. In the forward direction $\phi = \pi + \phi_o$, and we obtain from (2.27)

$$\left.\begin{aligned} F_\theta &= -\,i \sin(\phi_o - \phi_s) \\ F_\phi &= -\sin(\phi_o - \phi_s) \end{aligned}\right\} \qquad (2.30)$$

which indicates that the field is circularly polarized and the sense of polarization is clockwise, wave receding, i.e., right circular, which is similar to the incident polarization. In both the specular and forward directions the scattered field is a maximum since $C(\Omega t) = C(0) = 2\pi L_1 L_2/\lambda^2$.

(ii) Rotating Plate: Non Skewed

In this case, $\phi_s = 0$, $\theta_s = \Omega t \neq 0$. Again, for the case $\theta = \theta_o = \pi/2$ we obtain from (2.23) - (2.26) and (2.13):

$$\left.\begin{aligned} F_\theta &= -i \sin\phi_o \\ F_\phi &= \sin\phi \end{aligned}\right\} \qquad (2.31)$$

$$C(\Omega t) = \frac{2\pi L_1 L_2}{\lambda^2}\ \mathrm{sinc}\left[\frac{L_1}{\lambda}(\cos\phi_o + \cos\phi)\sin\Omega t\right] \cdot \mathrm{sinc}\left[\frac{L_2}{\lambda}(\cos\phi_o + \cos\phi)\cos\Omega t\right] \qquad (2.32)$$

The nature of the modulation waveform (i.e., $C(\Omega t)$ obtained from (2.32)) is similar to that for the linearly polarized case discussed in [2,4]. The behavior of the sense of polarization of the scattered field is similar to that obtained with the stationary plate discussed earlier.

(iii) Rotating Plate: Skewed

In this case $\phi_s \neq 0$, $\theta_s = \Omega t \neq 0$, the corresponding F_θ, F_ϕ and $C(\Omega t)$ are given by (2.25) (2.26) and (2.13). It can be seen that the scattered field in the forward direction is circularly polarized with the same sense of polarization as the incident wave. In other directions the scattered field is elliptically polarized and the sense of polarization may be obtained by studying the general expressions given earlier.

2.4 Reception of Direct and Scattered Waves

It is of practical interest to determine the open-circuit terminal voltage of a receiving antenna produced by circularly or elliptically polarized waves discussed in the previous section. Analysis of the reception of elliptically polarized waves by an arbitrarily polarized receiving antenna is a complicated problem and is discussed in [7-10]. For simplicity, here we shall assume that the receiving antenna is isotropic and circularly polarized, and that its polarization plane is matched [10] to that of the wave under consideration. Based on these ideal assumptions, we give a simplified but useful discussion of the reception of circularly polarized waves in the presence of a stationary metal plate.

Fig. 2-1 shows the location of an arbitrary receiving point $P(r,\theta,\phi)$ with respect to the plate and the direction of propagation of the incident wave. The analysis is simplified by assuming that $\theta = \theta_0 = \pi/2$, i.e., transmission and reception of waves take place in the horizontal xy plane. For

the purpose of the present discussion it is found convenient to represent the geometry as in Fig. 2-3 which shows the direct (or incident) ray and a scattered ray reaching the receiving point P located at $(r, \pi/2, \phi)$ with respect to the origin O. It is now assumed that P is located near the specular direction of the plate scattering, for the given angle of incidence ϕ_o (Fig. 2-3), such that

$$\phi = \pi - \phi_o + 2\phi_s + \alpha \ , \tag{2.33}$$

where α is a small quantity near zero. With a right circularly polarized incident plane wave of the form (2.21), the scattered electric field at P can be obtained from the results given in Section 2.3 and may be written as

$$\vec{E}^s(P) = [E_\phi^s \ \hat{\phi} + \hat{\theta} \ E_\theta^s \exp(-i\pi/2)] \exp(-ikr) \ , \tag{2.34}$$

where

$$\left.\begin{aligned} E_\phi^s &= \frac{E_o}{\sqrt{2}} \ \frac{C}{kr} \ \sin(\phi_o - \phi_s - \alpha) \\ E_\theta^s &= \frac{E_o}{\sqrt{2}} \ \frac{C}{kr} \ \sin(\phi_o - \phi_s) \end{aligned}\right\} \tag{2.35}$$

$$C = \frac{2\pi L_1 L_2}{\lambda^2} \ \text{sinc} \left[\frac{L_2}{\lambda} \{\cos(\phi_o - \phi_s) - \cos(\phi_o - \phi_s - \alpha)\}\right] \tag{2.36}$$

Note that for $\alpha = 0$ in (2.35), $E_\phi^s = E_\theta^s$, and it follows from (2.34) that the scattered field at P is left circularly polarized. The direct (or incident) field at P can be written as

$$\vec{E}^d(P) = \frac{E_o}{\sqrt{2}} (\hat{\phi} + i\hat{\theta}) \exp[-ikr \cos\{2(\phi_o - \phi_s) - \alpha\}], \tag{2.37}$$

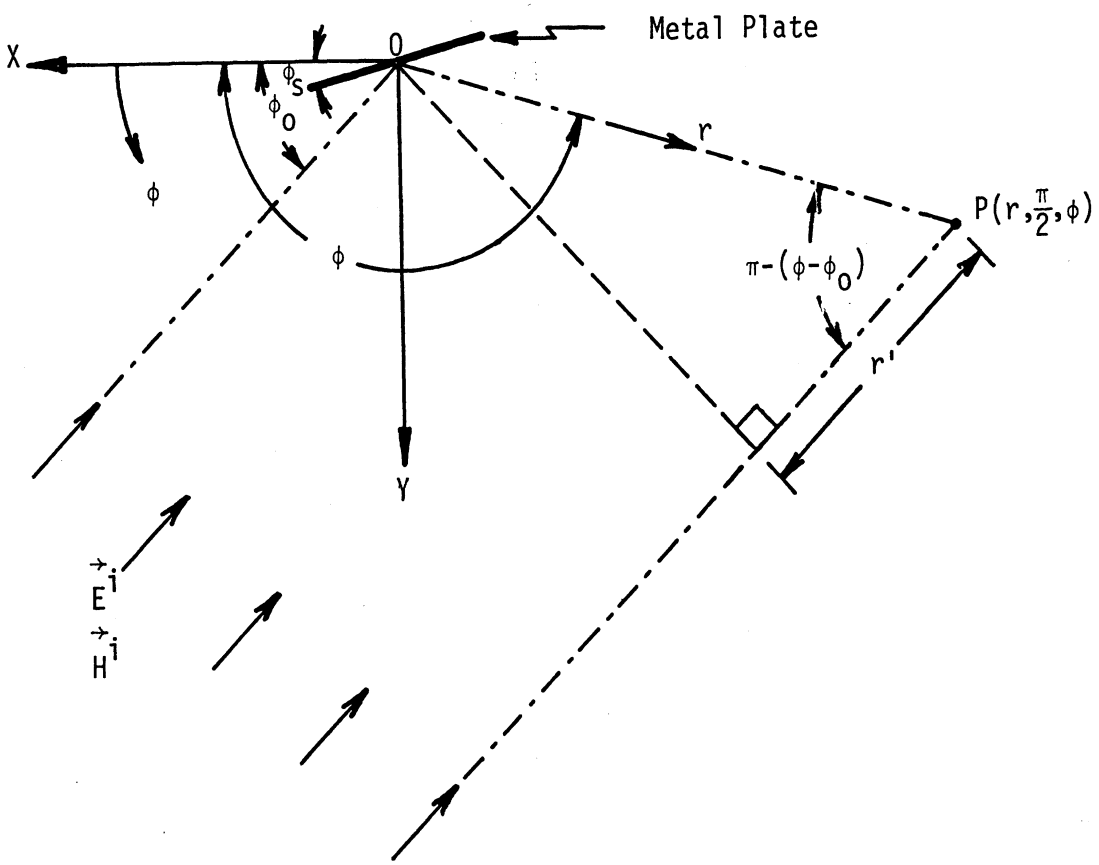

Fig. 2-3: Geometry showing the direct ray and a scattered ray reaching the receiving point P.

where the phase of the field has been expressed with reference to the origin O, $\hat{\phi}$ and $\hat{\theta}$ being the unit vectors at P defined earlier.

It has been found convenient to use the concept of vector effective height $\vec{h}$ [8,9] for an arbitrarily polarized antenna receiving elliptically polarized waves. Generally, $\vec{h}$ is a complex vector function [7], and may have both ϕ and θ components, both of which may be complex. However, without losing generality one of these components (say the ϕ-component) can be made a positive real quantity by a suitable choice of the origin for time, and we shall do so. Thus, for any antenna radiating elliptically polarized waves $\vec{h}$ can be written as

$$\vec{h} = [\hat{\phi}\, h_{\phi} + \hat{\theta} h_{\theta} \exp(i\delta)], \tag{2.38}$$

where δ is the phase angle by which the θ-component of the radiated field leads the ϕ-component, and h_{θ}, h_{ϕ} are real quantities. For a circularly polarized antenna $h_{\theta} = h_{\phi} = h$, and $\delta = \frac{\pi}{2}$ and $-\frac{\pi}{2}$, for right and left hand polarization, respectively. With a field $\vec{E}$ [$\vec{E}^{s}(P)$ or $\vec{E}^{d}(P)$ given by (2.34) or (2.37)] incident on a receiving antenna of vector effective height $\vec{h}$, the complex open-circuit voltage is given by [7]:

$$V = \vec{h} \cdot \vec{E}^{*}, \tag{2.39}$$

where $\vec{E}^{*}$ denotes the complex conjugate of $\vec{E}$.

Assuming the receiving antenna polarization matched to the incident field $\vec{E}$, the complex open-circuit voltage of the antenna is obtained by using (2.38) and (2.39) and is

$$V = [h_{\phi} E_{\phi} + h_{\theta} E_{\theta} \exp\{i(\delta + \pi/2)\}] \tag{2.40}$$

where E_{θ} and E_{ϕ} are the θ and ϕ components of $\vec{E}$.

With a circularly polarized receiving antenna matched to receive the scattered field given by (2.34), it can be shown from (2.40) that the open circuit voltage is

$$V_{\substack{R\\L}} = \frac{hE_o}{\sqrt{2}} \frac{C}{kr} [\sin(\phi_o - \phi_s - d) \mp \sin(\phi_o - \phi_s)] \exp(ikr), \tag{2.41}$$

where the upper and lower signs on the right-hand side are associated with the right circular (R) and left circular (L) receiving antennas, respectively. If the antenna is located exactly at the specular point,

$$V_{\substack{R\\L}} = \frac{hE_o}{\sqrt{2}} \frac{2\pi L_1 L_2}{\lambda^2 kr} \sin(\phi_o - \phi_s) [1 \mp 1] \exp(ikr), \tag{2.41}$$

which indicates that with a right circular incident plane wave a right circular receiving antenna will reject the specularly scattered field. However, with the same incident field, if a linearly polarized receiving antenna is used ($h_\phi = h$, $h_\theta = 0$) to receive the specularly scattered field, then it can be shown from (2.40) and (2.34) that

$$V = \frac{hE_o}{\sqrt{2}} \frac{2\pi L_1 L_2}{\lambda^2 kr} \sin(\phi_o - \phi_s), \tag{2.42}$$

indicating that the antenna now loses its capability of rejecting the scattered signal.

It is clear now that a right circular antenna should be used to receive the direct (or incident) field (2.57) which is right circular. Let us assume that a circularly polarized antenna is polarization matched to the direct wave $\vec{E}^d(P)$ and is used to receive both the direct and scattered waves. Using (2.40), (2.34) and (2.37) it can be shown that the open-circuit voltage on reception is

$$V_{\substack{R \\ L}} = \frac{E_o h}{\sqrt{2}} \exp\,[ikr\,\cos\{2(\phi - \phi_s) - \alpha\}]\,[1 \pm 1]$$

$$+ \frac{E_o h}{\sqrt{2}} \frac{C\,\exp(ikr)}{kr} \cos\{2(\phi_o - \phi_s) - \alpha\}$$

$$[\sin(\phi_o - \phi_s - \alpha) \mp \sin(\phi_o - \phi_s], \qquad (2.43)$$

where C is given by (2.36). If a horizontally polarized antenna is used to receive the same signals under similar conditions (i.e., $h_\phi = h$, $h_\theta = 0$), the open-circuit voltage is

$$V = \frac{E_o h}{\sqrt{2}} \exp\,[ikr\,\cos\{2(\phi_o - \phi_s) - \alpha\}]$$

$$+ \frac{E_o h}{\sqrt{2}} \frac{C\,\exp(ikr)}{kr} \cos\{2(\phi_o - \phi_s) - \alpha\} \sin(\phi_o - \phi_s - \alpha). \qquad (2.44)$$

It is now evident from (2.43) that a right circular antenna receiving right circularly polarized signals in the vicinity of a metal plate will discriminate against the scattered signals in the specular region and thereby will reduce any potential interference effects. Eq. (2.44) indicates that a linearly polarized receiving antenna will not have this capability.

2.5 Some Experimental Results

Limited experiments were carried out in an anechoic chamber to observe the signals scattered by a non-skewed rectangular metal plate (Fig. 2-1 with $\phi_s = 0$) rotating about an axis through its center when illuminated by circularly polarized plane electromagnetic waves. The frequency of the incident wave was 16.04 GHz corresponding to the wave length $\lambda = 1.87$ cm. The dimensions

of the plate were $L_1 = 24.5\lambda$ and $L_2 = 1.4\lambda$. The experimental arrangement was similar to that used in our previous studies with linearly polarized waves [2,4], and will be described in a later chapter. The plate and the circularly polarized transmitting and receiving antennas were in the far zone of each other according to the $2D^2/\lambda$ criterion, and throughout the measurements the phase centers of all three lay in the same horizontal plane, i.e., $\theta = \theta_0 = \pi/2$ (Fig. 2-1). The scattered fields were observed at a given bistatic angle $(\phi - \phi_0)$, as in Fig. 2-3.

The observed scattered field amplitudes as functions of time are shown in Figs. 2-4(a) and 2-4(b) with the receiver polarization opposite and similar to the incident polarization, respectively. The geometry used during this measurement was such that the observation angle was near specular — as a result, no sinc- like modulation [2,4] was observed. The sine wave-like modulation waveforms in Fig. 2-4 are similar to those observed with linearly polarized waves under similar conditions. It is important to note that the average amplitude level of the scattered field in Fig. 2.4(a) is about 15 dB higher than that in Fig. 2.4(b), which confirms the theoretical prediction (made in Sections 2.3 and 2.4) that the polarization of the specularly scattered field is opposite to that of the incident field. Similar measurements were taken with a stationary plate, and it was found that an oppositely polarized antenna received a signal about 14 dB higher than a similarly polarized antenna. Due to lack of time, a more detailed investigation was not carried out.

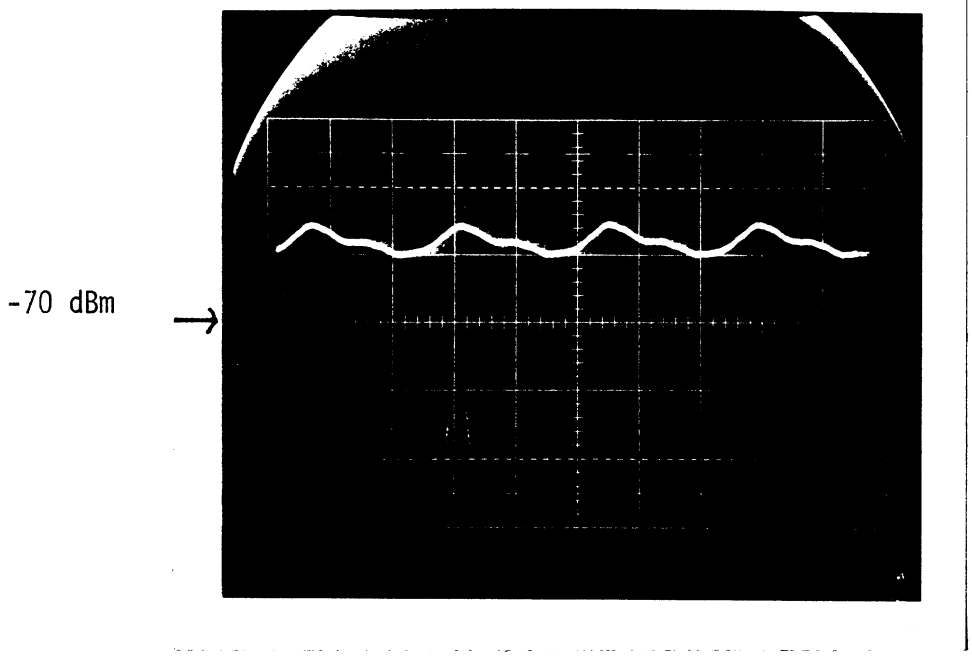

(a) transmit: clockwise
receive: anticlockwise

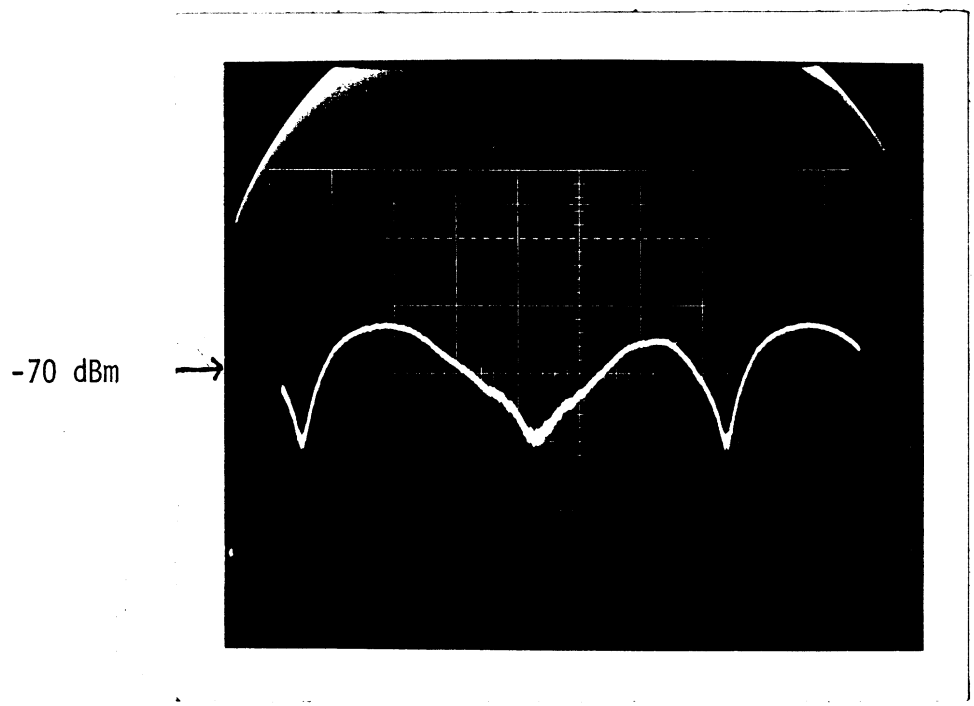

(b) transmit: clockwise
receive: clockwise

Fig. 2-4: The scattered field amplitude as a function of time for a rotating rectangular metal plate illuminated by circularly polarized plane electromagnetic waves (Note: (a) 10 dBm/vertical division and 0.5 sec/horizontal division, and (b) 10 dBm/vertical division and 0.2 sec/horizontal division).

2.6 General Discussion

The scattering of circularly polarized plane electromagnetic waves by a slowly rotating rectangular metal plate has been investigated. It has been found that the rotating plate amplitude modulates the incident wave. The nature of the modulation waveform depends on the orientation and electrical dimensions of the plate, its rotation speed, and most importantly, the directions of incidence and scattering. For a non-skewed plate rotating in its own plane, the modulation is independent of time in the directions of specular and forward scattering, i.e., in the directions where the scattering is a maximum. In directions near specular or forward, the modulation waveform is a sinusoid whose frequency is twice the rotation frequency; and away from these directions, the waveform consists mainly of sinc-like pulses repeating at twice the rotation frequency. The width of these pulses is inversely proportional to the maximum linear dimension of the plate. For a skewed rotating plate, the modulation waveform in the forward direction is sinusoidal with a frequency equal to the rotation frequency of the plate. In the specular direction with respect to the plane of rotation, the modulation waveform consists of a combination of sinusoids having frequency equal to the rotation frequency. In other directions, the waveform is primarily a sinc-like pulse, the width of the main pulse being inversely proportional to the maximum plate dimension. These findings are generally similar to those reported for the case of linearly polarized incident signals [2,4].

With a circularly polarized incident field, the scattered signal, in general, is elliptically polarized. In the forward and specular directions the scattered wave becomes circularly polarized with a sense of polarization similar and opposite, respectively, to the incident wave polarization. The

implications of these on reception would be that an antenna, polarization matched to receive the direct (or incident) circularly polarized signal, would discriminate against the specularly scattered interfering signal. As a consequence, any possible interfering effect caused by the scatterer would be significantly reduced.

CHAPTER 3

SOME PRACTICAL ASPECTS OF THE TV INTERFERENCE PROBLEM

In our previous studies [1,2] of the interference to TV reception produced by large horizontal axis windmills it was shown that the rotating blades can produce pulse-like amplitude modulation of the total received signal, and if the modulation is sufficiently strong, it can affect the TV picture. As a result of a detailed series of laboratory simulation experiments, it was found that the largest value of the amplitude modulation index for which the video distortion is still judged to be acceptable is $m = m_0 = 0.15$, and this threshold was confirmed by on-site measurements using the NASA-DOE 100 KW WTG at Plum Brook, OH.

In [3] the threshold was used to specify the region about a windmill where the interference to a given TV transmission could be unacceptable. It was assumed that the electromagnetic waves propagate in the free space medium above a homogeneous smooth spherical earth having a radius 6.34×10^3 km, with relative permittivity $\varepsilon_r = 15$ and conductivity $\sigma = 0.01$ siemens/m; and that the heights of the transmitting antenna, receiving antenna and blade scattering center are 1000, 10 and 30 m, respectively. The latter are reasonable for an antenna mounted on the roof of a home in the presence of a MOD-0 WTG, but two further assumptions were also made that are equivalent to a 'worst case' situation as regards the interference problem. Because the blade scattering is specular in nature, interference can only be observed when the windmill pointing direction and the blade pitch angle are such that at some point in a blade's rotation the scattering is directed to the receiving antenna. It was therefore assumed that for each receiver location the windmill is such as to direct the maximum reflected signal to the antenna, which was in turn treated as omnidirectional.

Under these assumptions three different computational techniques were proposed [3] to find the zone of (unacceptable) interference about a WTG. The third and most complicated technique gives the mathematically most precise specification of the zone, but for practical purposes it is generally sufficient to use the second or intermediate technique which leads to a zone in the form of a cardioid with a forward scattering spike. The zone is then defined as a function of the angular separation ϕ of the windmill-receiver and windmill-transmitter directions by

$$r = \begin{cases} r_1 \cos \frac{\phi}{2} & 0 \leq \phi \leq \pi - \lambda/L \\ r_2 \operatorname{sinc} \left(\frac{L}{\lambda} \sin \phi\right) & \pi - \lambda/L \leq \phi \leq \pi \end{cases} \tag{3.1}$$

where r_1 and r_2 are the zone radii in the backward and forward directions and L is the length (in m) of a WTG blade. The radii increase with the electrical size of blade and thus the interference is worst at the highest UHF frequency.

To illustrate the results, consider the case of the newly-erected WTG on Block Island for Channel 53 (f = 705 MHz) whose transmitter is located in Norwich, Connecticut, 56 km away. The equivalent scattering area of the MOD-0 blade is 12 m^2 and using then Figs. 4 and 5(f) of [3] with y_1 = - 2.0 dB we obtain

$$r_1 = 1.2 \text{ km}, \qquad r_2 = 1.7 \text{ km} \quad . \tag{3.2}$$

Since L = 18 m, the zone is as shown in Fig. 3-1, and we remark that the forward spike (directed away from the transmitter) is extremely narrow, being only 2.7^o in total width. For comparison we show also the zone

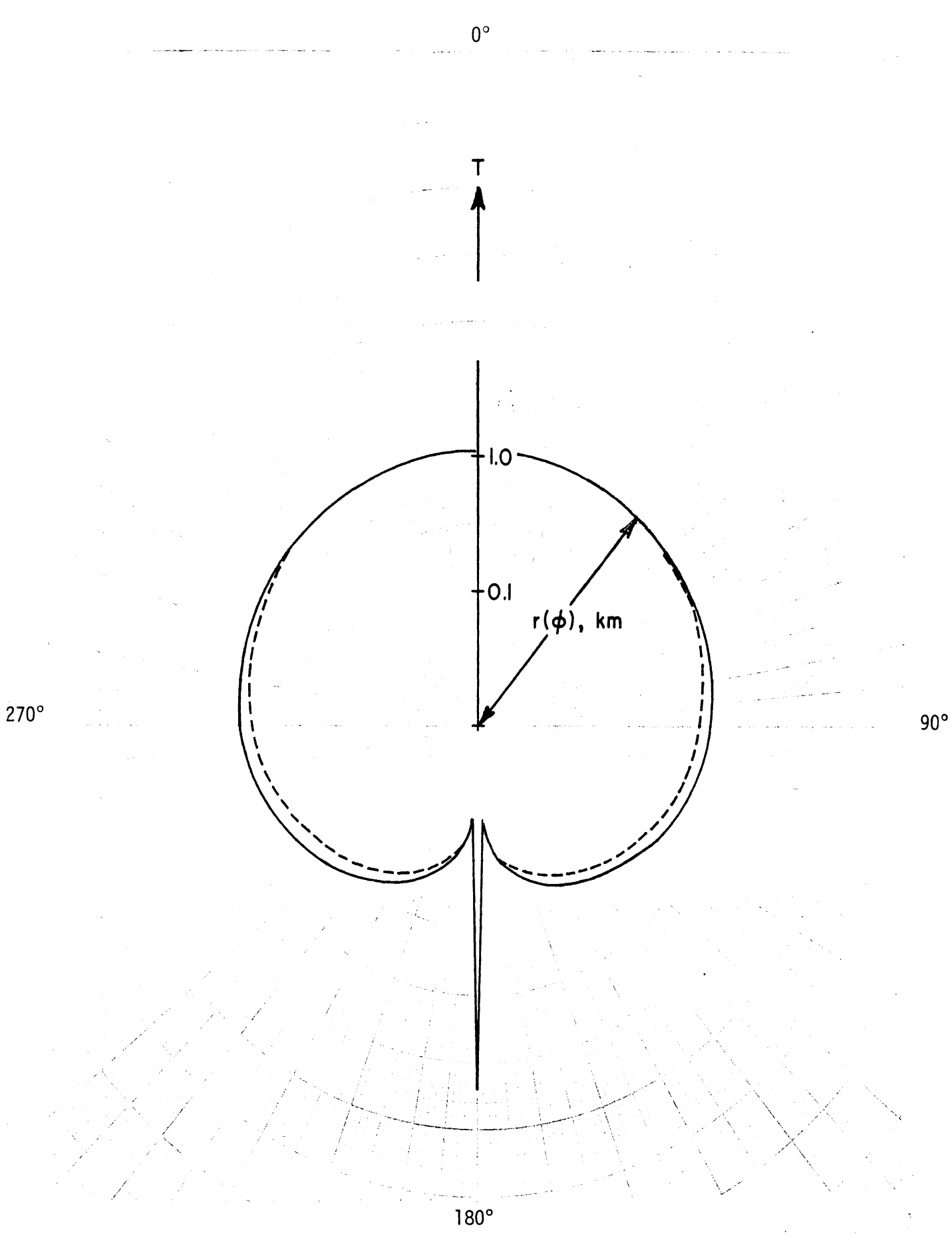

Fig. 3-1: Interference zone for Channel 53 on Block Island computed by the graphical (——) and intermediate (---) techniques.

computed by the third technique, and it is evident that for practical purposes the simplified formula is adequate.

Each TV Channel has its own interference zone and since, for a large windmill, the zones are quite extensive particularly at the higher UHF frequencies, it might appear that a windmill will produce video distortion over a significant geographical area around the WTG. This would obviously have a major impact on the siting of such machines and could lead to the elimination of sites which are otherwise most desirable. However, an interference zone is merely the region where video distortion could possibly occur, and gives no information about the probability of occurence. Even at a place well within a zone several conditions must be simultaneously met if a person viewing a TV picture is to see any interference whatsoever and in practice that person may be affected for only a very small fraction of his total viewing time. In order to assess the practical severity of the TV interference problem it is therefore important to examine the factors which govern the occurence of interference.

A major factor is the receiving antenna used. As we have remarked, the blade scattering increases with increasing frequency. The potential interference is worst at the highest UHF frequencies and, in practice, we can ignore the problem in the VHF band where the zone radii are typically only a small fraction of a kilometer. Thus, for Block Island with Channel 6 originating in Bedford, Massachusetts, $r_1 \simeq r_2$ = 0.13 km. Apart from urban areas where a windmill is hardly likely, the adequate reception of a UHF Channel requires a high gain antenna positioned with its beam directed at the TV transmitter. Such an antenna will then discriminate against signals coming in from other directions, including the interfering signal contributed by a windmill, and this could significantly reduce

the backward portion of the interference zone.

Another factor is the wind. Only if the wind is blowing can the blades rotate, and their pitch angle is then adjusted to maintain uniform power generation for varying wind speeds. In our on-site measurements at Plum Brook [2] the pitch angle was found to affect the direction of the specularly scattered signal from the blade, but this was largely compensated for by the blades' rotation -- a small change in pitch angle meant only that the specular lobe was picked up when the blade was at a different position in its rotation. The wind direction, however, is another matter. In computing the interference in a given direction ϕ it was assumed that the peak specular scattered signal was observed. As the wind shifts, so does the windmill. This in turn affects the direction of the specular beam, and a wind shift of only 10° will swing the specular beam 20^{0}, thereby eliminating interference in the original direction ϕ.

The number of TV Channels available at a given site and the viewing habits of the local population are also factors that affect the practical significance of the interference. It is obvious that interference can be perceived only if that Channel is being viewed and the more Channels there are available the lower the probability that a resident is tuned to any given one. Each Channel has its own interference zone and when one is being interfered with, the pointing direction of the windmill at that instant of time ensures that another Channel originating from a different point of the compass will not be interfered with. If several Channels are tied to the same network and transmitting the same program, the resident could now obviate the interference by simply switching to another Channel.

At a given WTG site most of the above factors could be estimated,

with some being deterministic and others statistical in nature. From an inspection of the homes in a neighborhood of the WTG, the availability of directional receiving antennas and their associated rotors could be ascertained. The use of such an antenna could drastically reduce the severity of the interference but only if the antenna is operating efficiently and the home owner is willing to take the trouble to point it appropriately. Local terrain will also affect the interference. If a hill or building were to shield the receiving antenna from the windmill-scattered signal the interference would obviously be less, but if the direct signal were similarly shielded, the reverse could be the case. This effect also is deterministic, and the necessary calculations could be performed.

At all existing and candidate WTG sites meteorological data are being gathered [11] giving wind speed and direction and can be processed [12] to provide monthly totals for the percent time the wind was in $22\frac{1}{2}^{o}$ sectors around the compass, and the percent time it exceeded a given speed in increments of 0.5 m/s. Although the $22\frac{1}{2}^{o}$ spread in direction is somewhat large for our purposes, such data can serve to indicate the probability that interference to a given TV Channel will occur at any location.

The other factors affecting the practical significance of the interference are much more difficult to quantify. Even at places where there are many TV Channels available, most people confine their viewing to a small number of these. Allegiances are built up which the TV stations take great pains to cultivate, but the allegiances are rather fragile, and a station which drops a single popular program or loses a newscaster may find its audience drastically reduced. The same fate would likely befall

the TV Channel whose signal was occasionally interfered with. In the case of Block Island, 14 TV Channels are listed as 'available', but it appears [13] that most residents watch only four of them: Channel 6 whose transmitter is in Bedford MA, NE of Block Island; Channels 10 and 12 with transmitters in Providence RI (NNE), and Channel 53 with transmitter in Norwich CT (NW). All of these transmitters are within 65 km of the island. To question the home owners living within (say) 1.5 km of the WTG could yield figures for the average time per day each Channel was being viewed, but it is doubtful how meaningful the figures would be. To watch a TV program as opposed to merely having the set 'on' are two very different things, and if one Channel were to suffer occasional interference more often than did the others, it is inevitable that the allegiance to that Channel would diminish. For these reasons, it does not seem profitable to pursue these matters further.

To examine the effect of using a directional receiving antenna and/or the influence of the wind characteristics on the interference, it is convenient to concentrate* on the backward portions of the interference zones using Block Island as an example. The first step is to recast the expression for the distance r_1 to bring out the dependence on the equivalent blade scattering area A_e and the wavelength λ. In the far field of the blade but at distances less than a few kilometers (the precise upper limit is a function of frequency), the blade-scattered field decreases at 0.3 V/km.

---

* The practical significance of the forward spike is difficult to assess, not least because of its very narrow width.

From (5) and (7) of [3] with K = 0.3 we then have

$$r_1 = \frac{2\Gamma}{150} \frac{A_e}{\lambda}$$

where Γ is the ratio of the primary signal at the blade to that at the receiver, and since Fig. 5(f) of [3] gives $\Gamma \simeq 3.0$ at distances of about a kilometer or less, it follows that

$$r_1 = 0.04\ A_e/\lambda$$

regardless of frequency. With Channel 53 (λ = 0.426 m) and A_e = 12 m^2, r_1 = 1.13 km, in close agreement with the more precise value in (3.2). The backward portion of an interference zone is then the region whose boundary is

$$r(\phi) = \frac{0.04}{\lambda} A_e \cos \frac{\phi}{2} \tag{3.3}$$

and we remark that $A_e \cos \frac{\phi}{2}$ is simply the projected area of a blade.

The use of a directional receiving antenna oriented towards the transmitter will reduce the blade-scattered or perturbing signal relative to the desired or direct one, and thereby reduce r. If $P(\phi)$ is the voltage polar diagram or pattern factor of the antenna with P(0) = 1, the resulting expression for $r(\phi)$ is

$$r(\phi) = \frac{0.04}{\lambda} A_e \cos \frac{\phi}{2} P(\pi-\phi). \tag{3.4}$$

Throughout most of the interference zone, the blade-scattered signal will be received via the backward lobes of the antenna, and the desirability of an antenna with a high front-to-back ratio is now evident.

The antenna used in our on-site measurements at Plum Brook is typical of the better UHF/VHF antennas, and its power polar diagram is shown in Fig. 5-2 of [2]. For $|\phi| \gtrsim 55^0$, P is down by at least 18 dB from its peak, and by averaging the left and right hand sides of the pattern, we arrive at the idealized but representative plot of $P(\phi)$ given in Fig. 3-2. With Channel 53, the effect of replacing the omnidirectional antenna with a directional one is shown in Fig. 3-3. The maximum value of $r(\phi)$ is reduced to 0.14 km (for $\phi = 0$), and $r(\phi) < 0.12$ km for $|\phi| > 55^0$. In the belief that values of r less than (say) 120 m are of no practical significance, we observe that the only locations where interference to Channel 53 could occur are those lying west to north of the WTG at distances of less than 140 m from the machine. For Channel 12, the next highest one in frequency, $r(\phi) \lesssim 330$ m even with an omnidirectional antenna, and the use of an antenna with only a 9 dB front-to-back ratio could make $r(\phi) < 120$ m for all ϕ.

We now turn to the role played by the wind and seek to use the wind data available for each WTG site to determine the probability of interference to a given TV Channel at any position relative to the WTG and the direction of the TV transmission. For simplicity we revert to the assumption of an omnidirectional receiving antenna.

In the previous Chapter an expression was derived for the field scattered by a rotating skewed rectangular plate when illuminated by a horizontal polarized field. For incidence and reception in the horizontal plane the expression is given by (2.12) in which L_1L_2 is clearly identifiable as the equivalent scattering area A_e of the blade. Let L_1 be the larger blade dimension. The scattering is a maximum when the arguments of both sinc functions are zero and for the backward portion of the interference

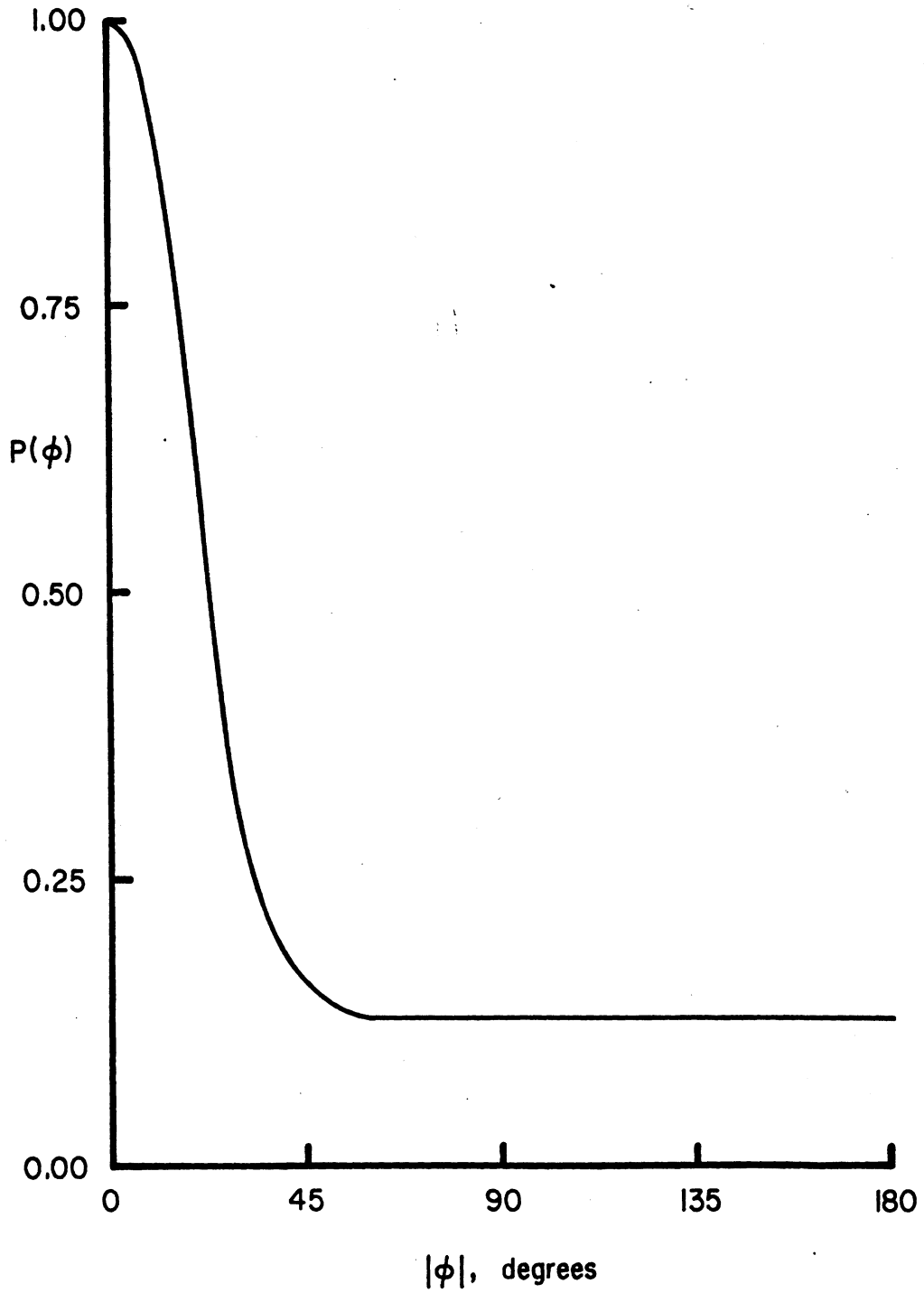

Fig. 3-2: Voltage polar diagram of the receiving antenna used in the analysis.

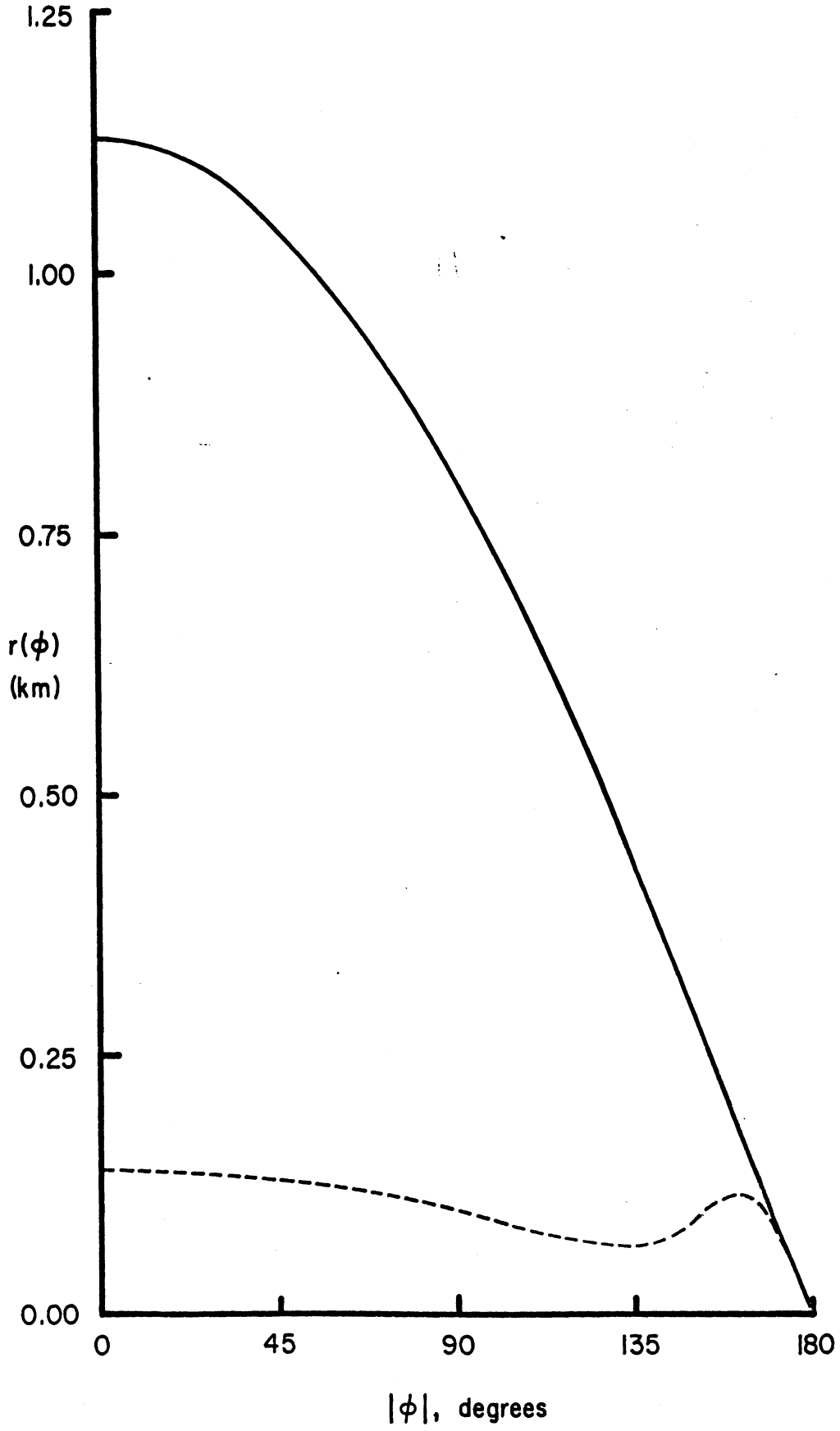

Fig. 3-3: The radius r(ø) of the interference zone for Channel 53 on Block Island with an omni-directional receiving antenna (————) and the directional one (---) whose polar diagram

zone the case that is appropriate is

$$\Omega t = 0, \qquad \tilde{\phi} - \phi_s = \pi - (\tilde{\phi}_o - \phi_s) \ ,$$

where the tildas has been added to avoid confusion with the angle ϕ used in the zone specification. To compute the zone radius $r(\phi)$ it was assumed that the windmill is oriented to direct the maximum blade-scattered signal to the receiver as shown in Fig. 3-4a, implying

$$\tilde{\phi} - \phi_s = \pi - (\tilde{\phi}_o - \phi_s) = 1/2(\pi + \phi) \ .$$

Thus

$$E = iE_o \frac{e^{-ikr}}{\lambda r} A_e \cos \frac{\phi}{2} \tag{3.5}$$

from which (3.3) follows, but if the windmill were to turn through an angle α, thereby rotating the specular beam 2α (see Fig. 3-4b),

$$\tilde{\phi} - \phi_s = 1/2(\pi + \phi) - \alpha, \qquad \tilde{\phi}_o - \phi_s = 1/2(\pi - \phi) - \alpha$$

and (2.12) then gives

$$E = iE_o \frac{e^{-ikr}}{\lambda r} A_e \cos (\frac{\phi}{2} - \alpha) \operatorname{sinc} (\frac{2L_2}{\lambda} \cos \frac{\phi}{2} \sin \alpha).$$

With the windmill driven off azimuth in this manner, the resulting expression for the zone radius in a direction ϕ is

$$r(\phi,\alpha) = \frac{0.04}{\lambda} A_e \cos (\frac{\phi}{2} - \alpha) \operatorname{sinc} (\frac{2L_2}{\lambda} \cos \frac{\phi}{2} \sin \alpha). \tag{3.6}$$

The sinc function provides the main dependence on the angle α and for most practical purposes we can ignore the asymmetric dependence of the cosine factor. We then have

$$\frac{r(\phi,\alpha)}{r(\phi,0)} = \operatorname{sinc} (\frac{2L_2}{\lambda} \cos \frac{\phi}{2} \sin \alpha) \tag{3.7}$$

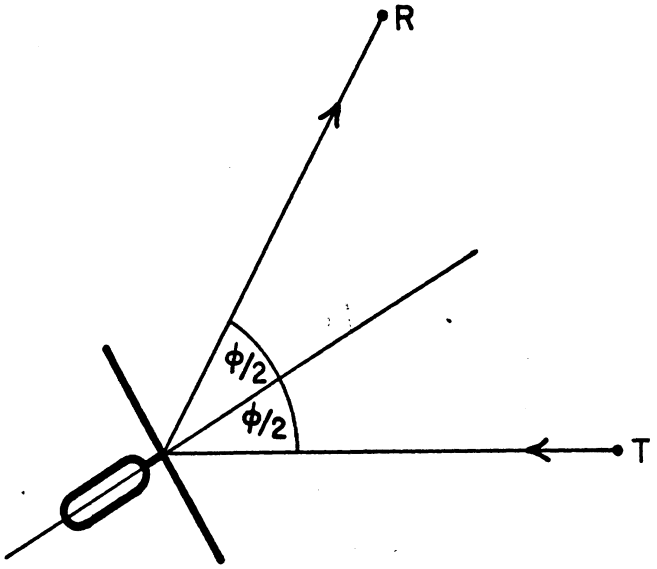

Fig. 3-4a: Windmill orientation for the standard computation of the interference zone radius in a direction ø relative to the incident field.

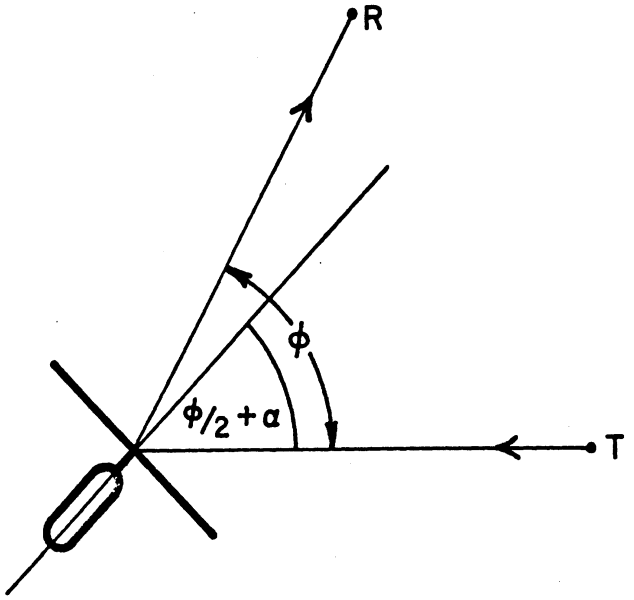

Fig. 3-4b: Windmill rotated in azimuth through an angle α.

and this is plotted in Fig. 3-5 for L_2 = 0.9 m (corresponding to a MOD-0 blade), λ = 0.426 on Channel 53 and ϕ = 0, 45 and 90 degrees. In these three directions, deflections α of 11.3, 12.2 and 16.0 degrees respectively are sufficient to reduce the zone radius by a factor 5.

At all existing and potential WTG sites the wind speed and direction are being monitored, and monthly totals are available for the percent time the wind lies in 22 1/2 degree sectors around the compass. Since the back of the blades scatter energy as well as the front, winds in diametrically opposite directions are equally effective in aligning the WTG, and for a recent month [12] on Block Island the results obtained by adding the percent times for winds in directions β and $\beta + 180^0$ are shown in Fig. 3-6. Although a spread of 22 1/2 degrees in wind direction is too large for interference calculations, by linear interpolation and subsequent renormalization of the tabulated data we can deduce the probability $p'(\beta)$ of a wind in directions $(\beta - 2.5^0, \beta + 2.5^0)$. However, not always is the wind speed sufficient for the blade rotation to produce modulation, and if we set the minimum required speed at (say) 6.5 m/s ($\sim$ 14.5 m.p.h.), the cumulative wind data [11] for the period December 1976 to September 1978 yields a probability p_0 = 0.63 for Block Island. The probability of an adequate wind in directions $(\beta - 2.5^0, \beta + 2.5^0)$ is therefore

$$p_0 p'(\beta),$$

and if we widen the spread to $\pm 7.5^0$ the corresponding probability is

$$p_0 \{ p'(\beta - 5^0) + p'(\beta) + p'(\beta + 5^0) \} .$$

To illustrate the use of these data, consider the case of Channel 53

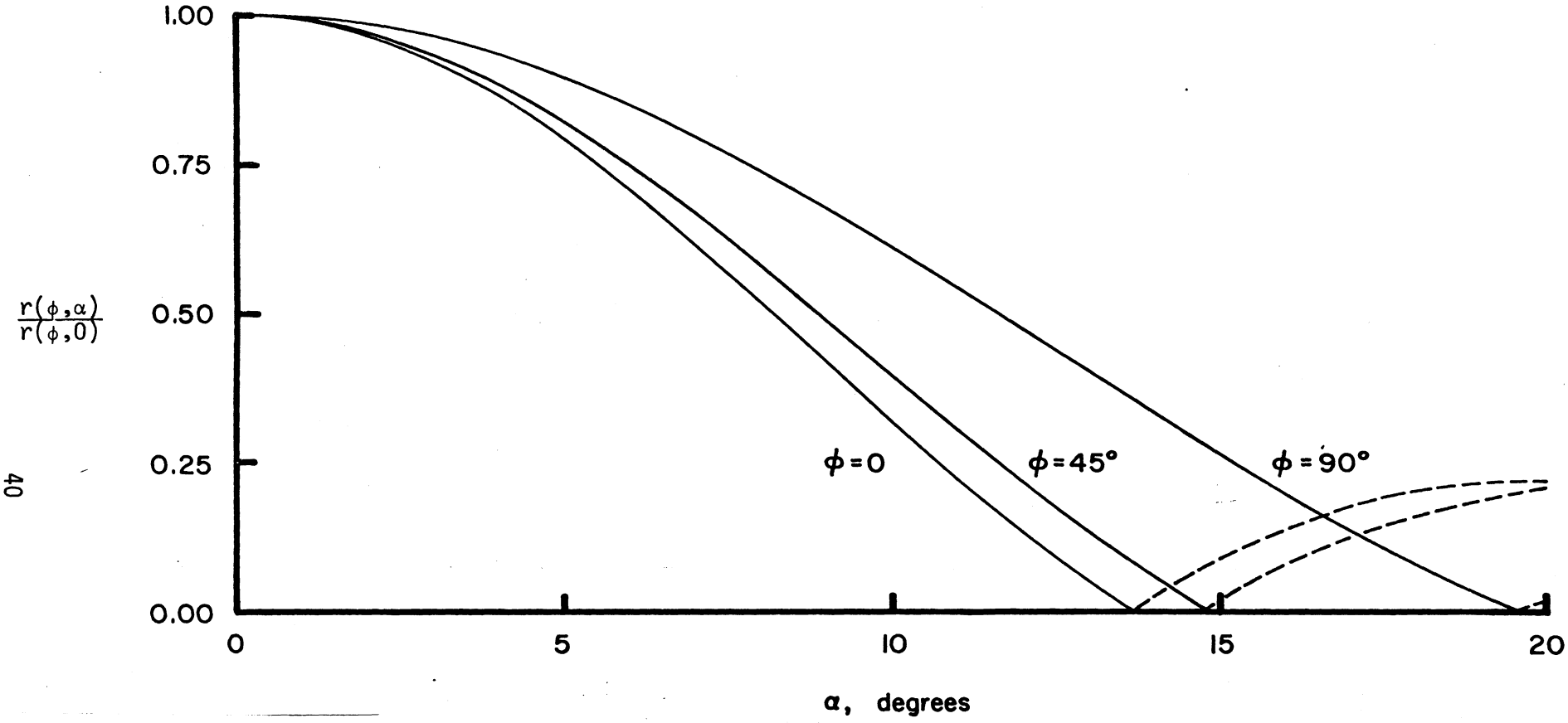

Fig. 3-5: $\frac{r(\phi,\alpha)}{r(\phi,0)} = \text{sinc}\left(\frac{2L_2}{\lambda}\cos\phi\sin\alpha\right)$ with $2L_2/\lambda = 4.23$ corresponding to a MOD-0 blade on Channel 53. The broken lines correspond to the first side lobes, which are ignored in the analysis.

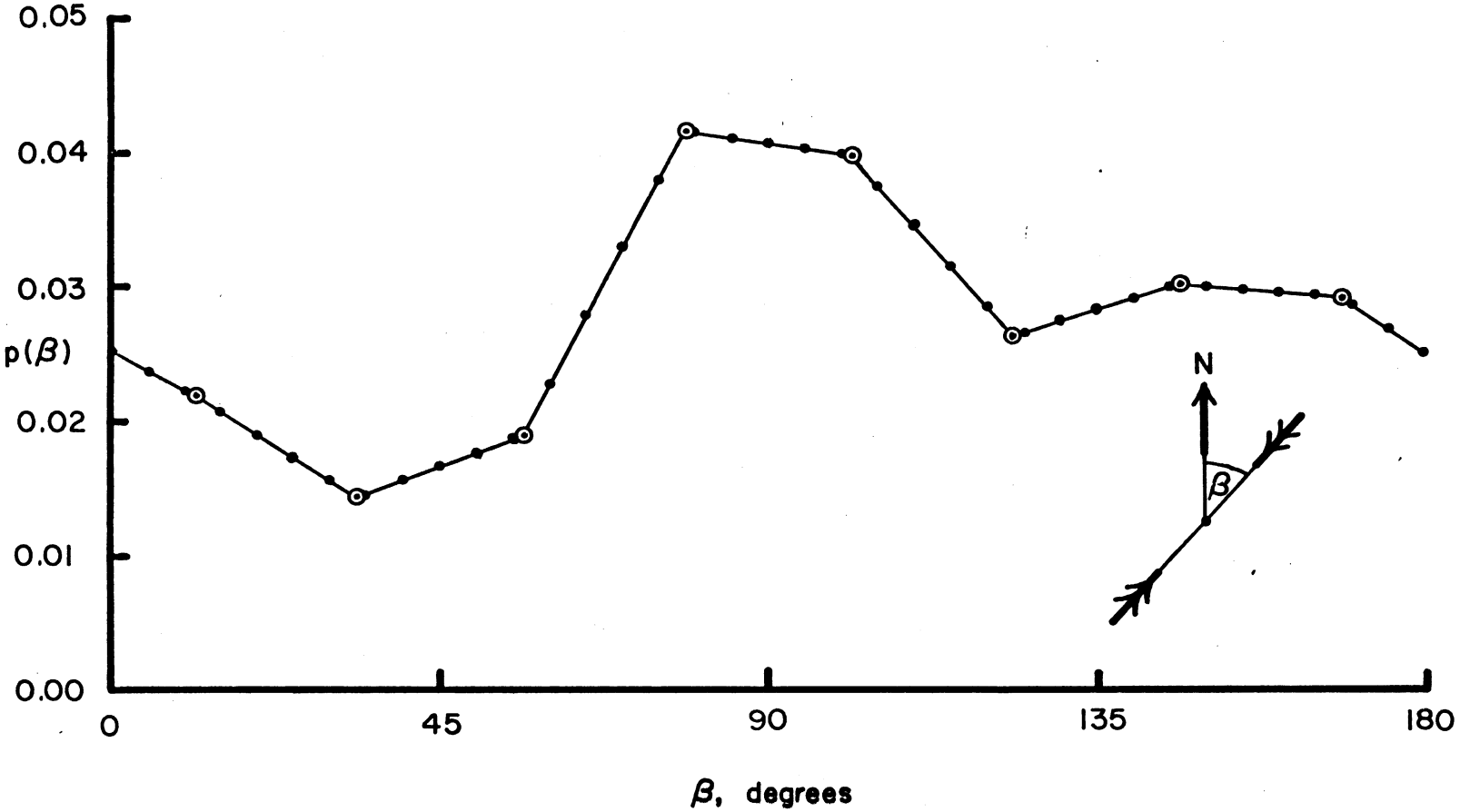

Fig. 3-6: Probability of wind in 5^{o} sectors centered on the dots, obtained by linear interpolation of 22 1/2-degree sector data (⊙ ⊙ ⊙) for a recent month on Block Island [12].

on Block Island whose transmitter (in Norwich, CT) will be treated as NW of the WTG. For a receiver SW of the windmill ($\phi = 90^0$) an east or west wind would orientate the windmill appropriately to direct the specularly scattered signal to the receiving antenna, and if the wind speed was sufficient, interference would be observed out to a distance r = 0.80 km (see Fig. 3-1) from the machine. The probability of a wind within $\pm 2.5^0$ of these directions is, from Fig. 3-6 with $\beta = 90^0$,

$$0.63 \times 0.041 = 0.026$$

and for $0 \leq \alpha \leq 2.5^0$ with $\phi = 90^0$, the sinc function in (3.7) varies from 0.97 to 1.0, averaging 0.985. There is consequently a 2.6% probability of interference out to $0.80 \times 0.985 \simeq 0.80$ km from the machine or, conversely expressed, 97.4% probability of no significant interference beyond 0.80 km. Within $\pm 7.5^0$ of east or west, the probability of an adequate wind is

$$0.63\ (0.041 + 0.041 + 0.040) = 0.077,$$

so that the probability of the wind being outside this range and/or of insufficient speed is 92.3%. The maximum value of the sinc function for $\alpha = 5^0$ is 0.97 (the average for $\alpha = 5 \pm 2.5^0$ is 0.71), and the probability of no significant interference beyond $0.97 \times 0.80 = 0.78$ km is therefore 92.3%. Continuing in this manner we ultimately arrive at $\alpha = 20^0$ for which the sinc function is always less than 0.11 . The corresponding r is then 0.088 km, and in line with our previous assumption, we treat this as a case of no interference.

These results are plotted in Fig. 3-7 along with the analogous ones for reception NW of the WTG ($\phi = 0$), and we observe that at a distance of 0.5 km the probability of experiencing significant interference on Channel 53 is 15 percent SW of the machine and 9 percent NW. This is for an omni-

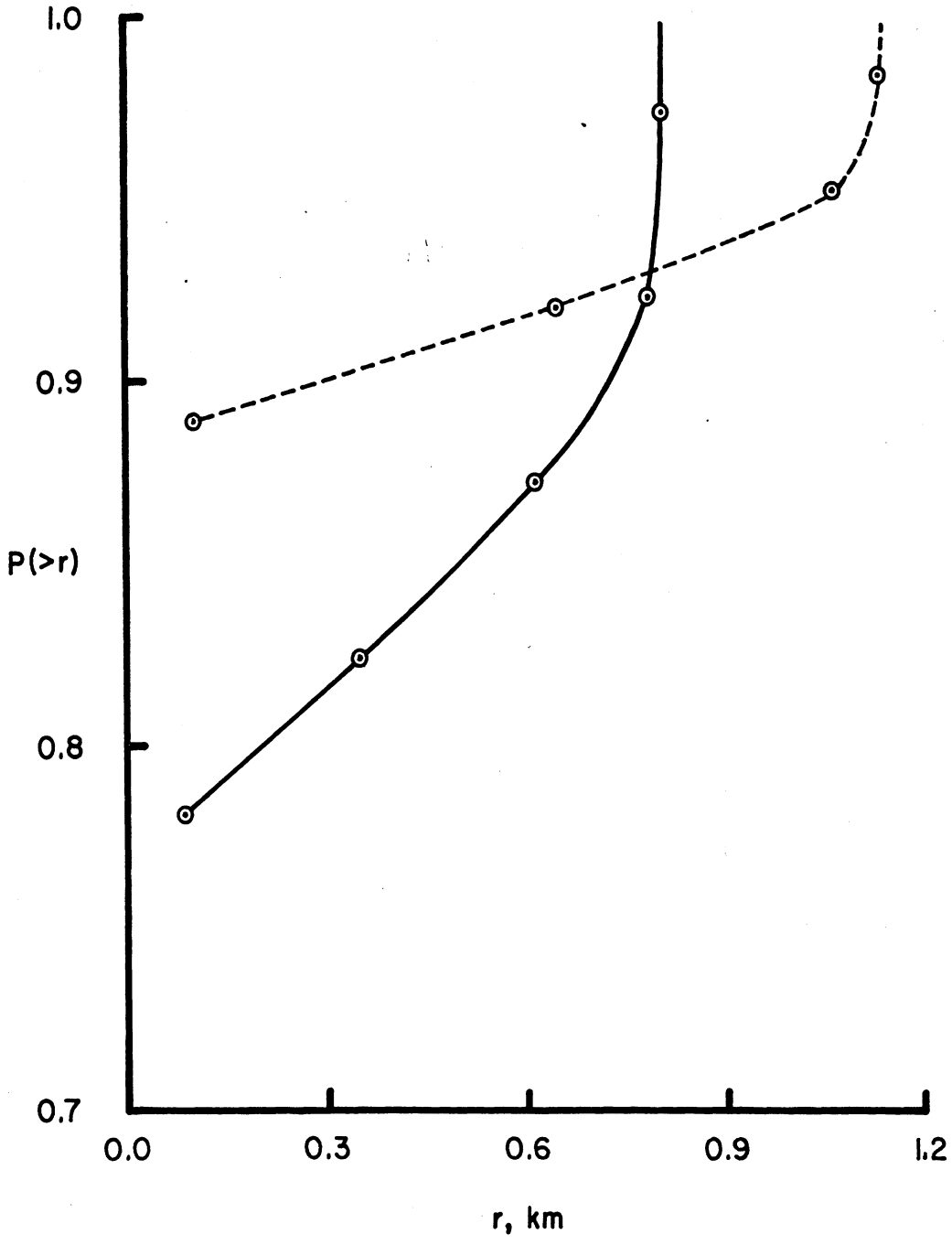

Fig. 3-7: Probability of observing no significant interference to Channel 53 on Block Island at a distance greater than r south-west of the WTG (——) and north-west (---).

directional antenna, and were a directional one employed, r should be multiplied by $P(\pi-\phi)$ where P is the voltage polar diagram of the receiving antenna.

From the above analyses it is clear that the availability and correct orientation of a directional antenna will decrease the possibility of interference throughout the backward portion of the interference zone, and that the probability of interference occurring can be deduced from data on wind speed and direction. In practice, therefore, the interference problem could be much less severe than is suggested by the basic interference zones, but it is still true that these zones define the region where interference could occur. Indeed, were a directional antenna operated incorrectly, i.e., pointed at the windmill, interference could exist even beyond the zone.

CHAPTER 4

SCATTERING FROM VERTICAL AXIS MACHINES

The Darrieus and Giromill are very different structures from the large horizontal axis machines that have been the focus of our previous studies, and since it is not obvious what their electromagnetic scattering is, a variety of scattering measurements were carried out in an anechoic chamber using small scale models of varying degrees of fidelity. All had maximum dimension 15 in. purporting to be 1/40 scale models of the full size machines. The measurements were performed with a standard cw set-up at a frequency of 16.04 GHz (λ = 0.736 in.) corresponding to 401 MHz full scale.

Each model was placed vertically on a support pedestal and was rotated through a full 360^{o} about a vertical axis either by rotating the pedestal or by driving the model using a small electric motor buried in the top of the pedestal, thereby allowing the pedestal to remain stationary. The measurements were made for the bistatic angle (separation of the transmit and receive directions) $2\alpha = 44^{o}$ and 90^{o}, but since the dominant features of the scattering patterns were the same for the two angles, we shall present data only for $2\alpha = 44^{o}$. The polarizations transmitted were vertical, horizontal and right circular. In each instance the same polarization was received and, in the third case, the left circularly-polarized signal as well. We remark that because of the phase change on reflection at a metal surface, a right circularly-polarized receiver will discriminate against the specular reflection of a right circularly-polarized field incident on the surface. However, other types of scattering can produce a cross polarized return.

Wherever appropriate, the calibration of the measured patterns was with respect to the scattering from a sphere 14 in. in diameter, whose cross section at 16.04 GHz is 154 in.^{2}, i.e., -10.0 dB m^2. This level is shown as a small vertical line on each pattern. For convenience we shall express all cross sections relative to that of the sphere, writing (for example) -4.1 dB m^2 as 5.9 dB (sph).

4.1 Scattering Formulas

To better understand the patterns that follow, it is desirable to list the bistatic scattering formulas for some of the elementary shapes that make up the Darrieus and Giromill models. For the most part the formulas are based on the physical optics approximation which is applicable for angles not too far from the specular direction if all relevant dimensions of the scatterer are larger than the wavelength.

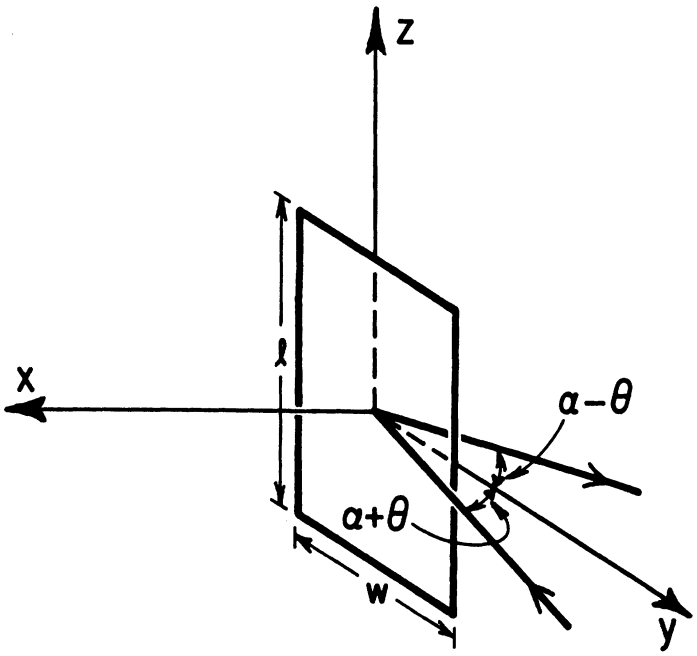

Fig. 4-1: Geometry for single planar strip

A thin metallic strip of length ℓ and width w lies in the plane $x = 0$ as shown in Fig. 4-1. A plane wave is incident in a direction making an angle $\alpha + \theta$ with the negative y axis, and the far zone scattered field is observed in the direction $\alpha - \theta$. The case $\theta = \pi/2$ therefore corresponds to specular scattering off the face of the strip for a bistatic angle 2α. For vertical and horizontal polarizations (electric vector parallel and perpendicular to the z axis) the bistatic scattering cross sections as functions of θ are, respectively,

$$\sigma_V(\theta) = \pi \left\{ \frac{2w\ell}{\lambda} \sin(\alpha+\theta) \frac{\sin X}{X} \right\}^2 \tag{4.1}$$

$$\sigma_H(\theta) = \pi \left\{ \frac{2w\ell}{\lambda} \sin(\alpha-\theta) \frac{\sin X}{X} \right\}^2 \tag{4.2}$$

where

$$X = \frac{2\pi w}{\lambda} \cos\alpha \cos\theta \ . \tag{4.3}$$

The formulas are valid for incidence and observation well away from edge-on, thereby excluding $\theta = \pm \alpha$. If $\theta = \pm \alpha$ the strip is invisible for horizontal polarization, i.e., $\sigma_H = 0$, and with vertical polarization the cross section is comparable to that of the leading edge of the strip, i.e.,

$$\sigma_V \simeq \frac{\ell^2}{4\pi} (\sec\alpha + \sec\theta)^2 \ . \tag{4.4}$$

If a second identical strip is placed a distance $d >> \lambda$ behind the first one in the plane $x = -d$, the cross section of the combination is

$$\sigma(\theta) = \sigma^{(1)}(\theta)\ 2\left\{1 + \cos\left(\frac{4\pi d}{\lambda} \cos\alpha \sin\theta\right)\right\} \tag{4.5}$$

where $\sigma^{(1)}(\theta)$ is the cross section of a single strip. The multiplicative factor varies from 0 to 4 corresponding to destructive and constructive

interference, and can produce a very rapid variation as a function of θ.

If a single strip is bent to form a blade of the Darrieus machine (see Fig. 4-2), the scattering cross section can be obtained by

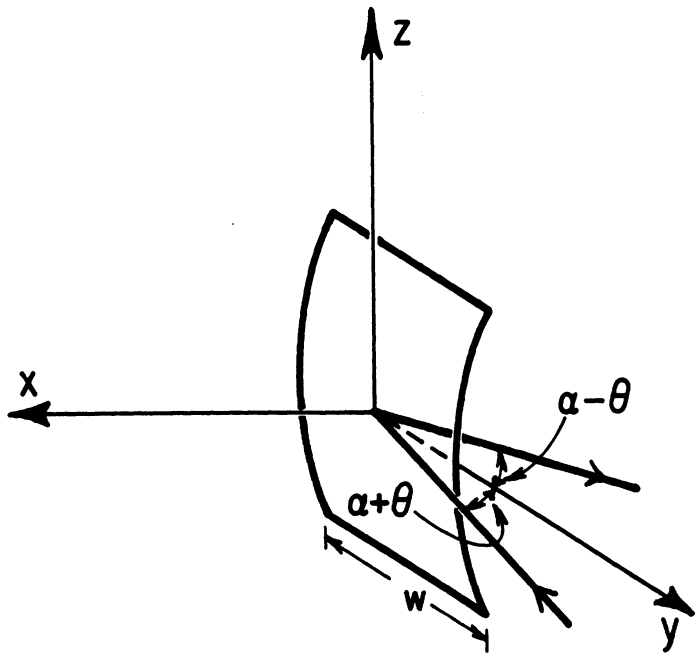

Fig. 4-2: Geometry for single curved strip

replacing the factor ℓ^2 in (4.1) and (4.2) by $\rho\lambda/2$, where ρ is the radius of curvature at the center of the strip. Thus,

$$\sigma(\theta) = \sigma^{(1)}(\theta)\,\frac{\rho\lambda}{2\ell^2} \tag{4.6}$$

valid for incidence not too far from normal to the face. Since this holds for θ negative as well as positive, it follows that if two strips are combined to form a Darrieus 'loop', the resulting cross section can be found by inserting (4.6) into (4.5) where d is now the separation of the mid points of the strips. Though the formula breaks down for incidence close to the normal to the loop, the cross section is then

$$\sigma_{V,H}(\theta) = \gamma A \cos^2(\alpha \pm \theta) \tag{4.7}$$

where A is the area spanned by the loop and $\gamma \simeq 0.6$, depending somewhat on the strip width.

Finally, for a cylindrical metal shaft of length ℓ and radius b with incidence and observation in a plane perpendicular to its axis, the cross section is independent of θ and, for $\alpha < 90^0$,

$$\sigma_{V,H} = \frac{2\pi b \ell^2}{\lambda} \quad . \tag{4.8}$$

4.2 Measured Data

We shall now examine the measured scattering patterns for the Darrieus and Giromill in the light of these formulas.

The first model considered was a crude replica of the Giromill consisting of a square of Styrofoam 15 in. along a side and 1 in. thick with conducting tape 1 in. wide applied around the edges (Fig. 4-3). The purpose of the Styrofoam was only to support the tape. The structure was placed

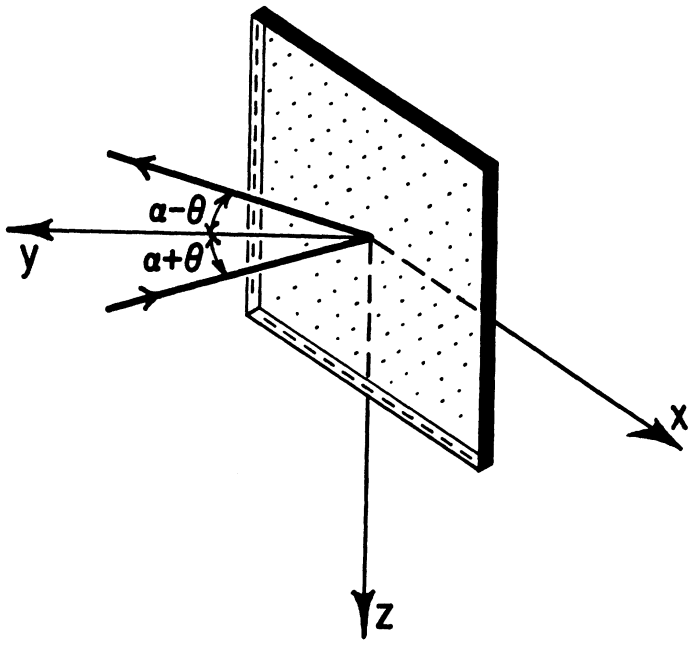

Fig. 4-3: Geometry of the first Giromill model

vertically on top of a pedestal, and data were recorded for $\alpha = 22^0$ and various polarizations as the pedestal was rotated.

The pattern for vertical polarization is shown in Fig. 4-4. According to the preceding formulas, the top and bottom strips should be invisible, and the scattering due entirely to the vertical strips, and perhaps the Styrofoam slab. The data support this and the envelope is almost identical to the pattern of a single strip raised 6 dB corresponding to in-phase addition of the scattering from two strips. Thus, for θ in the vicinity of 0^0 we have, from (4.4) with $\ell = 15$ in., $\alpha = 22^0$ and $\theta = 0^0$, $\sigma =$ 3.0 dB (sph) compared with the measured envelope value of about 2.5 dB (sph). The rapid oscillation is due to the interference between the strip returns, and this is also the source of the well-separated peaks in the vicinity of $\theta = \pm 90^0$ when the strips are being viewed near broadside. At $\theta = 90^0$ with $\ell = 15$ in., $w = 1$ in. and $\alpha = 22^0$, (4.1) gives $\alpha_V = 14.7$ dB (sph). From (4.5) with $d = 15$ in. we then have $\sigma\ (90^0) = 18.7$ dB (sph) compared with the measured value 12.6 dB (sph), but we remark that if d were actually 14.94 in. rather than 15 in. the agreement would be precise. Certainly neither the model nor its dimensions were accurate enough to distinguish between these two values; and using $d = 14.94$ in. the peaks adjacent to the one at $\theta = 90^0$ would occur at

$$\theta = \sin^{-1} \frac{74}{75.26} = 90^0 \pm 10.5^0 \quad ,$$

in full agreement with the measured locations.

The corresponding pattern for horizontal polarization is shown in Fig. 4-5. The main effect of the polarization change is the creation of the deep nulls near $\theta = \pm 22^0$ and this is, of course, due to the illumination of the vertical strips edge-on where they are invisible. For θ closer to 0^0 the vertical strips continue to be the main source of the scattering,

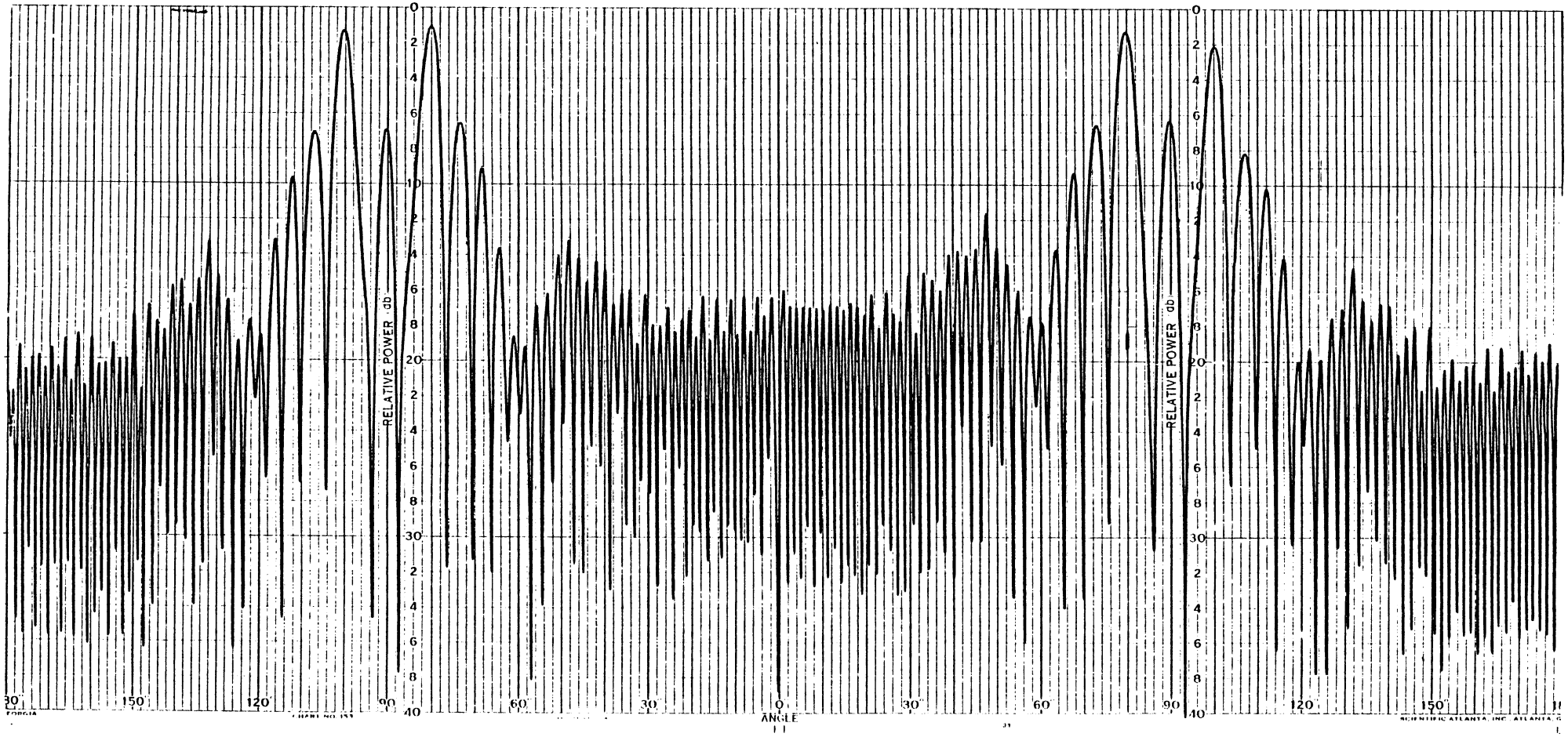

Fig. 4-4: Scattering cross section of a 1/40 scale model of the Giromill machine: vertical polarization.

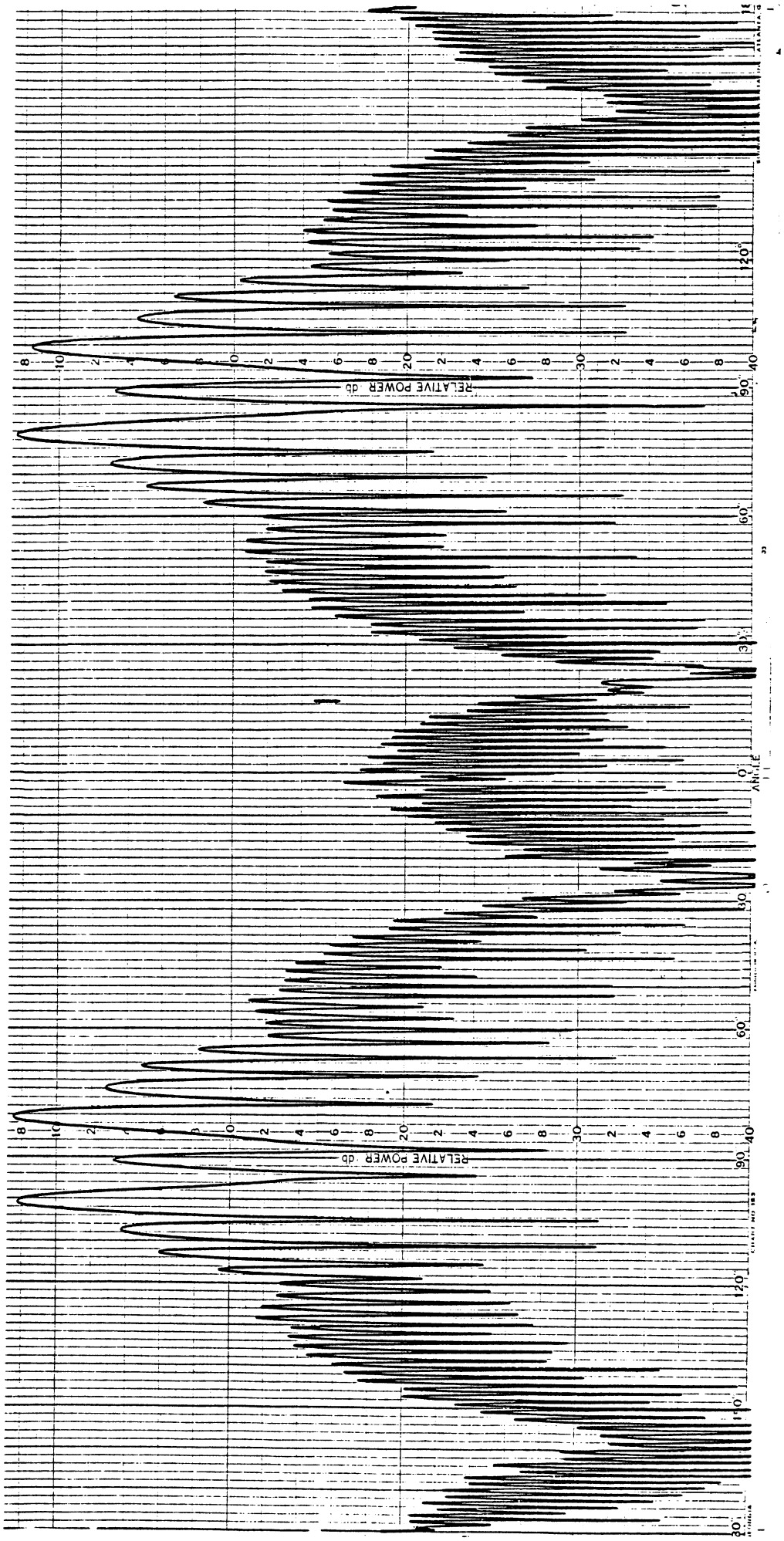

Fig. 4-5: Scattering cross section of a 1/40 scale model of the Giromill machine: horizontal polarization.

and though the two horizontal strips could dominate at $\theta = 0$ and produce a cross section of about 2 dB (sph), the lobe is only a degree or two in width and very sensitive to the precise alignment of the loop.

To confirm the dominant role of the vertical strips, measurements were also made with the horizontal strips removed: the patterns were virtually indistinguishable from those with all four strips present. We then replaced the horizontal strips and removed the vertical. With both polarizations, the scattering dropped to 13 dB or more below the sphere apart from a narrow peak of width $\sim 3^0$ and height -2.9 dB (sph) for horizontal polarization and 1.6 dB (sph) for vertical at $\theta = 0$. The fact that the return was larger with vertical polarization (for which the strips are invisible edge-on) can be attributed to the presence of the Styrofoam. Because the relative permittivity of the Styrofoam is only 1.035, the power reflection coefficient is -41.3 dB, and the specular return from the front face of the slab is therefore -3.1 dB (sph). When the rear face is taken into account as well, the cross section could be almost zero or as high as 2.9 dB (sph), and since the scattering is confined to the same narrow angular range as that from the strips, it is evident that the two could interfere to produce the cross sections that were measured.

A central vertical drive shaft was now added to the original Giromill model. The shaft was, in effect, a metal rod 0.25 in. in radius and approximately 15 in. long, and the entire structure was mounted on a small electric motor recessed into the support pedestal. From (4.7) with b = 0.25 in. and ℓ = 15 in. the cross section of the shaft is 4.9 dB (sph), and the expectation was that the presence of the shaft would serve to fill in the nulls at $\theta = \pm 22^0$ in the pattern of the stucture for vertical polarization, and raise the other lower portions of the patterns by about 2 dB for both

polarizations. This is what was found. We also repeated the measurements with the shaft replaced by single or double center strips 1 in. in width. The main effect was to increase the cross section for θ near zero, corresponding to the larger scattering from a strip at broadside compared with that of the shaft.

It would therefore appear that the dominant scattering from a Giromill machine occurs at angles close to the direction of specular scattering from the vertical strips, and can be adequately approximated by

$$\sigma(\theta) = \pi\left\{\frac{4w\ell}{\lambda}\sin\alpha\ \mathrm{sinc}\left(\frac{2w}{\lambda}\cos\alpha\cos\theta\right)\right\}^2\cos^2\left(\frac{2\pi d}{\lambda}\cos\alpha\sin\theta\right) \tag{4.9}$$

where

$$\mathrm{sinc}\ X = \frac{\sin\pi X}{\pi X} \tag{4.10}$$

and the dimensions and angles are as before. The last factor on the right hand side of (4.9) is the one responsible for the lobing structure and can be replaced by unity in any computation of the envelope alone.

The model of the Darrieus is shown in Fig. 4-6 and here again a piece of Styrofoam 1 in. thick was used to hold the various parts in position. The slab was 15 in. by 15 in. in its maximum dimensions. A central shaft 0.25 in. in radius was embedded in the slab, protruding slightly at the top and bottom, and this was attached to a small electric motor recessed into the top of the support pedestal. The visible length of shaft was about 16 in. To simulate the cross braces, metallic strips 1 in. wide inclined at 22 1/2^{o} to the horizontal were inserted through the Styrofoam. Including the necessary breaks where they met the central shaft, the overall

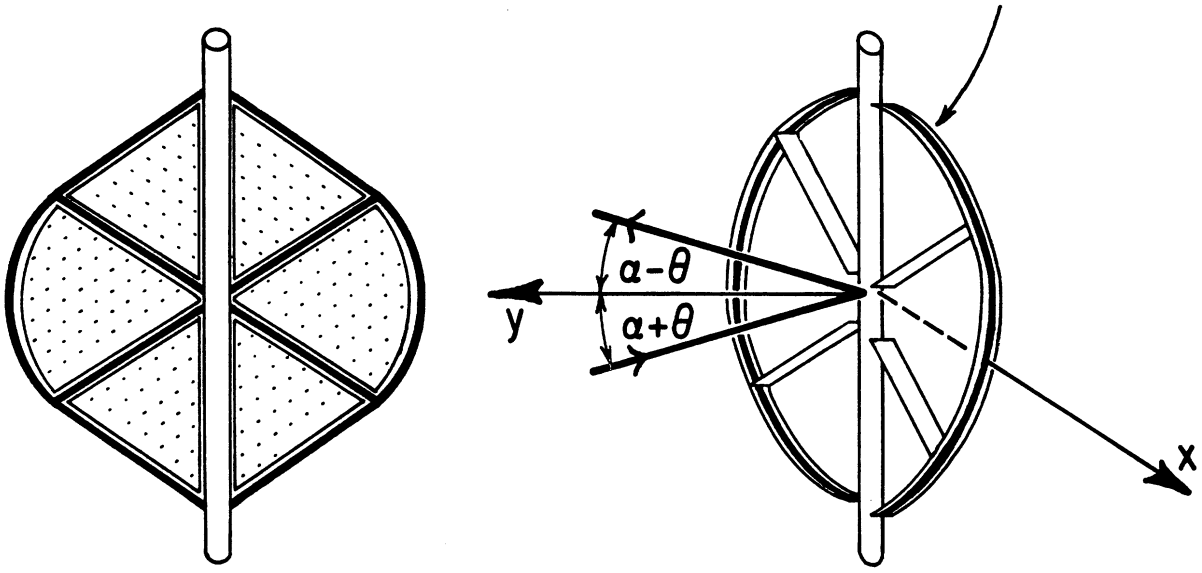

Fig. 4-6: Geometry of the Darrieus model.

length of these strips was 14.5 in. Finally, to complete the model, 0.5 in. wide strips of metallic tape were attached to the outer edges of the Styrofoam.

The scattering patterns for vertical and horizontal polarizations are shown in Figs. 4-7 and 4-8 respectively, and are much more complicated than for the Giromill machine. They are also less regular and symmetric and some of the asymmetry is undoubtedly due to the difficulty of maintaining the axis of rotation vertical throughout the measurements. However, for both polarizations the key feature is that the maximum scattering occurs near broadside to the loop, i.e., $\theta = 0$, where the cross section has a $\text{sinc}^2 X$ behavior riding on a uniform background. At $\theta = 0$ the cross sections are, respectively, 7.7 and 9.0 dB (sph) for vertical and horizontal polarizations. As $|\theta|$ increases the lobe widths increase and the cross sections decrease,

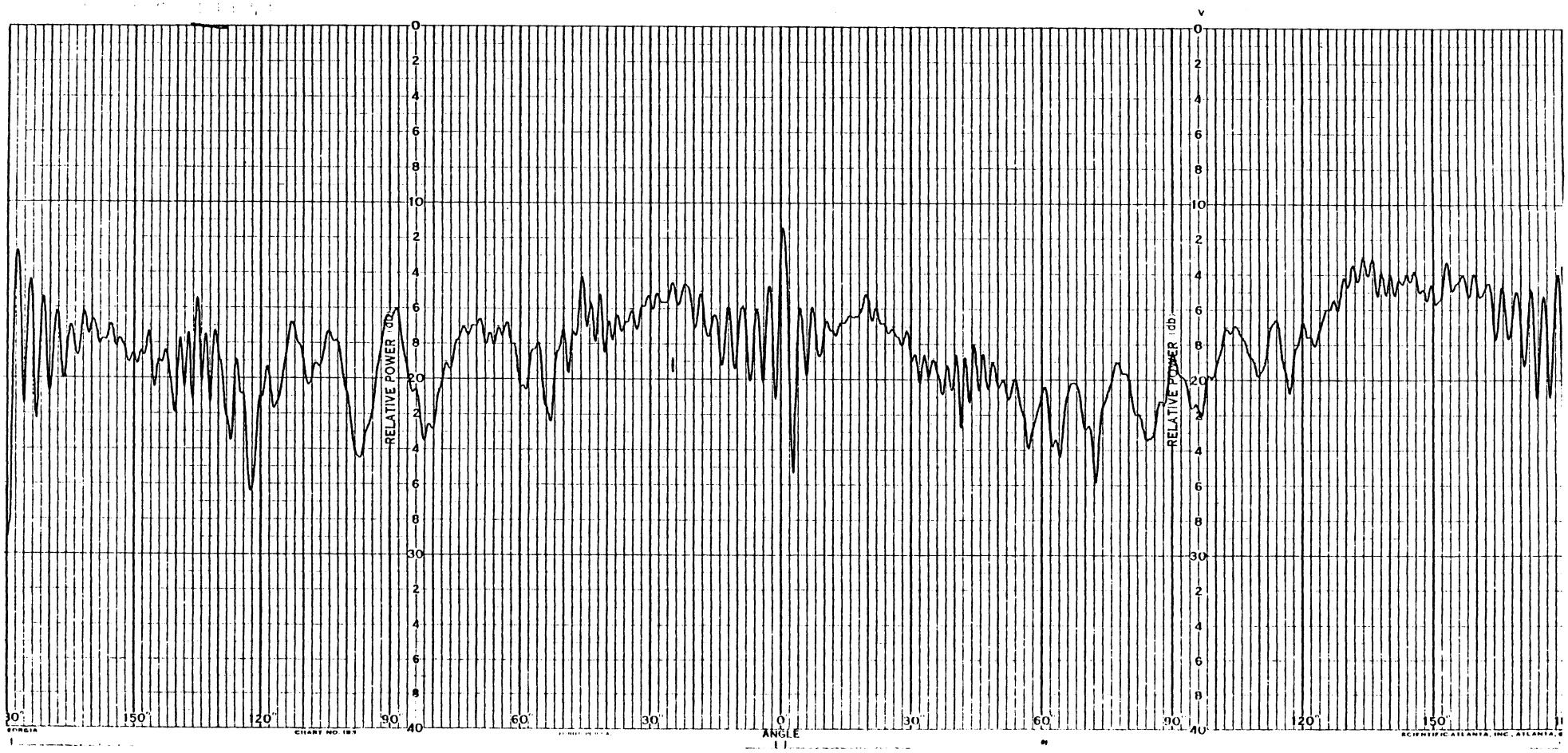

Fig. 4-7: Scattering cross section of a 1/40 scale model of the Darrieus machine: vertical polarization.

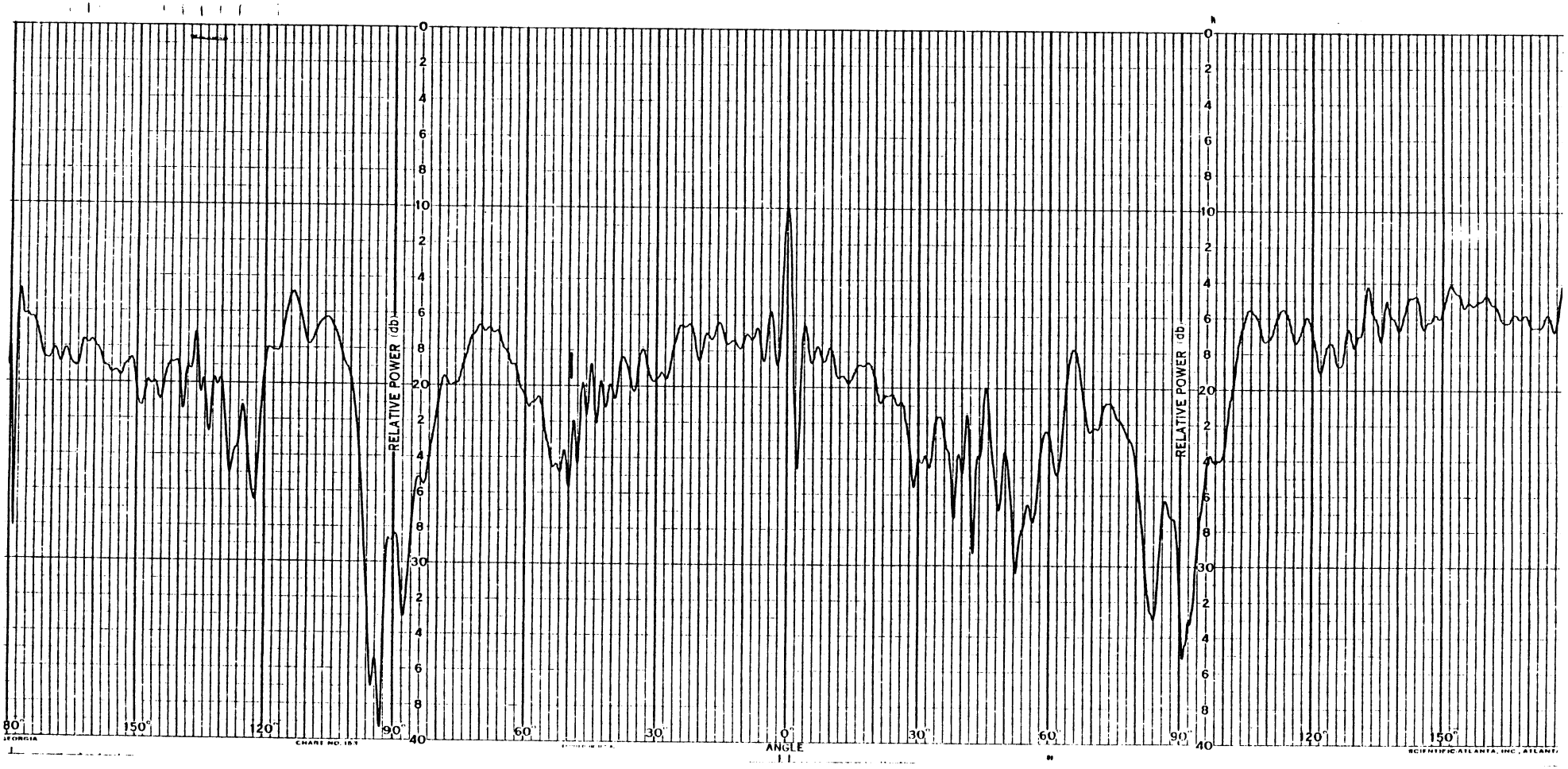

Fig. 4-8: Scattering cross section of a 1/40 scale model of the Darrieus machine: horizontal polarization.

with the decrease being particularly noticeable for horizontal polarization. With the exception of the peaks near $\theta = 0$, the cross sections average about 3 dB (sph) and 1 dB (sph) for vertical and horizontal polarizations respectively.

In seeking to provide an explanation for the behavior we first remark that the Styrofoam 'slab' is almost certainly not a significant contributor. Its scattering is concentrated in the vicinity of $\theta = 0$ and since the area of the slab is less than 60 percent of that used in the Giromill model, its contribution is about 5 dB less. The contribution from the curved outer strips is also negligible, being less than -10 dB (sph), but the central shaft now has a dominant role. Indeed, from (4.8) with b = 0.25 in. and ℓ = 16 in., we obtain $\sigma_{V,H} = 5.5$ dB (sph), and it would seem logical that this should be the average cross section as a function of angle. Nevertheless, the cross braces do have an effect. As $|\theta|$ approaches 90^0 the braces provide progressively more shadowing of the vertical shaft whilst contributing little themselves, and this is almost certainly the major source of the reduced scattering at these angles.. Moreover, at $\theta = 0$ the strips are being viewed edge-on. From (4.4) the in-phase contributions of two such strips inclined at angles $\pm \beta$ to the horizontal are

$$\sigma_V(0) = \frac{1}{\pi}\{\ell_1 \sin\beta\,(\sec\alpha + 1)\}^2$$
$$\sigma_H(0) = \frac{1}{\pi}\left\{\ell_1 \cos\beta\,(\sec\alpha + 1)\right\}^2 , \qquad (4.11)$$

and with ℓ_1 = 14.5 in., $\beta = 22\ 1/2^0$ and $\alpha = 22^0$, $\sigma_V = -5.6$ dB (sph) and $\sigma_H = 2.0$ dB (sph). Constructive interference with the shaft return now gives 8.0 and 10.2 dB (sph) for vertical and horizontal polarizations

respectively, in good agreement with the measured values, and the rapid decrease with increasing $|\theta|$ is then due to the common sinc^2 behavior of the scattering from each strip.

It would thus appear that the dominant scattering from a Darrieus machine occurs at angles close to the direction of specular scattering from the plane of the loop, i.e., θ near zero, and can be attributed to an interference between the scattering from the vertical shaft and the two cross braces. The appropriate formulas are

$$\sigma_V(\theta) = \frac{2\pi b \ell^2}{\lambda} \left[1 + \frac{\lambda}{2b} \left\{ \frac{\ell_1}{\pi \ell} \sin \beta \, (\sec \alpha + \sec \theta) \, \text{sinc } Y \right\} \right]^2$$

$$\sigma_H(\theta) = \frac{2\pi b \ell^2}{\lambda} \left[1 + \frac{\lambda}{2b} \left\{ \frac{\ell_1}{\pi \ell} \sin \beta \, (\sec \alpha + \sec \theta) \, \text{sinc } Y \right\} \right]^2 \qquad (4.12)$$

where

$$Y = \frac{2\pi \ell}{\lambda} \cos \alpha \cos \beta \sin \theta \, , \qquad (4.13)$$

ℓ and ℓ_1 are the lengths of the shaft and braces respectively, and the other symbols are as defined previously.

4.3 Remarks

In addition to the measurements using vertical and horizontal polarizations, data were also obtained for both models using a right circularly polarized transmitting antenna and left and right circularly polarized receiving antennas. With the left circularly polarized receiver (direct polarization) the gross features of the scattering patterns were the same as for the linear polarizations, but when the receiver was cross polarized the previously-dominant features of the patterns were suppressed and the scattering at other angles reduced by 5 or more dB. It is therefore evident that the

use of circular polarization with the receiver matched to the primary signal would provide substantial discrimination against the scattering and, hence, interference, produced by a Giromill or Darrieus as well as a horizontal axis machine.

To appreciate the significance of the cross sections that were measured with a linear polarization, it may be helpful to compare the scattering from the Giromill and Darrieus models with that from a 1/40 scale model of a horizontal axis machine. From prior measurements [2] of the scattering from a MOD-0 windmill each of whose blades has an effective scattering area of 12 m^2, the cross section of a 1/40 scale blade at 16.04 GHz would have a peak value

$$\sigma = \frac{4\pi}{\lambda^2}\left(\frac{12}{40\text{x}40}\right)^2 \ m^2$$

implying σ = 13.1 dB (sph). This is about 5 dB greater than for the Darrieus, and 5 dB less than for the Giromill. Nevertheless, it is the modulation waveform which determines the interference, and this is affected by the (static) lobe width and the rotation frequency of the scatterer in addition to the cross section. With the MOD-0 blade the specular lobe width measured at (say) the -10 dB level is as narrow as 3^o but could be an order of magnitude larger than this if the blade were far from the horizontal when the specular lobe was picked up by the receiver. By comparison the lobe width for the Giromill is larger by at least a factor 2 and that for the Darrieus is smaller, but since the rotation frequency of these machines is greater than for a horizontal axis one, it is not evident how the modulation waveform will be affected. It is therefore desirable to measure the waveform and the resulting interference directly, and a set-up that has been developed for this purpose is described in Chapter 5.

CHAPTER 5

TV INTERFERENCE STUDIES

Our previous experimental studies of windmill interference to TV reception [1,2,14] were carried out in two stages: on-site measurement with the operational MOD-0 windmill at Plum Brook and laboratory simulation measurements. In both cases commercially available local TV signals were used as the source of the desired signals. To eliminate the dependence on outside signal sources, and the need for laboratory measurements to quantify the observed interference effects, we have developed a microwave test system of TV signal transmission and reception in the presence of small scale models of windmills. The system enables us to observe and quantify the interference effects produced by a variety of windmills under controlled conditions.

The present chapter describes the laboratory microwave TV system developed, and gives some representative TV interference results obtained using it. Since the system is still undergoing improvement, the results should not be regarded as conclusive. Most of the results are for the Giromill and the Darrieus, typical of vertical axis machines [15,16], but some data are presented for a small scale model of the MOD-0 windmill. The purpose of the latter is to demonstrate that the laboratory microwave TV system does yield results confirming those obtained during on-site measurement with the full scale horizontal axis machine using commercial TV signals.

5.1 Scale Model Windmills

The Giromill and Darrieus are vertical axis machines [15], the former having been developed by the University of Virginia, and the latter by Sandia Laboratories. One-tenth scale models of both machines were built in our laboratory.

The Giromill was constructed from the engineering sketch in Fig. 5-1. The model was essentially a vertically oriented square loop 5 ft. along a side with a central metallic rod simulating the machine axis. The vertical and horizontal sides of the loop consisted of aluminum strips 6 and 2 in. wide respectively, and the whole structure was supported using wires and metallic rods as shown in Fig. 5-2. Fig. 5-3 is a portion of the engineering sketch from which the 1/10 scale model of the Darrieus machine was fabricated. The key elements are the curved blades, the machine axis, and the cross supports (see inset to Fig. 5-3), and the model was 5 ft. tall and 5 ft. wide at its broadest dimension. The blades and cross supports were made of 2 in. wide aluminum strips and the axis was a 2.35 in. diameter aluminum rod 6 ft. high. Fig. 5-4 shows a photograph of the model.

A common motor drive mechanism was constructed to accomodate each model and this was capable of providing a turbine rotation speed up to 130 rpm. During operation rope guys were used to anchor the models to the ground.

For comparison purposes we also built and tested a crude model of a MOD-0 horizontal axis machine. The blades were the ones used in our previous study [2]. Each was a 1/37.5 scale version of a MOD-0 blade 18.7 in. long, and was cut from a block of wood. To facilitate construction, the blades were made with linear variations of thickness and twist from root to tip, and were finally coated with conducting silver paint. They were then attached to the shaft of a small DC motor mounted on a lucite column 7 ft. in height to allow the two blades to be rotated together in a vertical plane at speeds up to 40 rpm. The entire model is shown in Fig. 5-5.

5.2 Laboratory Microwave TV System

The small scale models of the windmills described in the previous section can be used for a meaningful study of TV interference phenomenon,

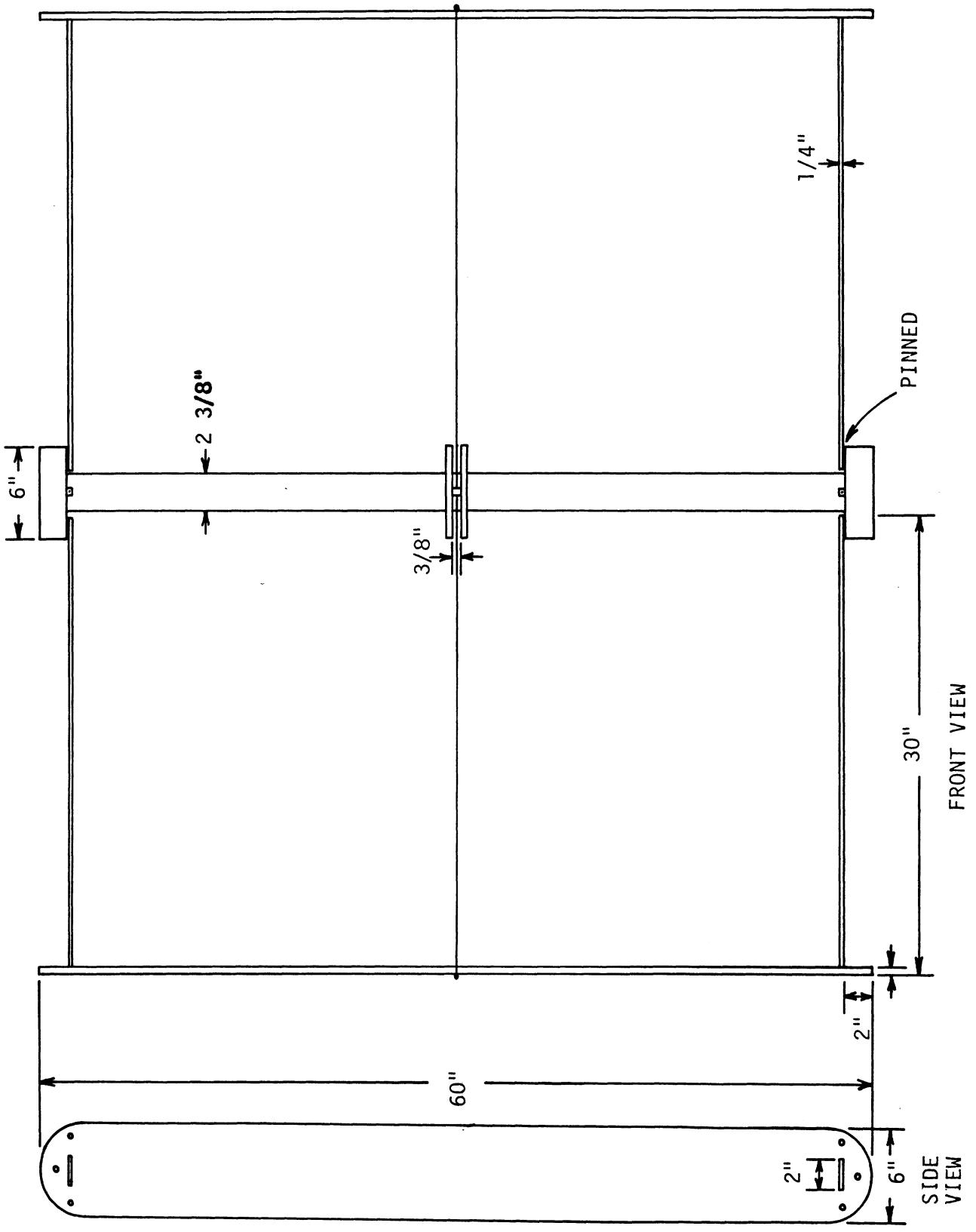

Fig. 5-1: Engineering sketch of a 1/10 scale model of the Giromill.

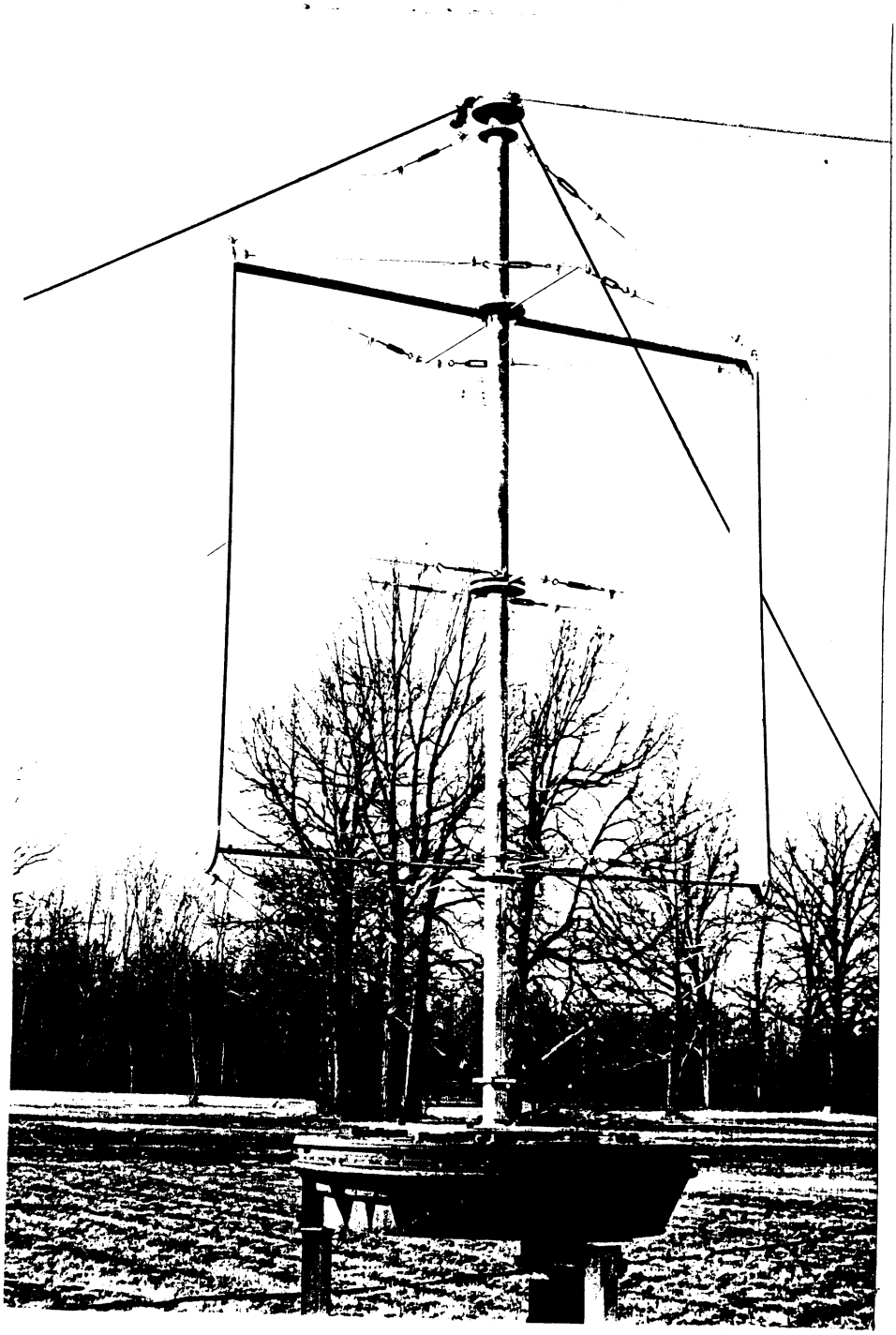

Fig. 5-2: Photograph of the 1/10 scale model of the Giromill.

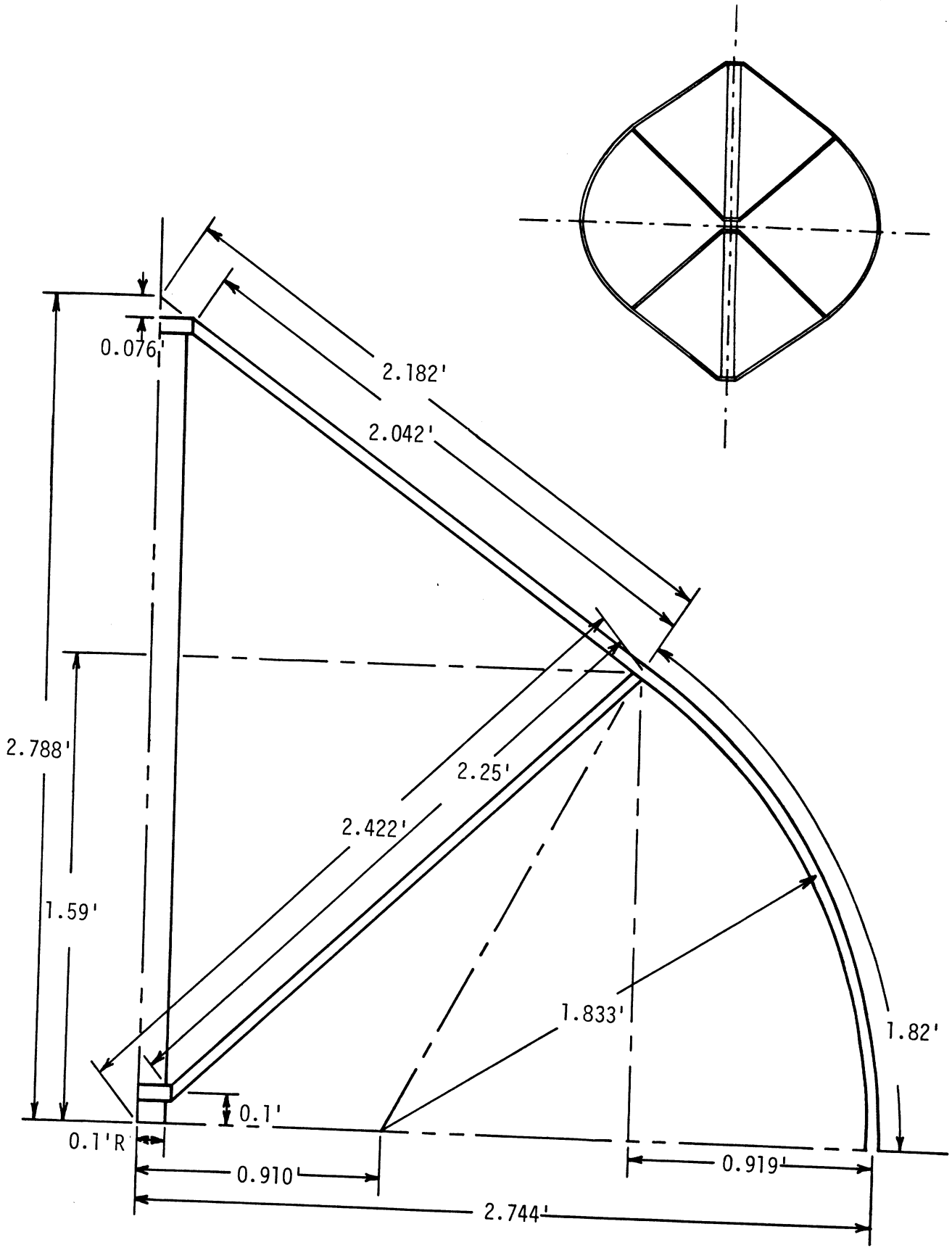

Fig. 5-3: Portion of the engineering sketch of a 1/10 scale model of the Darrieus.

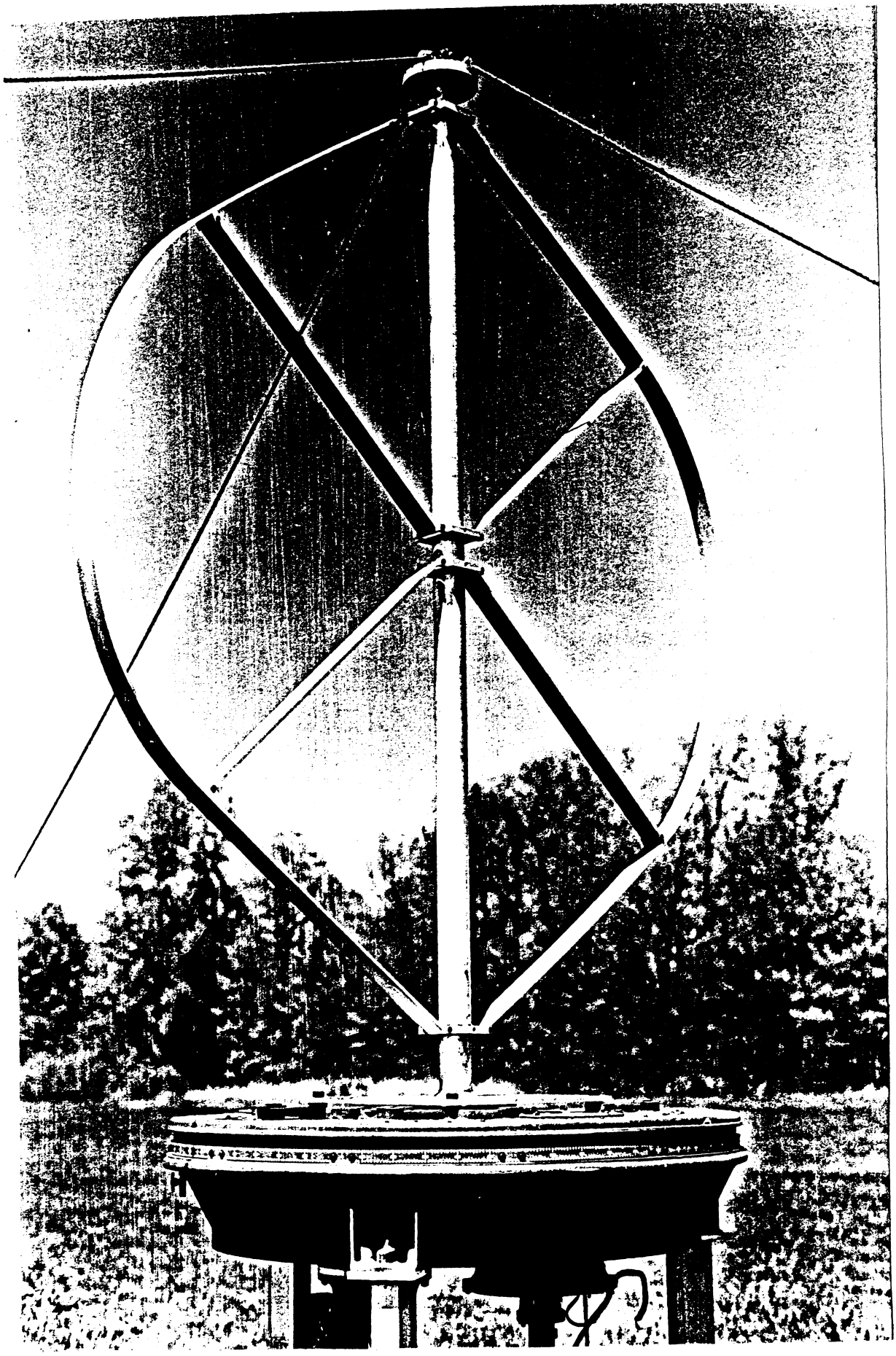

Fig. 5-4: Photograph of the 1/10 scale model Darrieus.

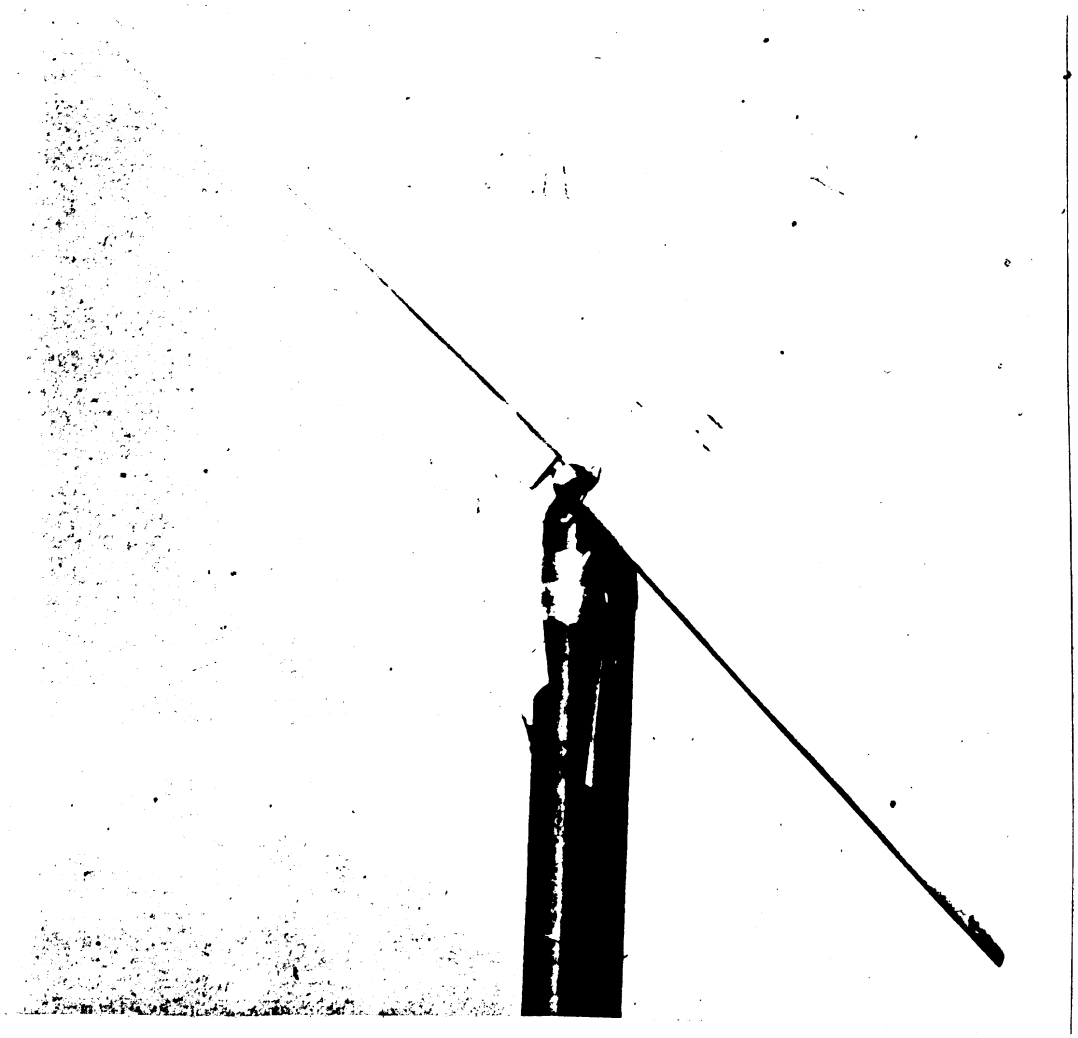

Fig. 5-5: Photograph of the 1/37.5 scale model of the MOD-0 windmill blades.

provided the signal frequencies of interest are sufficiently high. For example, with a 1/10 scale model windmill the signal frequency should be 10 times greater than the frequency of the commercial TV channel for which the interference effects are desired. TV channel frequencies lie within the range 50 - 900 MHz, and TV receivers are designed to accept these frequencies only. The use of the above scale model windmills in the present study therefore necessitated proper processing of the normal TV signal, up-converting its frequency to the microwave range before transmission, and down-converting the frequency of the received signal to a frequency acceptable to the TV test receiver. The present section describes the laboratory system assembled to accomplish these tasks.

A block diagram of the microwave TV transmitting and receiving system is shown in Fig. 5-6. The signal generator section (within the dotted box in Fig. 5-6) consisting of three main components provides a 83.25 MHz signal output which is compatible with the conventional on-the-air TV signal at Channel 6. The color-bar generator was assembled at the laboratory using a commercially-available chip. The circuit diagram of the color-bar generator is shown in Fig. 5-7, and provides the basic video base-band signals (0 - 5 MHz) with the desired test pattern encoded. The test pattern can be any one of the sixteen different patterns shown in Fig. 5-8, which are selected with the help of four two-position switches (the positions of the switches are indicated by numbers under each sketch of Fig. 5-8) on the color-bar generator. During our test we used the switch position 1000 (Fig. 5-8) which provided a gated rainbow test pattern consisting of ten vertical colored bars.

The video signal from the color-bar generator via the inverting amplifier modulates a 83.25 MHz carrier generated by a crystal oscillator located within

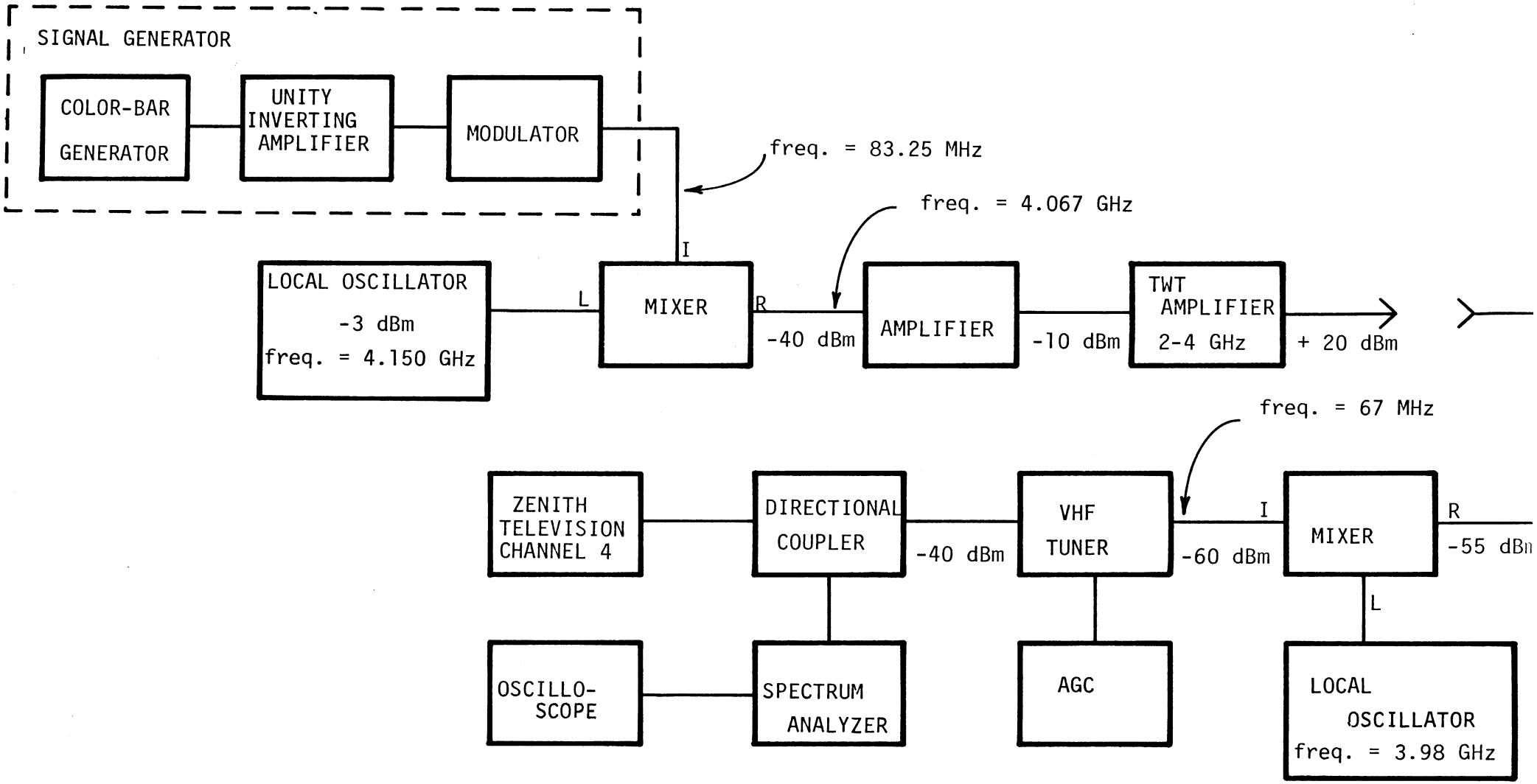

Fig. 5-6: Block diagram of the equipment for the microwave TV System.

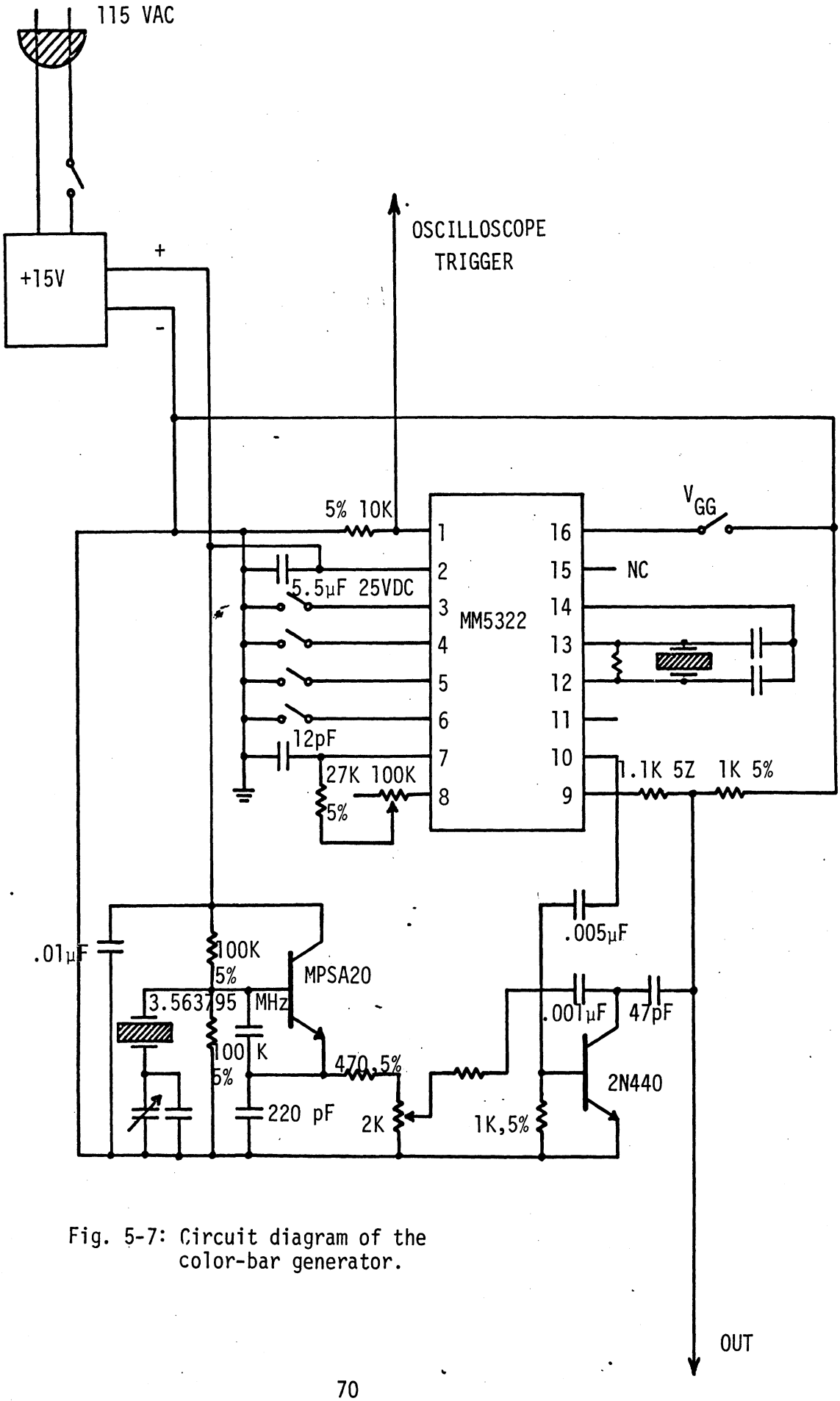

Fig. 5-7: Circuit diagram of the color-bar generator.

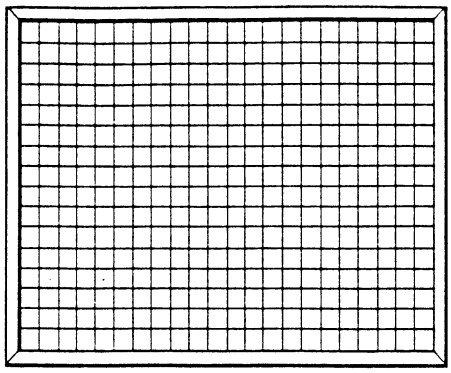

15 x 21 Cross Hatch
0010

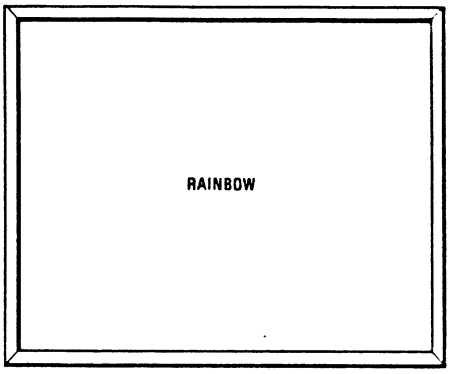

Ungated Rainbow
1111

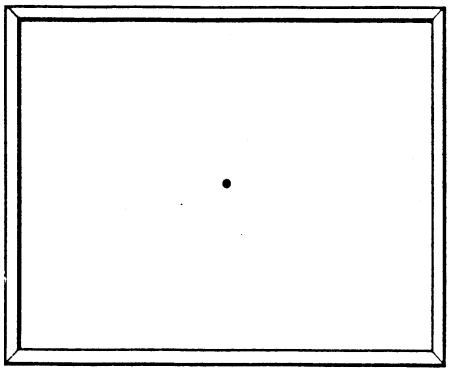

Single Dot
0111

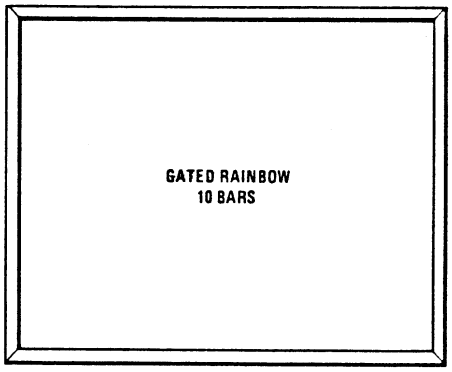

Gated Rainbow
1000

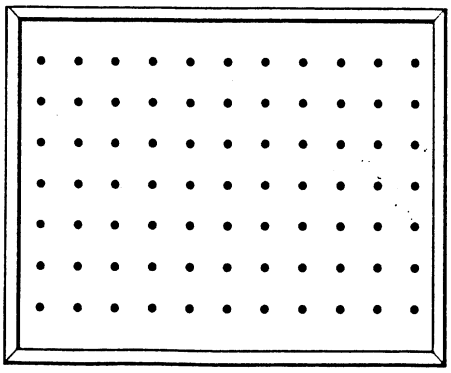

Dots 7 x 11
0110

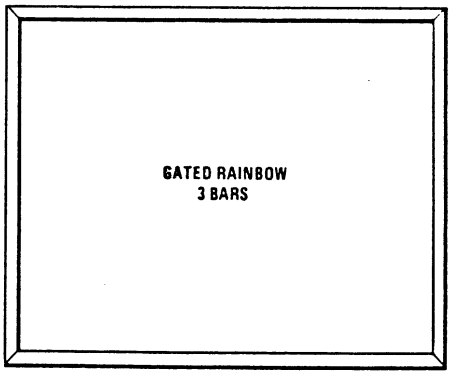

Gated Rainbow
0011

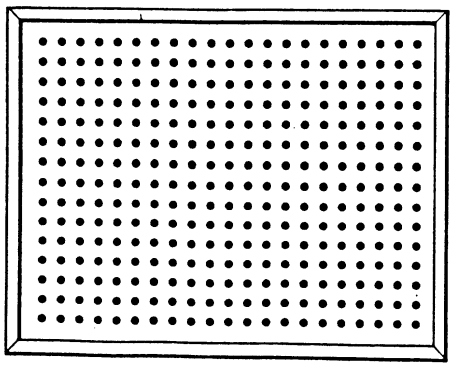

Dots 15 x 21
0100

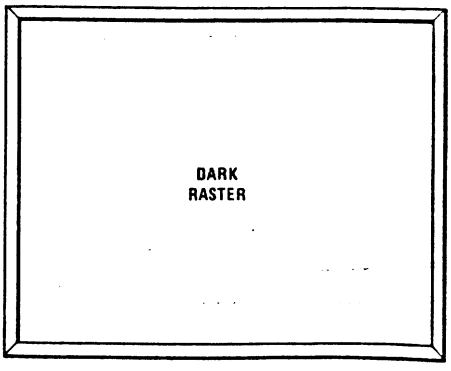

Note: Pattern switch codes are BCD 1248 positive logic.

Purity
0101

Fig. 5-8: Various video test patterns.

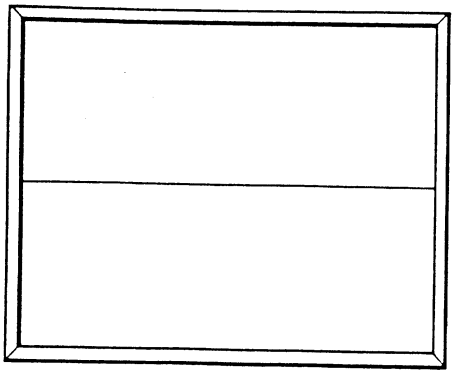

Single Horizontal Line
1100

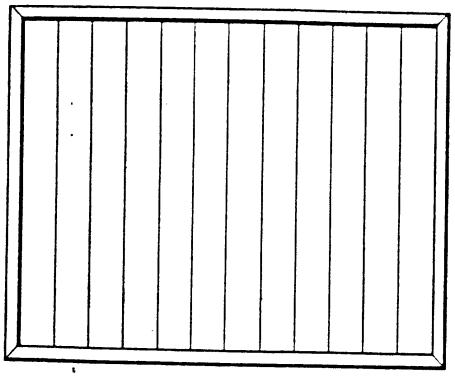

11 Vertical Lines
1110

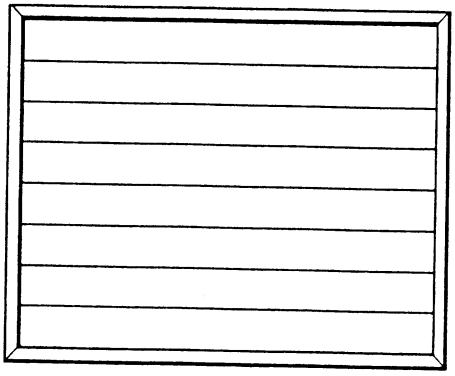

7 Horizontal Lines
1101

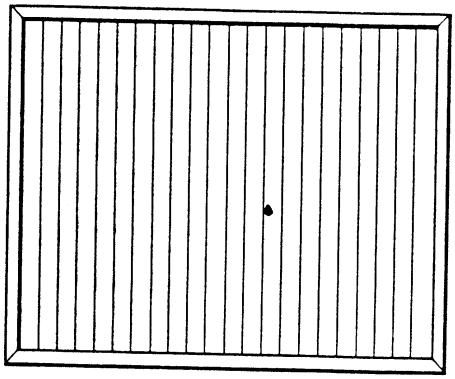

21 Vertical Lines
0001

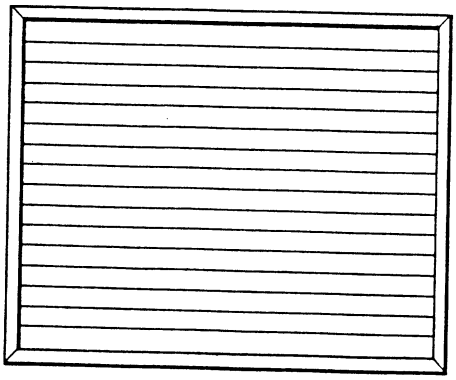

15 Horizontal Lines
0000

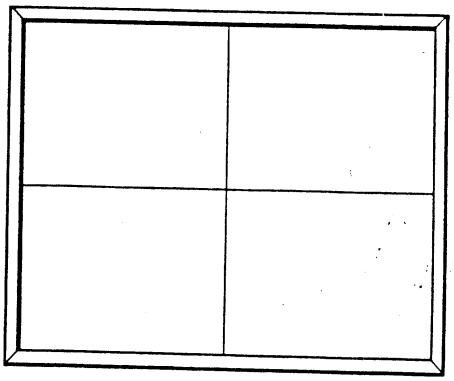

Single Crosshair
1011

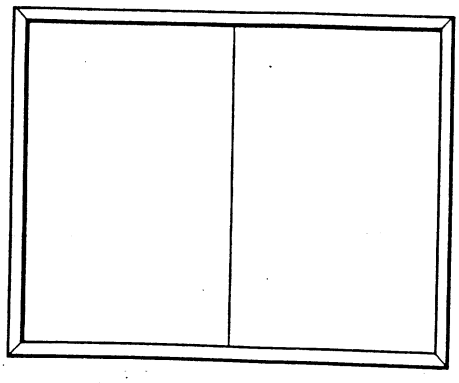

Single Vertical Line
1001

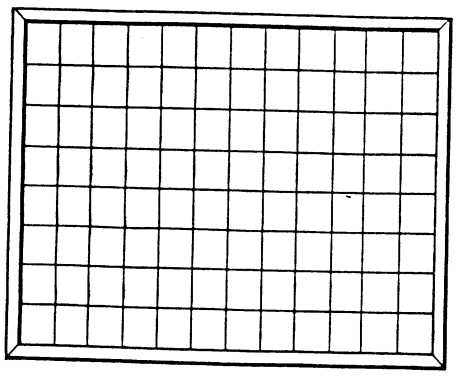

7 x 11 Cross Hatch
1010

Fig. 5-8: (continued).

the modulator whose circuit diagram is shown in Fig. 5-9. The unity gain inverting amplifier between the color-bar generator and the modulator (Fig. 5-6) is an operational amplifier which is required to provide the modulating signal with a polarity acceptable to the modulator. The signal generator is capable of supplying a signal carrying both video and audio information, although we have not used the latter capability during the present study. If a video signal different from that provided by the color-bar generator is desired, it can be achieved by replacing the color-bar generator with the desired video signal source. In fact, the signal generator described here provides a degree of flexibility not usually found in off-the-shelf color-bar generators.

The frequency of the signal output from the signal generator is now up-converted with the help of a mixer. As shown in Fig. 5-6, the local oscillator frequency being 4.15 GHz, the frequency of the mixer output signal is 4.07 GHz. With the variable frequency local oscillator used, the present mixer is capable of providing an output signal having a frequency anywhere in the range 2.5 - 5.0 GHz.

Following the mixer on the transmit side (Fig. 5-6) is a solid state amplifier providing a gain of 30 dB at 4.4 GHz. The amplifier can operate over a range of frequencies from 4 to 8 GHz. Cascaded with this amplifier is a TWT amplifier providing a nominal gain of 30 dB at 4 GHz. The operating frequency of the TWT amplifier lies in the range 4 - 8 GHz. With the help of a 165 ft. long coaxial cable, the output signal from the TWT amplifier is carried outside to a horizontally polarized rectangular horn which radiates the signal in the presence of a suitably located scale model windmill. The radiating horn has a gain of 18 dB with respect to an isotropic antenna.

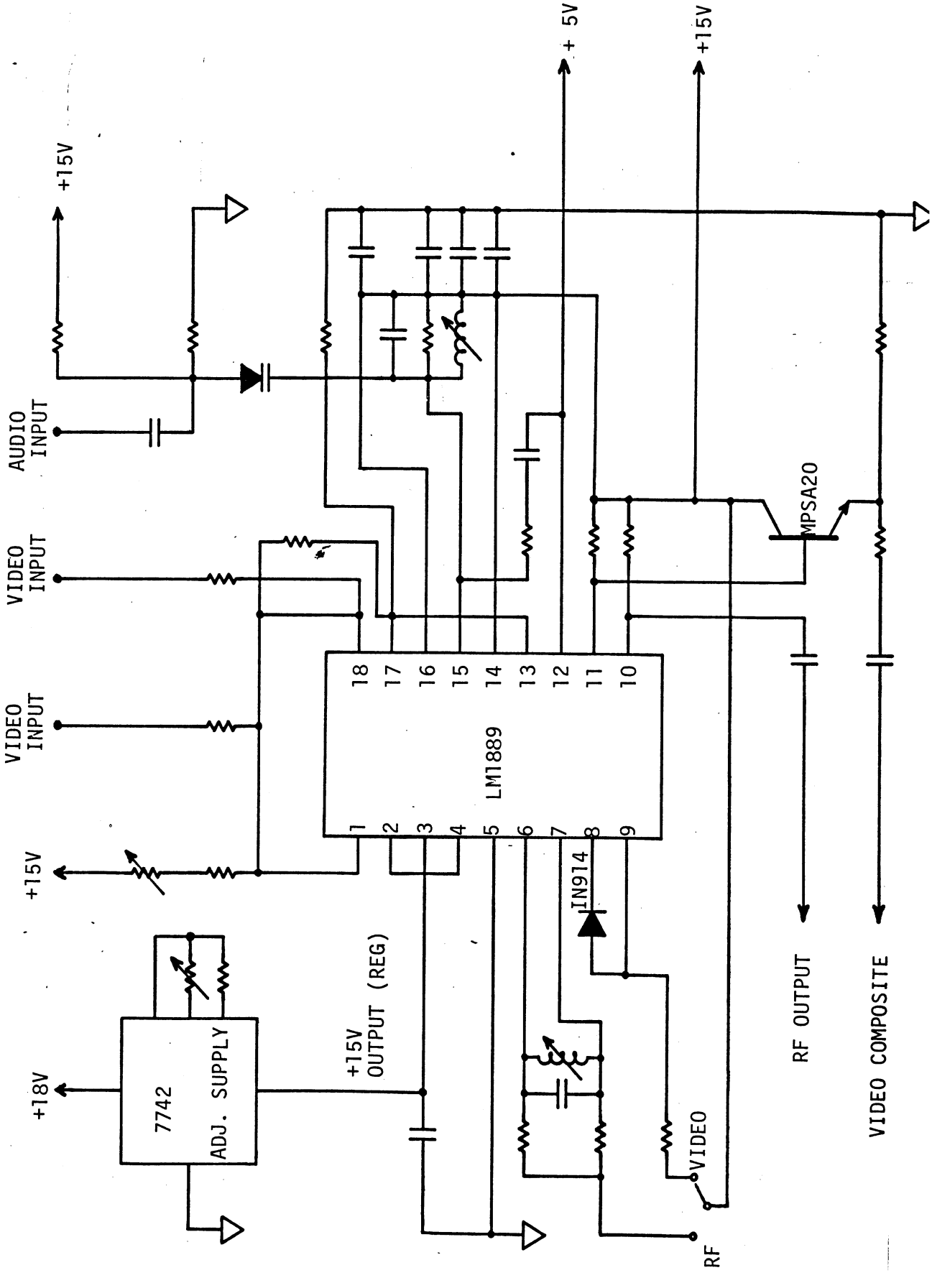

Fig. 5-9: Circuit diagram of the modulator section.

An identical rectangular horn is used to receive the radiated signal which is carried inside through a 200 ft. long coaxial cable (identical to that used on the transmit side), and fed to the mixer on the receive side as shown in Fig. 5-6. The receiving side mixer is identical to that on the transmit side, and down-converts the frequency of the received signal to 67 MHz, i.e., the TV Channel 4 frequency). It is important to observe that the two mixers, although identical, use two separate local oscillators. This is done to eliminate any direct coupling of signals between the transmitter and the receiver which would otherwise reduce the overall system sensitivity to interference produced by the windmill. The mixer output is now fed to a video tuner-amplifier and filter having 10 dB gain over a 6 MHz band (nominally, 1.25 and 5 MHz below and above the video carrier respectively). This amplifying and filtering action is available for each TV channel of interest. The output from the video tuner-amplifier is fed to the TV test receiver (Zenith model 17 GC 45) where it is now examined for interference effects produced by the scale model windmill. As shown in Fig. 5-6, a portion of the signal going to the TV test receiver is sampled with the help of a directional coupler and fed to a spectrum analyzer. The vertical output of the spectrum analyzer, containing the desired video signal along with any modulation introduced by the rotating windmill is fed to an oscilloscope which reproduces on its screen the combined direct and scattered video signals, which can be photographed if desired. In addition to the above signal, the oscilloscope also reproduces a timing signal derived from the synchro-motor (not shown in Fig. 5-6) driving the windmill so that the total received signal can be correlated with the windmill rotation. With a 1/10 scale model windmill, the system reproduces the interference appropriate to the corresponding full scale windmill at a TV frequency close to that of Channel 14.

The main components used in the entire system and their nominal performance characteristics are given in Table 5-1. The extra set of mixers (mixer set #2), shown in Table 5-1 and having RF operating frequencies in the range 1 - 750 MHz would, in conjunction with appropriate local oscillators, enable the system to provide interference results appropriate for VHF TV reception (i.e., at channels lower than 14) in the presence of the same 1/10 scale model windmill. The possibility of obtaining results for higher UHF TV channels will be discussed later.

5.3 Initial Testing of the System: Inside the Laboratory

The microwave TV system described above was initially tested inside the Field Laboratory for optimum performance. During this test, the two rectangular horns and their associated feeding cables were eliminated, and the output signal from the TWT amplifier on the transmit side in Fig. 5-6 was attenuated 75 dB and fed to the appropriate terminals of the mixer on the receiving side. This attentuation in the signal level was used to simulate the transmission loss when transmission and reception take place outdoors.

The signal levels measured at various stages of the system are shown in Fig. 5-6. It is recommended that these signal levels be maintained for best performance of the system outdoors. The system performance was optimized by adjusting the signal generator section to give the best possible color-bar test pattern on the TV test receiver screen. As mentioned earlier, during all interference measurements we used the same color-bar test pattern, i.e., switch at position 1000.

The insertion loss of the modulator section on the transmit side was found to be 7 dB. For satisfactory performance, the signal level at the output of the local oscillator associated with the mixer on the transmit side was

EQUIPMENT TYPE	FREQUENCY RANGE	GAIN
Color-Bar Generator	Video Signal	--
Video Modulator	83.25 MHz (Channel 6)	--
Inverting Operational Amplifier	0-10 MHz	Unity
Video Amplifier and Filter	VHF Frequencies	10 dB
Mixer (2 Available)	#2 1-750 MHz	-7 dB
Mixer (2 available)	#1 0.5 - 5 GHz	-6.5 dB
Solid State Amplifier	4-8 GHz	20 dB
TWT Amplifiers	4-8 GHz	30 dB (1 watt max. amp.)
Horn Antennas (2)	4 GHz	18 dB with respect to isotropic
Television Receivers (2)	Zenith	--
Variable Freq. Oscillators (2)	2-4 GHz	--

Table 5-1: Available test equipment.

maintained at -3 dBm, although the manufacturer's recommended value is 9 dBm. The discrepancy may be due to some malfunction in the mixer itself.

5.4 Initial Testing of the System: Outside the Laboratory

During this test as well as the actual TV interference studies to be discussed later, the main components of the system except the transmitting and receiving horns were located inside a Field Laboratory. A typical arrangement of the two antennas and the scale model windmill with respect to the Field Laboratory is shown in Fig. 5-10. The 165 and 200 ft. coaxial cables feeding the transmitting and receiving horns attenuated the signal 10 and 12 dB, respectively. The carrier frequency of 4.07 GHz was the maximum frequency of operation for the cables. The 450-feet distance between the two horn antennas in Fig. 5-10 introduced about 88 dB attenuation in the received signal in the absence of the windmill.

The two horizontally polarized horn antennas were identical, each having a gain of 18 dB above an isotropic antenna and mounted 7 ft. above ground. The receiving patterns of the horn in the presence of the stationary and rotating scale models of the Darrieus, measured at 4.07 GHz, are shown in Fig. 5-11(a) and 5-11(b), respectively. It can be seen from the results that the rotation of the windmill has no significant effect on the pattern for angles outside the range $200° \leq \theta \leq 310°$.

Two brief experiments were carried out with the Darrieus and the two antennas arranged in the configurations shown in Figs. 5-12(a) and 5-12(b). With each configuration, the transmitting and receiving antennas were located in the far and near zones respectively of the windmill regarded as a scatterer. A black and white TV camera and video equipment were used to photograph the windmill, and thereby permit correlation of the interference on the test receiver screen with the rotational position of the windmill. In each case,

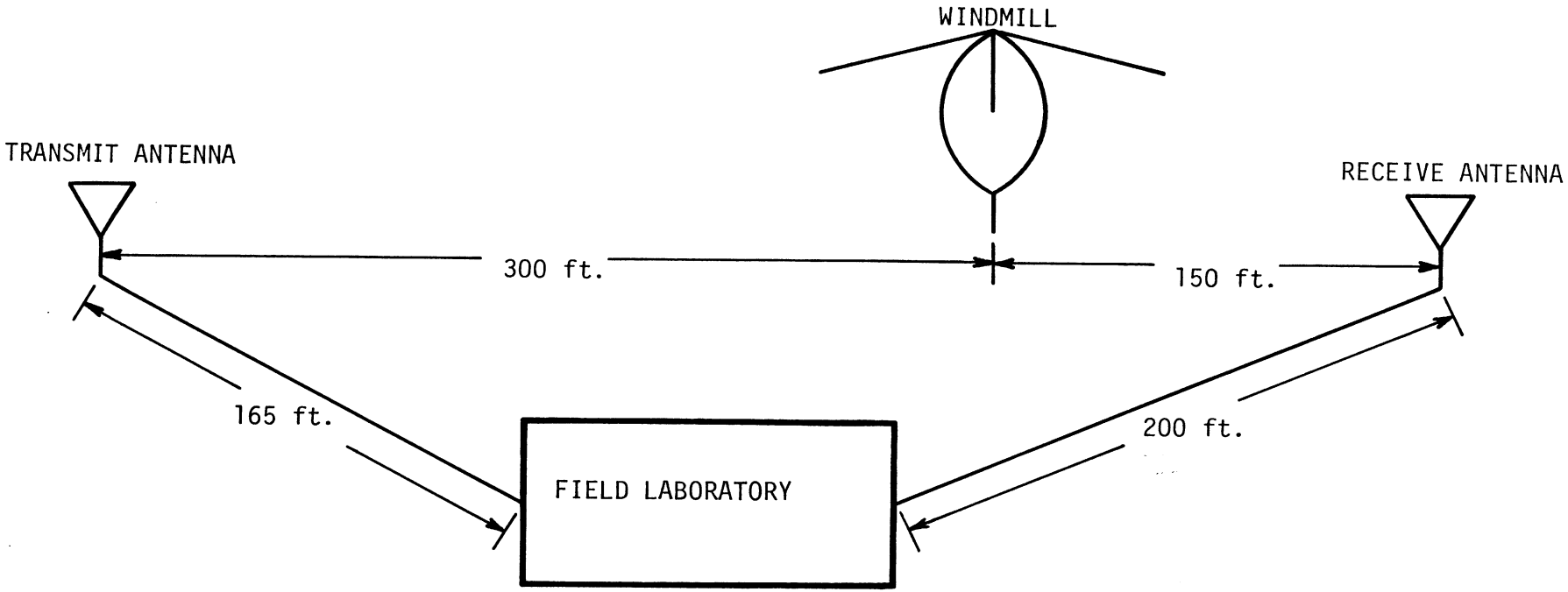

Fig. 5-10: A typical arrangement of the antennas and the windmill.

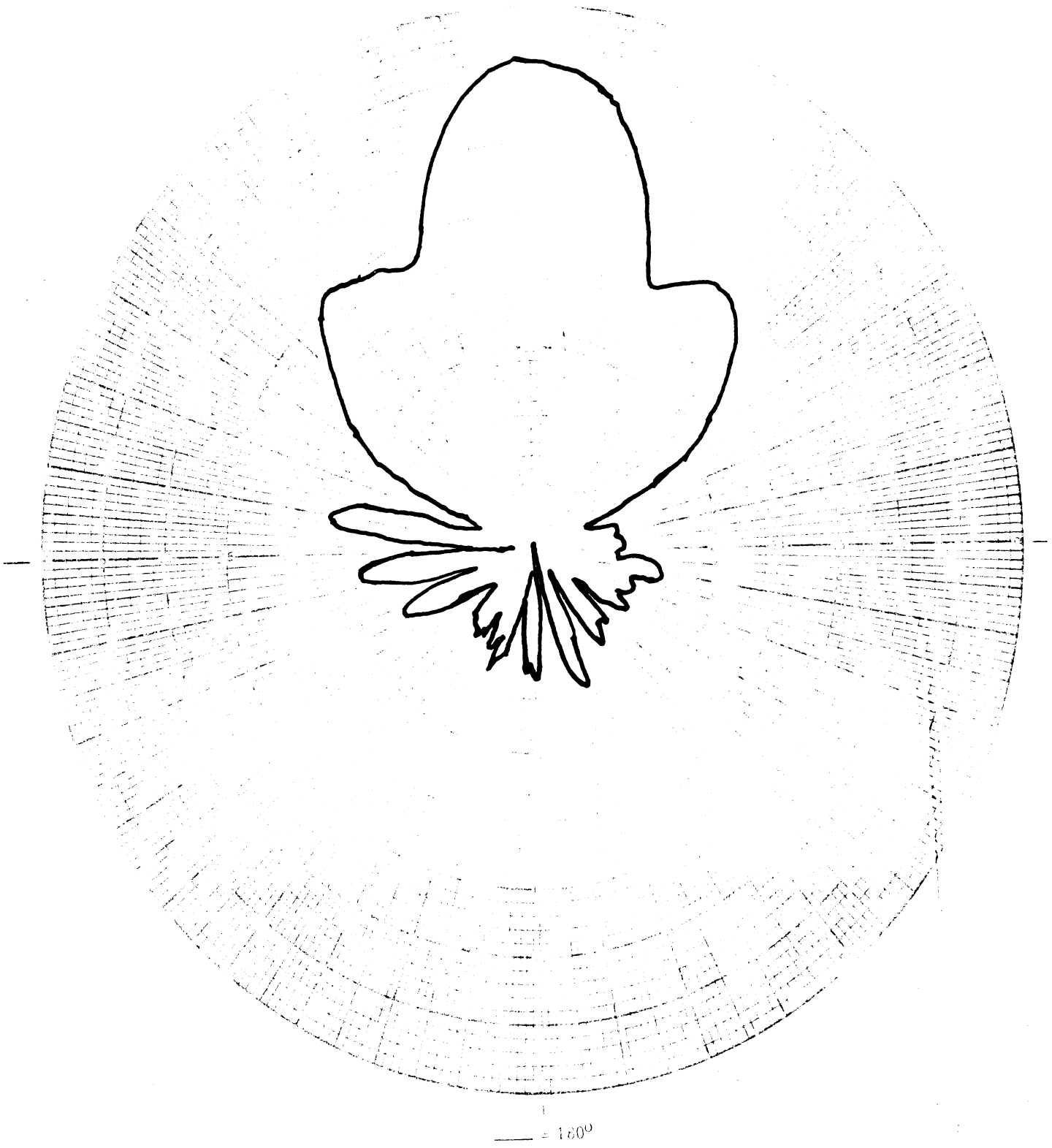

Fig. 5-11 (a): Horizontal plane receiving pattern of the horn antenna in the presence of the stationary Darrieus. Receiving horn located 40 ft. from the windmill and in a direction normal to the transmitter-to-windmill direction (f = 4.04 GHz).

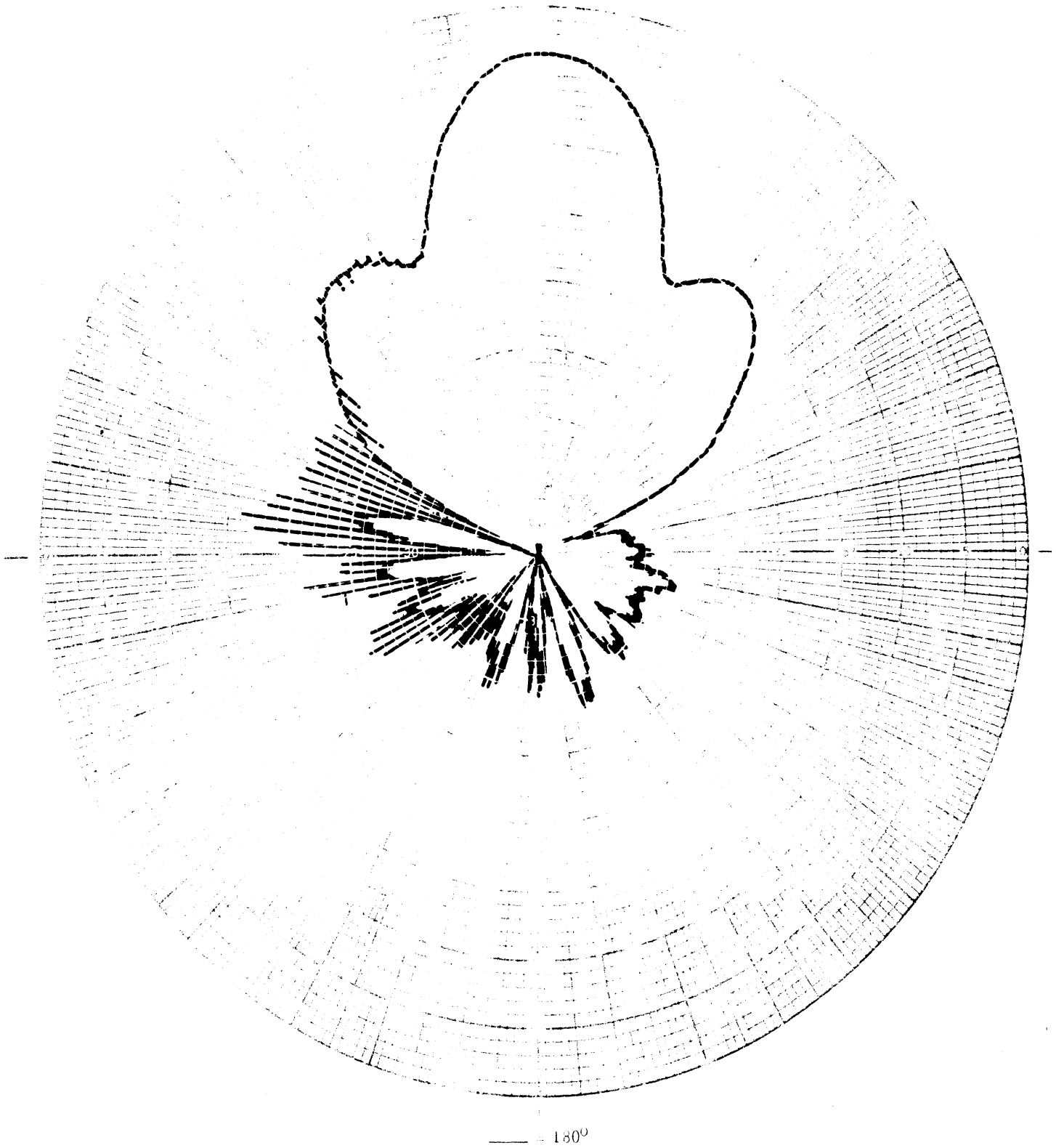

Fig. 5-11 (b): Horizontal plane receiving pattern of the horn antenna in the presence of the rotating Darrieus. The receiving horn is located 40 ft. from the windmill and in a direction normal to the transmitter-to-windmill direction. Rotation speed of the windmill = 100 rpm; f = 4.04 GHz.

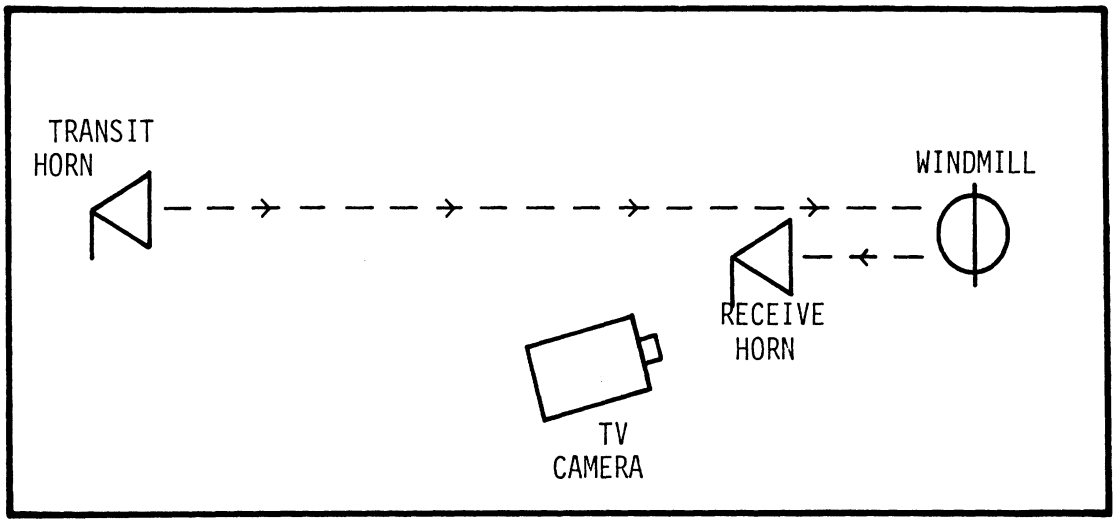

(a) receiving horn in the backscattering direction

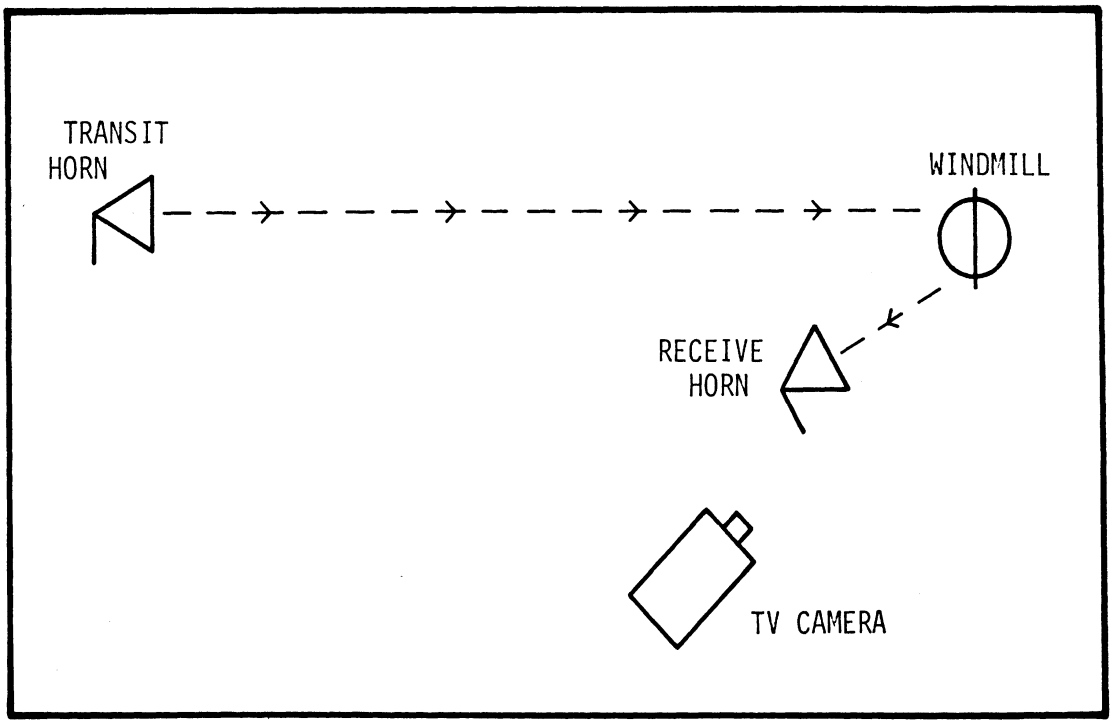

(b) receiving horn in an off backscattering direction

Fig. 5-12: The two arrangements of the antennas and the Darrieus used during the preliminary test.

the transmitted signal level and the rotational speed of the windmill were varied and the received signal was observed. The interference was more apparent at low signal levels, and appeared as a sudden increase in the snow content in the received picture. This increase seemed to coincide with each passage of the curved vertical blades of the Darrieus through the receiving antenna beam.

5.5 TV Interference Tests and Results

A number of TV interference tests was carried out by receiving the laboratory generated microwave TV signals, in the presence of a rotating scale model windmill. The windmill and the transmitting and receiving antennas were all located outdoors where no other significant scattering object existed. The frequency of the source signal being 4.07 GHz ($\lambda \simeq 2.9$ in.), the two 1/10 scale model vertical axis windmills gave results equivalent to those produced by the corresponding full scale windmills at 407 MHz (i.e., TV Channel 14, approximately), and the 1/37.5 scale model horizontal axis windmill simulated the full scale MOD-0 windmill at 102 MHz (i.e., Channel 6, approximately).

The data gathering process consisted of recording the total electrical signal received (including any modulation caused by the windmill) while observing the received picture on the test TV receiver for any video interference. No audio interference test was conducted, since our previous studies [1,2] indicated that no such interference would occur under normal conditions.

5.5.1 Recording of the Received Signal

The recording of the received signal was done as follows. A portion of the signal going to the test receiver was sampled with the help of a directional coupler and fed to a spectrum analyzer (see Fig. 5-6). The vertical output

of the spectrum analyzer contained the desired video information along with any modulation introduced by the rotating windmill. This signal was then used to drive an oscilloscope which reproduced on its screen the combined direct and scattered video signals which were then photographed. In addition to the above signal, the oscilloscope reproduced a timing signal derived from the synchro-motor driving the windmill: this signal appeared on the screen as a series of timing pulses whose separation was equal to the rotation period of the windmill. On each photograph of the received signal, to be discussed later, the upper trace is the actual signal received and the lower trace shows the timing signal for correlating the former signal with the windmill rotation.

5.5.2 Geometry

Fig. 5-13 gives a cross-sectional view of a typical arrangment of the two antennas and the windmill, where T, W, and R represent the phase centers of the transmitting horn, the windmill and the receiving horn, respectively. The two 18 dB gain horns were horizontally polarized with phase centers 7 ft. above the ground. Normally, the distance d_{TW} between the transmitting horn and the windmill was kept constant at d_{TW} = 300 ft., and the distance d between the windmill and the receiving horn was varied.

The transmitting antenna beam pointing direction is represented by α_T, where α_T is measured clockwise from the line TW (Fig. 5-13). Thus, $\alpha_T = 0$ indicates that the transmitting antenna beam is pointed towards the windmill, and as a rule $\alpha_T = 0$. Sometimes, it was necessary to rotate the transmitting antenna beam, and in these cases the α_T values will be stated explicitly. Similarly, the receiving antenna beam pointing direction is denoted by the angle α_R, where α_R is measured clockwise from a line RT' parallel to WT (Fig. 5-13); $\alpha_R = 0$ corresponds to a receiving antenna beam pointing direction

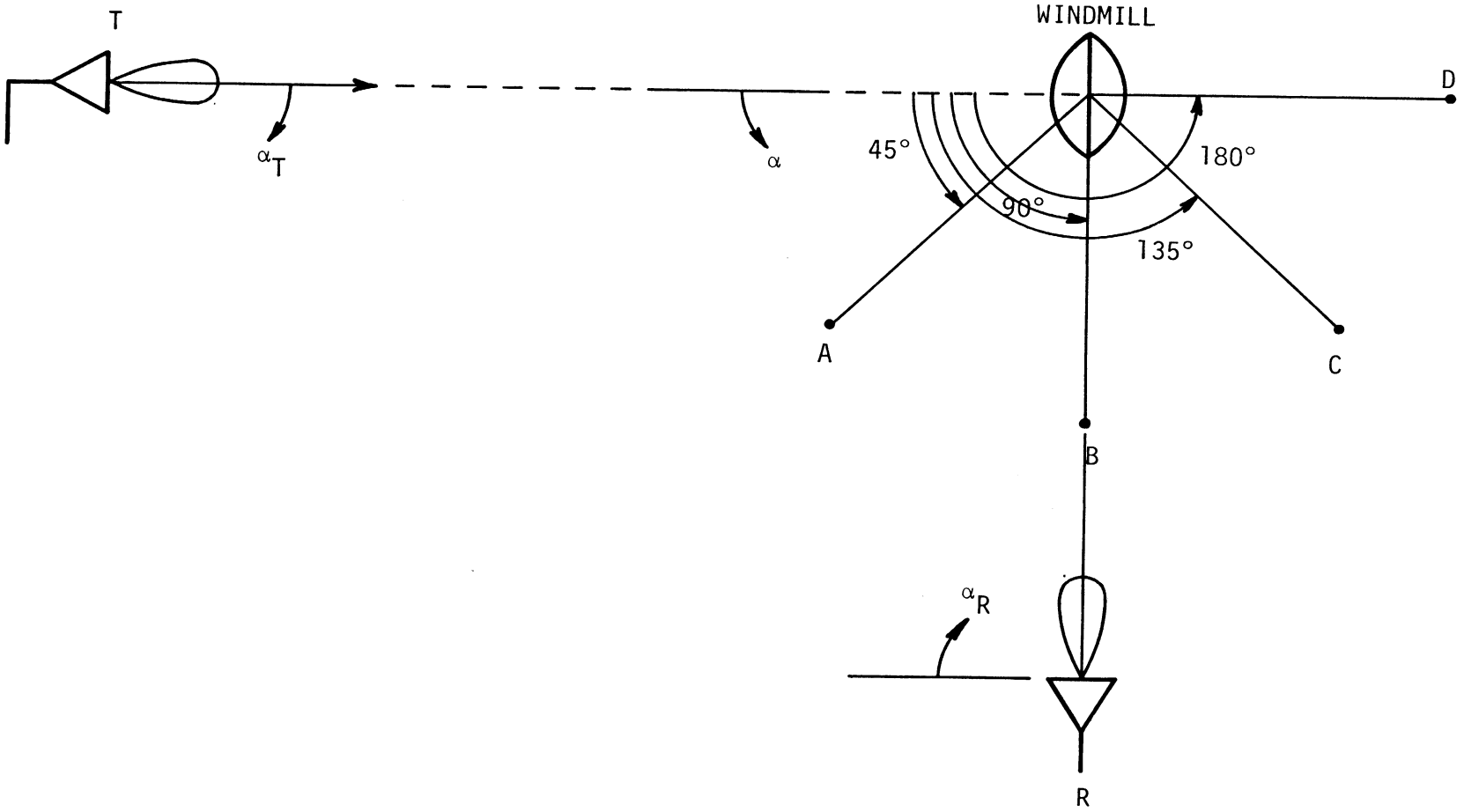

Fig. 5-13: Geometry and notation showing the arrangement of the antennas and the windmill during the TV interference tests.

parallel to the vector WT.

The location of a receiving point R is represented by a system of polar coordinates (d/α) with origin located at W as shown in Fig. 5-12, where d is the distance of R from W and α is the polar angle of R measured anti-clockwise from the line WT. With $\alpha_T = 0$, the location of R and the orientation of the receiving antenna beam with respect to W and T are represented by $(d/\alpha,\alpha_R)$ where d/α denotes the location of R, and α_R the pointing direction of the receiving antenna beam. For example, the location of R and the receiving antenna beam pointing direction in Fig. 5-12 are denoted by (d/90°, 90°).

The plane of the vertical axis windmill blade in Fig. 5-13 is oriented broadside to the line WT and it rotates clockwise around its vertical axis.

5.5.3 Giromill Test Results

A typical outside arrangement of the scale model Giromill and the transmitting and receiving antennas is shown in Fig. 5-13. During the test the distance between the transmitting antenna and the windmill was kept constant at d_{TW} = 300 ft.; unless otherwise stated the transmitting antenna beam was directed towards the windmill, i.e., $\alpha_T = 0$.

The upper trace in Fig. 5-14(a) shows the received signal as a function of time with R located at (50 ft./90°, 0°), i.e., the receiving antenna located at a distance of 50 ft. from the windmill along the 90° radial and the receiving antenna beam oriented along the direction $\alpha_R = 0$. With this orientation, the total received signal consisted mainly of the direct signal from the transmitter having a level of about -39 dBm, as can be seen from Fig. 5-14(a). The received picture (color-bar) was good, and since little or no scattered (or

secondary) signal was received, no significant video interference was observed. The lower trace in Fig. 5-14(a) shows that the time between two adjacent pulses is 0.52 sec. indicating that the windmill was rotating at about 115 rpm.

Fig. 5-14(b) shows the signal received at the same location as in Fig. 5-13(a), but with the receiving antenna beam pointing to the windmill, i.e., the coordinates of R were (50 ft./90°, 90°). At this orientation, little or no direct signal was received; the received signal consisted mainly of the secondary signal having a level about -62 dBm. Note that the period of the received signal in Fig. 5-14(b) is half the period of the timing pulses, indicating that the antenna received the scattered signals twice in every rotation. With little or no direct signal received, the picture (color-bar) flashed on and off with the passage of the scattered signal through the receiving antenna beam.

Fig. 5-14(c) shows the received signal with R located as before but the receiving antenna beam pointing in the direction $\alpha_R = 30°$, i.e., the coordinates of R were (50 ft./90°, 30°). As can be seen from the figure the received signal level was -50 dBm. Although the recorded signal in Fig. 5-13(c) does show the existence of a scattered signal, it is not sufficiently strong to produce any noticeable video distortion in the received picture, which was good.

The receiving antenna was now located on the 45° radial at a distance of 45 ft. from the windmill. The receiving antenna was then rotated to control the ratio of the direct to scattered signals received. Typical of the results obtained are the two shown in Figs. 5-15. The received signal at a level of -50 dBm in Fig. 5-15(a) does not contain an appreciable scattered signal and consequently no video distortion was observed in the picture (compare with Fig. 5-14(a)). The results shown in Fig. 5-15(b) were obtained with the

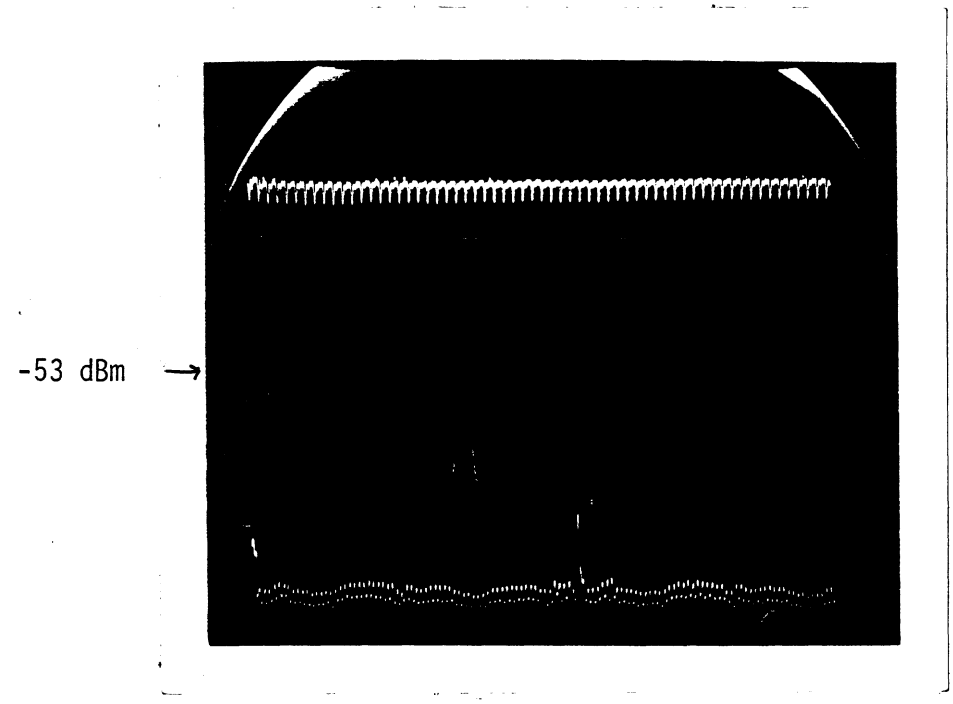

(a) R at (50 ft./90°, 0°)

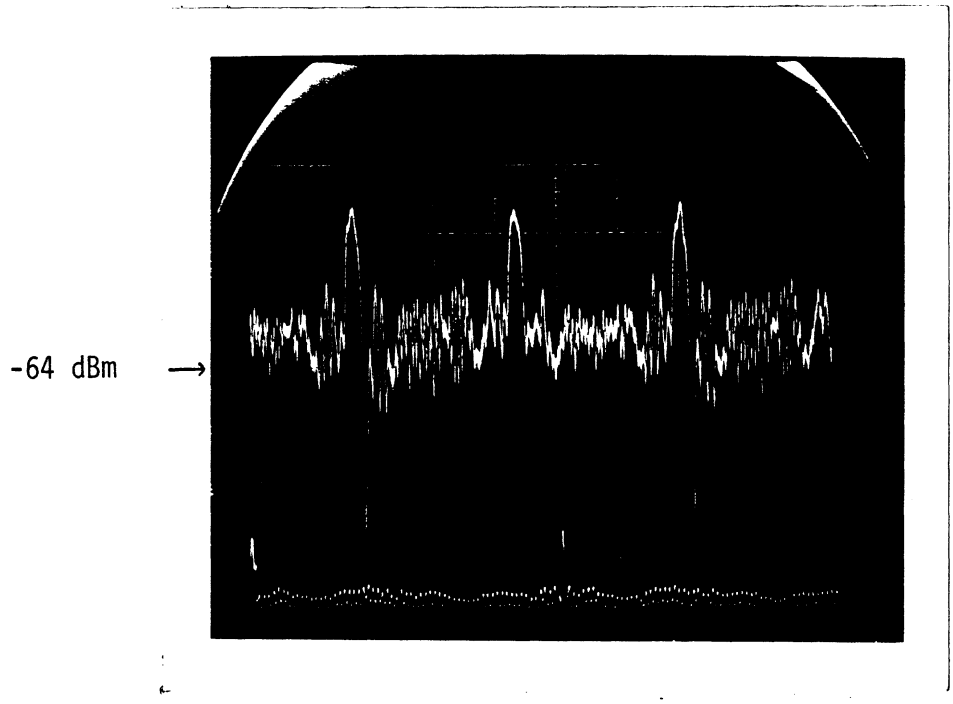

(b) R at (50 ft./90°, 90°)

Fig. 5-14: Video signal as a function of time received in the presence of the Giromill rotating at 115 rpm (Note: 5 dBm/vertical division and 0.1 sec/horizontal division).

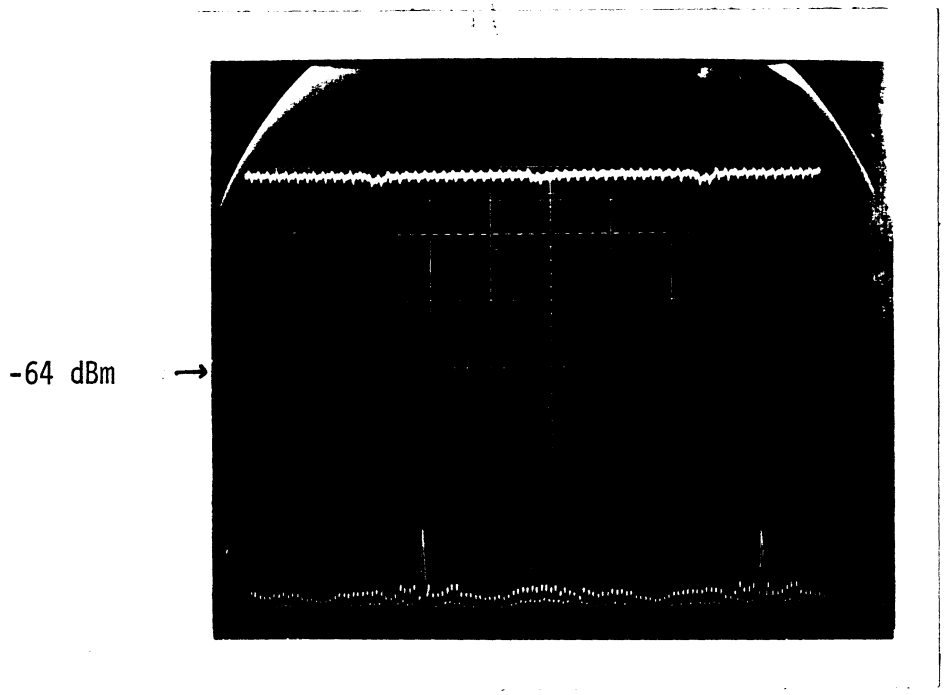

(c) R at (50 ft./90°, 30°)

Fig. 5-14 (continued).

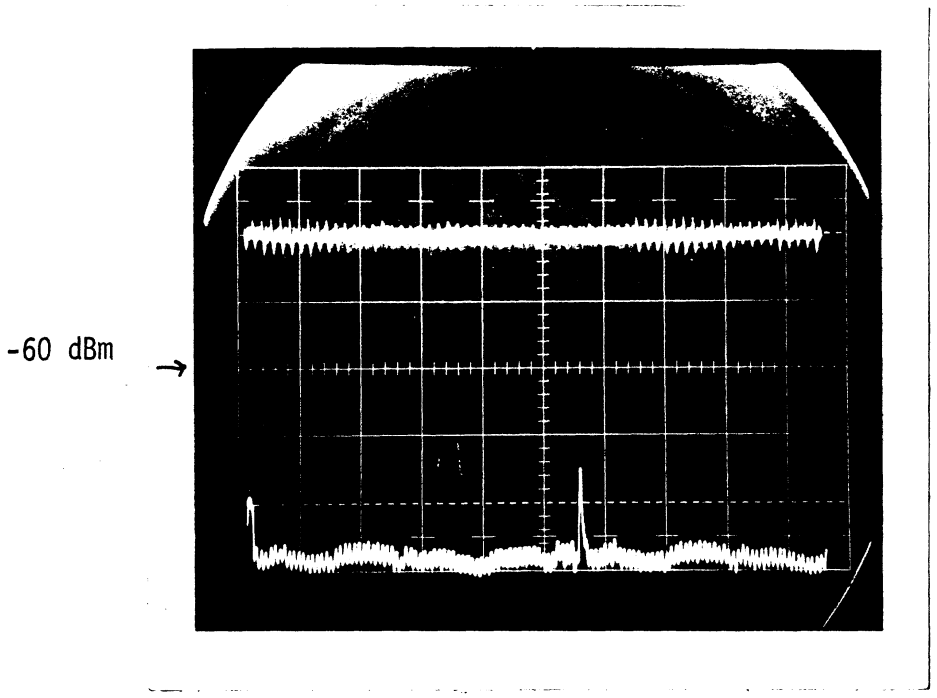

(a) R at (50 ft./45°, 60°)

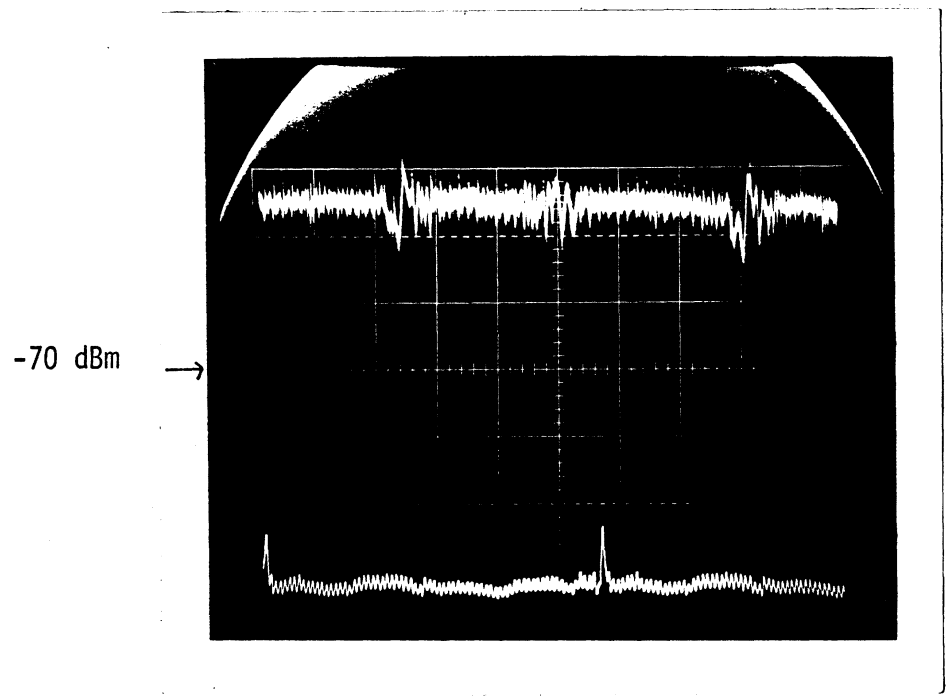

(b) R at (50 ft./45°, 80°)

Fig. 5-15: Video signal as a function of time received in the presence of the Giromill rotating at 115 rpm (Note: 5 dBm/vertical division and 0.1 sec/horizontal division).

receiving antenna beam oriented more towards the windmill. As a result, stronger scattered signal pulses were received in addition to the direct signal whose average level was -58 dBm. The received picture in this case was snowy with video distortion in synchronism with the received scattered pulses.

Next, a series of tests were conducted with the receiving antenna located on the $\alpha = 90°$ radial but at variable distances from the windmill. At each location of the receiver, α_R and α_T were varied, as needed, to obtain barely visible video distortion of the received picture. The purpose of these tests was to determine the level of the interfering (scattered) signal relative to the direct signal to produce barely visible distortion of the received picture. In effect, this would yield the threshold modulation for interference [1,2]. Figs. 5-16a,b, and c show some typical results obtained with the receiving antenna located at 150, 75, and 25 ft., respectively. The pulse-like modulations of the received signal introduced by the rotation of the windmill are evident in the figures. In all three cases the peak-to-peak variation in the signal introduced by the windmill scattering effects is about 5 dB, corresponding to an amplitude modulation index of about 0.27 [2]. The results show that the modulation waveform varies with the distance of the windmill from the receiving antenna. This is due to the fact that the receiving antenna was located within the near zone of the windmill: since the maximum linear dimension of the windmill D is about 5 ft. and $\lambda = 2.9"$, $2\,D^2/\lambda \simeq 200$ ft.

Fig. 5-17 shows the results obtained with R at (50 ft./135°, 45°). The ambient signal level was -55 dBm. The received picture was good and although the existence of modulation pulses is evident in Fig. 5-17, their amplitude was not strong enough to cause any noticeable video distortion. With this orientation, it was not possible to further adjust α_R and/or α_T to obtain significant

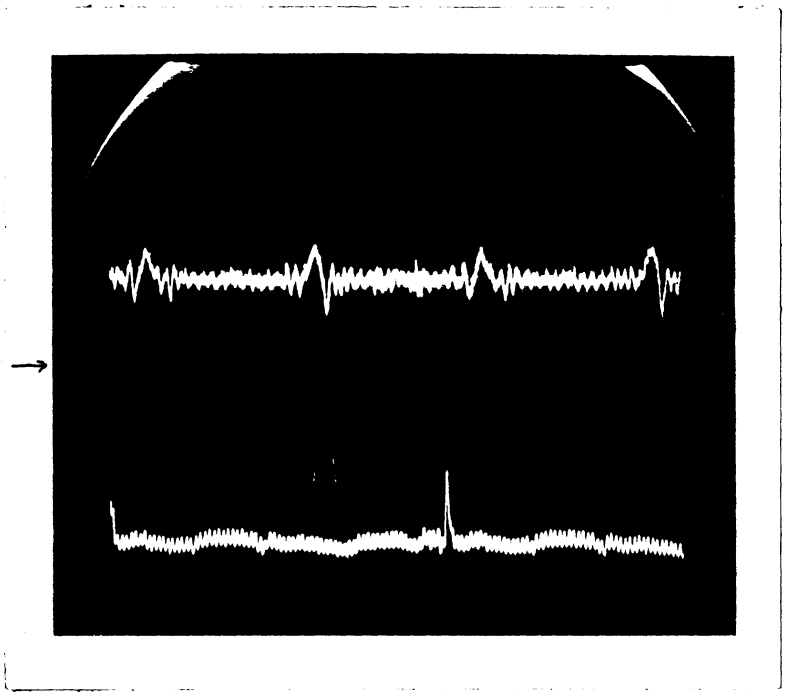

(a) R at (150 ft./90°, 80°), α_T = 10°

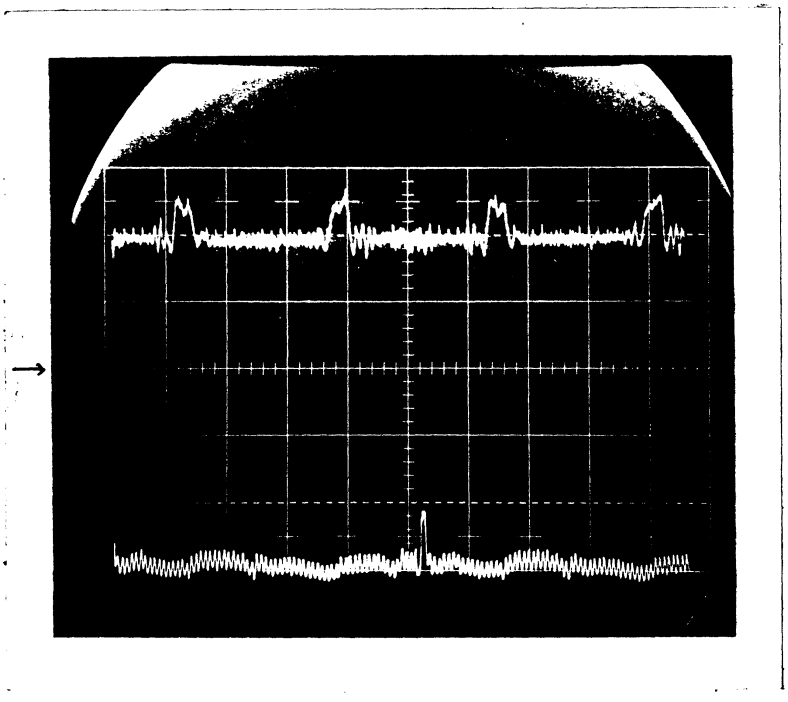

(b) R at (75 ft./90°, 72°), α_T = 5°

Fig. 5-16: Video signal as a function of time received in the presence of the Giromill rotating at 115 rpm (Note: 5 dBm/vertical division and 0.1 sec/horizontal division).

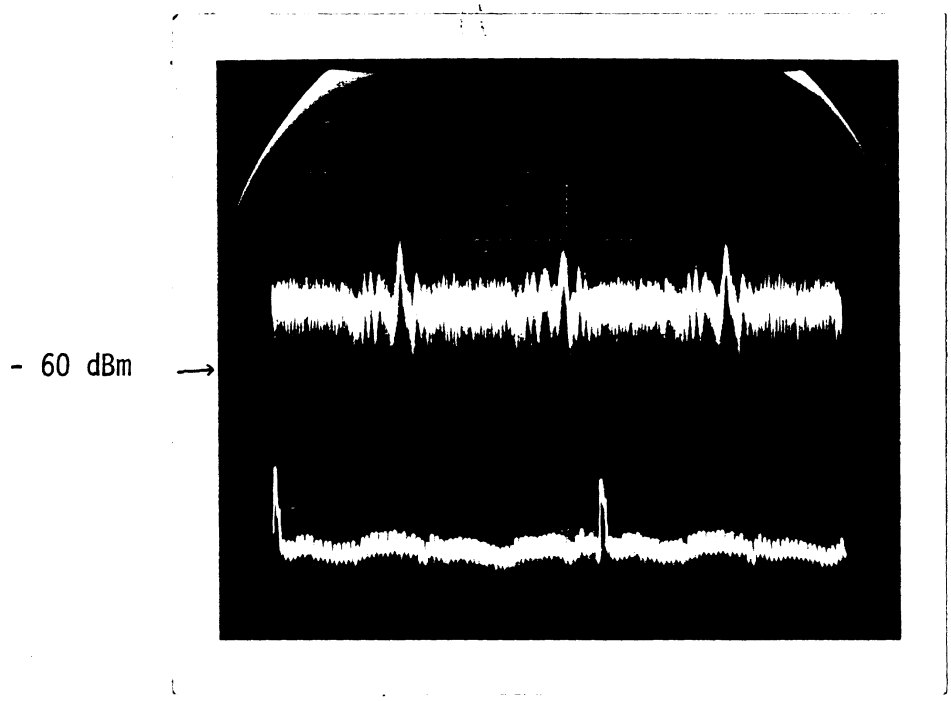

(c) R at (25 ft./90°, 60°), $\alpha_T = 0°$

Fig. 5-16 (continued).

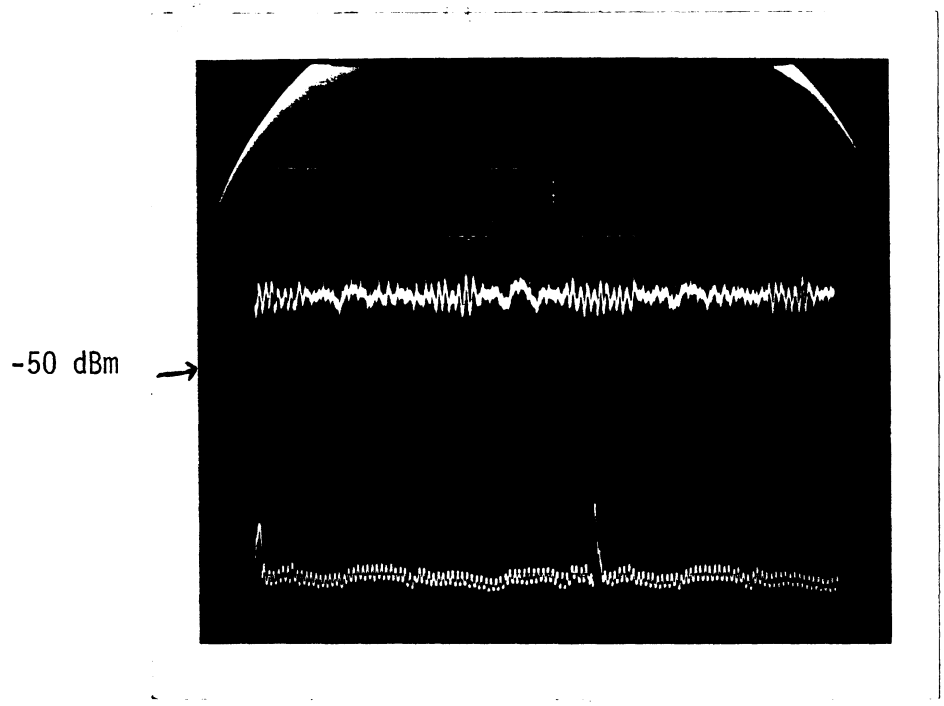

Fig. 5-17: Video signal as a function of time received in the presence of the Giromill rotating at 115 rpm: R at (50 ft./ 135°, 45°) (Note: 5 dBm/vertical division and 0.1 sec/horizontal division).

amounts of video distortion.

Fig. 5-18 shows the results obtained with the receiving antenna located in the forward direction with respect to the scattering by the windmill and at a distance of 50 ft., i.e., with R at (50 ft./180°, 0°). With this orientation the antenna was receiving both the direct and scattered signals via its main beam. The results indicate that the desired video signal is riding on a low frequency sinusoidal waveform, which is characteristic of the modulation waveform introduced by a windmill in the forward direction [2]. In Fig. 5-18, the modulation being sinusoidal-type and the average signal level being -42 dBm, the received picture was good and no video distortion was observed. In the forward direction it was not possible to control the scattered signal relative to the direct signal received, and hence no further test was carried out.

5.5.4 The Darrieus Test Results

Due to limitations on time, results were obtained with the receiving antenna located at a constant distance of 50 feet from the Darrieus. The transmitter-to-windmill distance was kept 300 feet, as before, and the windmill was rotated at about 115 rpm.

Figs. 5-19a, b, and c show the results obtained with R located at a distance of 50 feet from the windmill and on the 90° radial, for α_R = 60°, 80°, and 90°, respectively. At the location of R corresponding to Fig. 5-19(a), the received signal consisted mainly of the direct signal and the received color-bar was good with no video distortion. The results of Fig. 5-19(b) were obtained by rotating the receiving antenna beam towards the windmill; consequently the received signals contain the scattered signals. The results indicate that the scattering effect of the Darrieus introduces two types of modulation waveforms: a broad

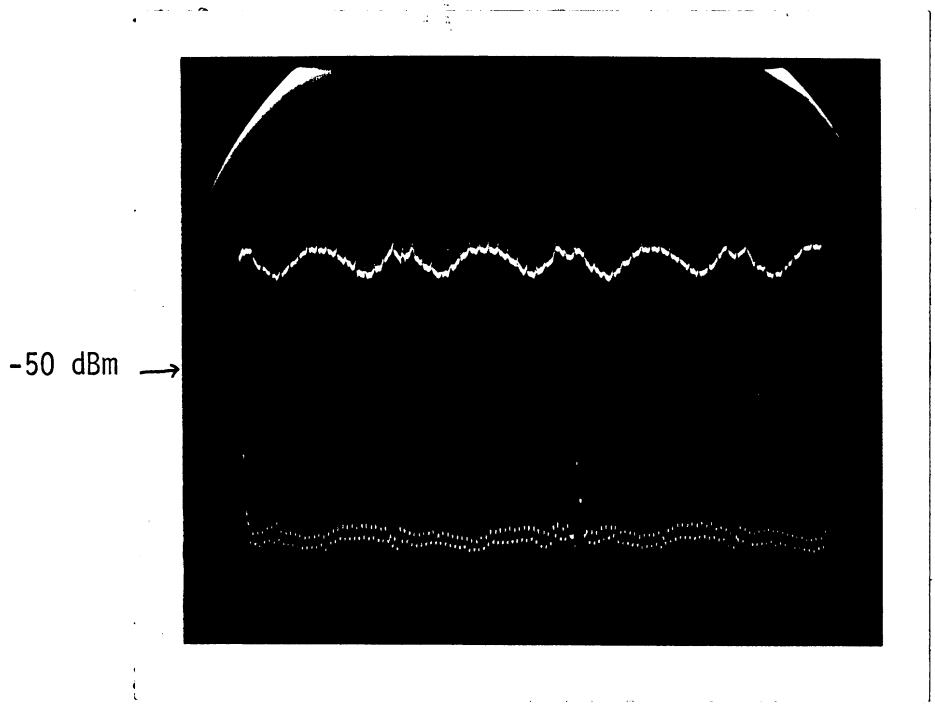

Fig. 5-18: Video signal as a function of time received in the presence of the Giromill rotating at 115 rpm: (50 ft./180°, 0°) (Note: 5 dBm/vertical division and 0.1 sec/horizontal division).

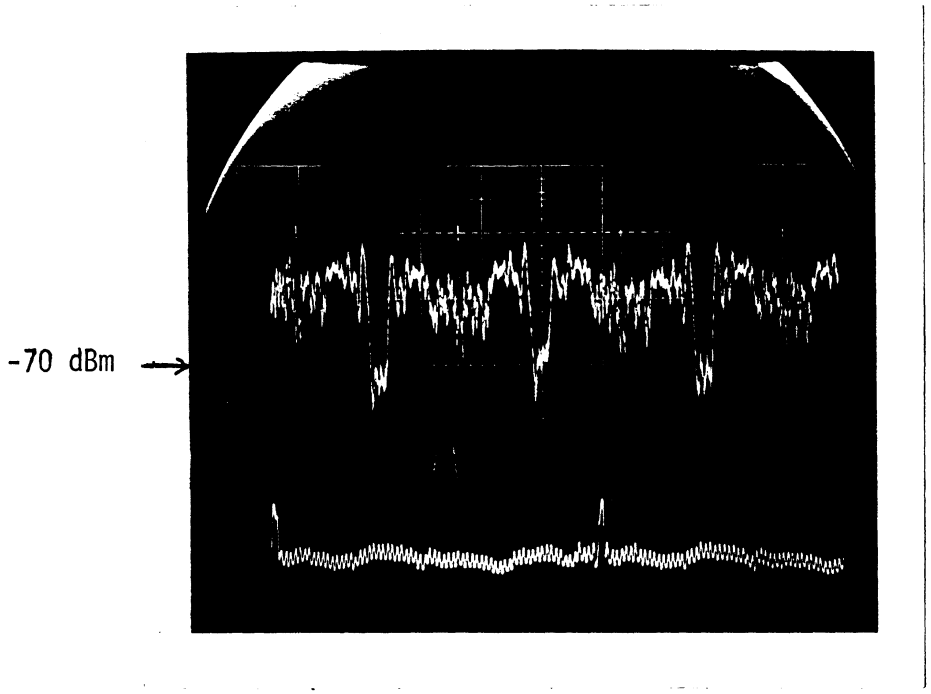

(a) R at (50 ft./90°, 60°)

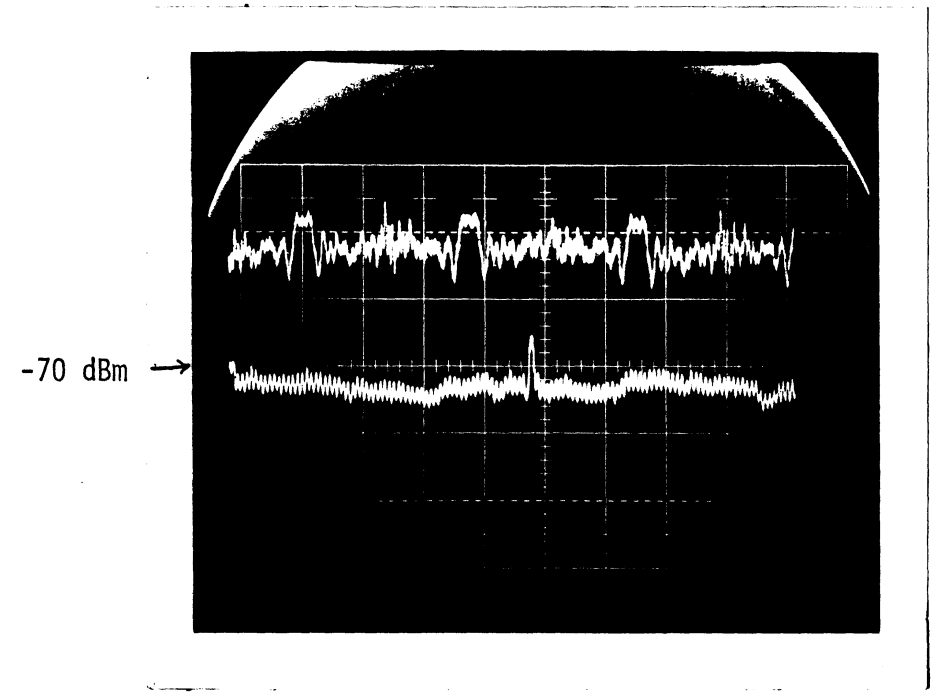

(b) R at (50 ft./90°, 80°)

Fig. 5-19: Video signal as a function of time received in the Presence of the Darrieus rotating at 115 rpm. (Note: 5 dBm/vertical division and 0.1 sec/horizontal division).

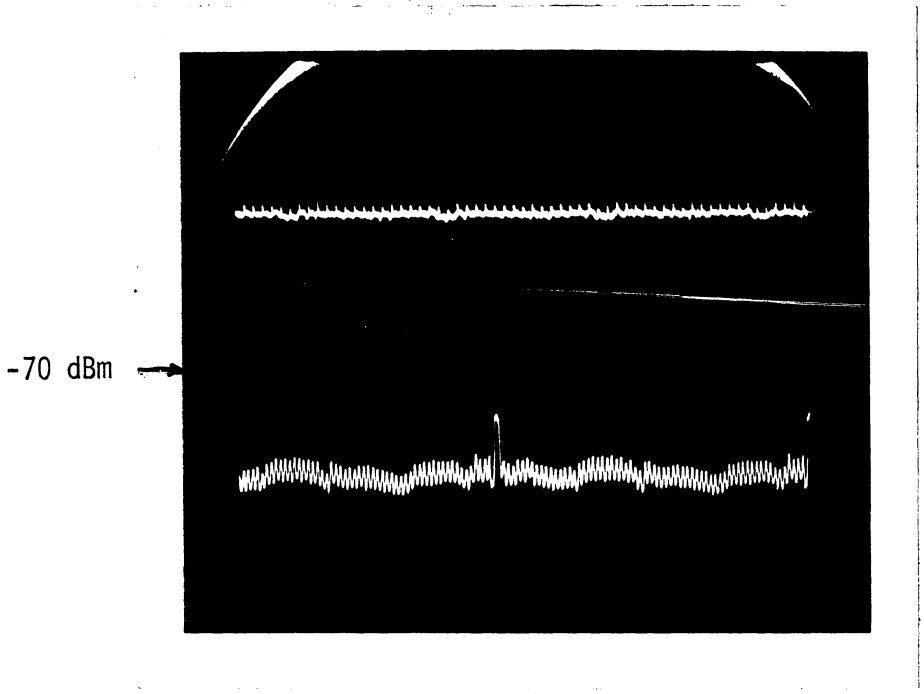

(c) R at (50 ft./90°, 90°)

Fig. 5-19 (continued).

pulse-like waveform and a sharp spike-like waveform. The peak-to-peak variation in the received signal caused by the broad pulse is about 5 dB. The received picture was poor, and threshold type of video distortion was observed coinciding with the occurrence of the broad pulses in Fig. 5-19(b). The narrow spikes did not produce any distortion. Fig. 5-19(c) shows the results obtained when the receiving antenna beam was directed towards the windmill to receive only the scattered signals. The stronger narrow spikes are again visible in the received signal. No color-bar was seen on the test TV screen, although the background color blinked on and off with the occurrence of the broad pulses in the received signal.

Fig. 5-20 gives the results obtained with R at (50 ft./90°, 55°). At this position, the received signal contains a modulation waveform which builds up gradually to a peak value and thereafter gradually diminishes to zero. The received picture was found to be noisy, and video interference occurred in synchronism with the modulation pulses in Fig. 5-20.

Fig. 5-21 shows the results obtained with R at (50 ft./180°, 0°), i.e., in the forward direction. There appears to be a weak sinusoidal pulse-like modulation waveform introduced by the scattering effects of the Darrieus. The received picture was good and no video distortion was observed.

5.5.5 MOD-0 Windmill Test Results

The size of the scale model MOD-0 windmill being small (~1/40), the transmitter was moved to a distance of 100 ft. from the windmill so as to increase the scattered field within the test area. Even then, the scattered field was very small and it was difficult to obtain any clearly noticeable video distortion on reception. The windmill was rotated at 40 rpm and no

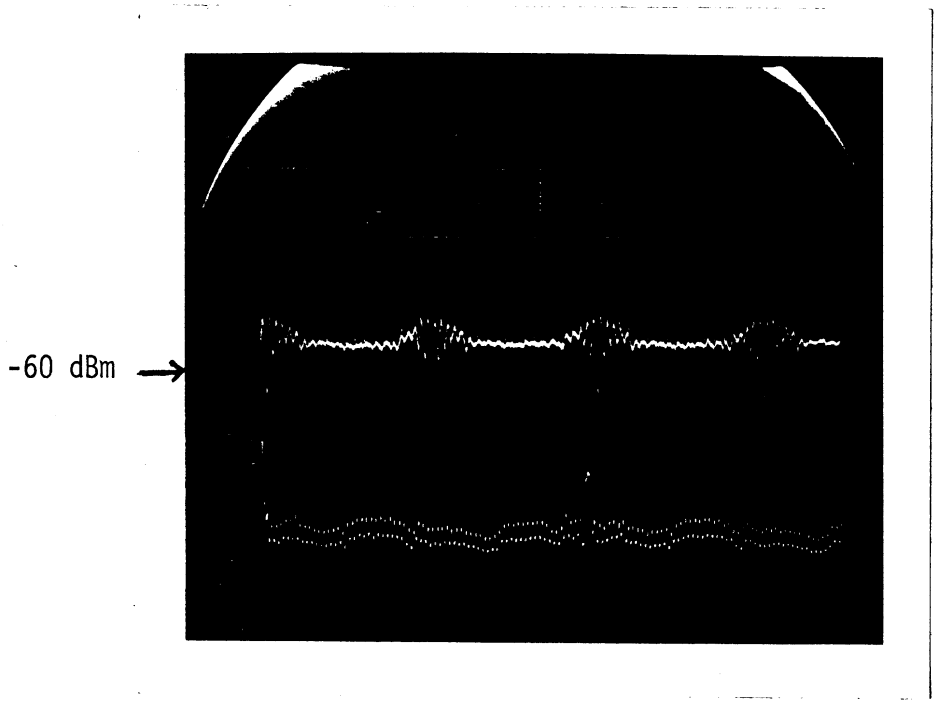

Fig. 5-20: Video signal as a function of time received in the presence of the Darrieus rotating at 115 rpm: R at (50 ft./135°, 55°) (Note: 5 dBm/vertical division and 0.1 sec/horizontal division).

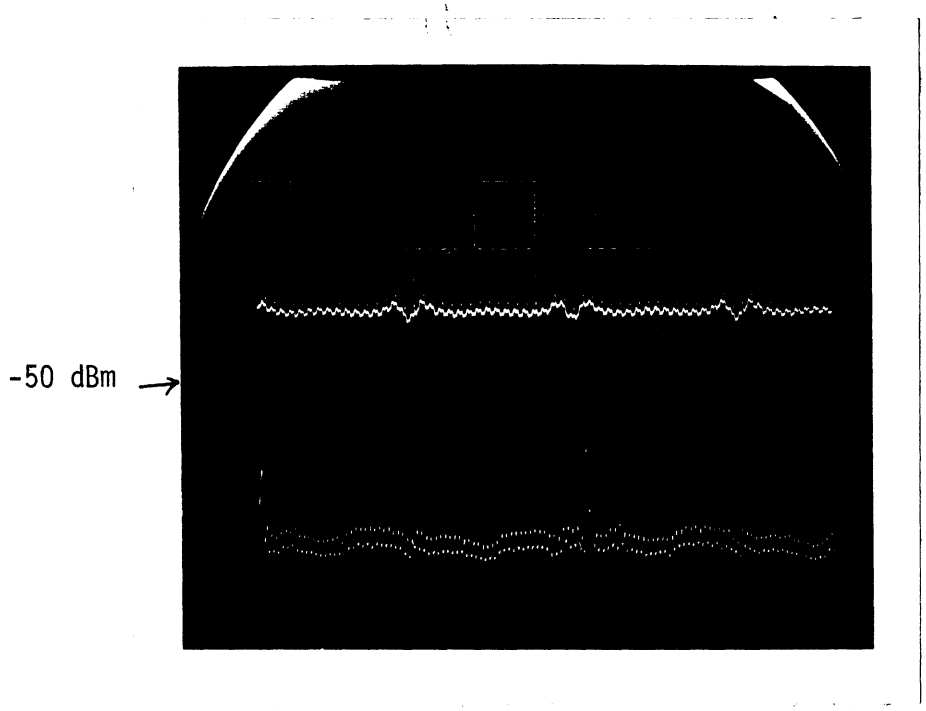

Fig. 5-21: Video signal as a function of time received in the presence of the Darrieus rotating at 115 rpm: R at (50 ft./ 180°, 0°) (Note: 5 dBm/vertical division and 0.1 sec/ horizontal division).

timing signal was used during these tests.

Figs. 5-22a, b, and c give results obtained with R located at 25 ft./90°, for the receiving antenna beam pointing directions α_R = 75°, 80°, and 90°, respectively. The results indicate that the modulation introduced by the windmill is increased as the receiving antenna beam is rotated towards the windmill; the modulation waveform, particularly the one in Fig. 5-22(b), resembles that observed at on-site measurement at Plum Brook during our previous study [2]. In all three cases the received picture was fair; video interference was observed for the cases with α_R = 80° and 90°, the amount of distortion being larger at the latter angle. As can be seen from Fig. 5-22(b) the modulation level introduced is about 3 dB ($\sim$ 0.17) for which the interference observed was threshold type. This is consistent with results obtained with our previous studies of MOD-0 windmill [1,2].

Fig. 5-23 shows the results obtained with R at (50 ft./180°, 26°), i.e., in the forward direction. At this location, the received picture was poor but no video distortion caused by interference was observed. This was because the signal did not suffer appreciable modulation, as can be seen from Fig. 5-23.

5.5.6 Discussion

The results presented above, although not complete, indicate that the electromagnetic interference to TV reception caused by various windmills can be studied and quantified with the help of a laboratory microwave TV system in conjunction with rotating scale models of the windmills. The exact TV channel frequency at which these effects are applicable for a given full-scale windmill is determined by the scale factor of the model and the frequency of the microwave signal used.

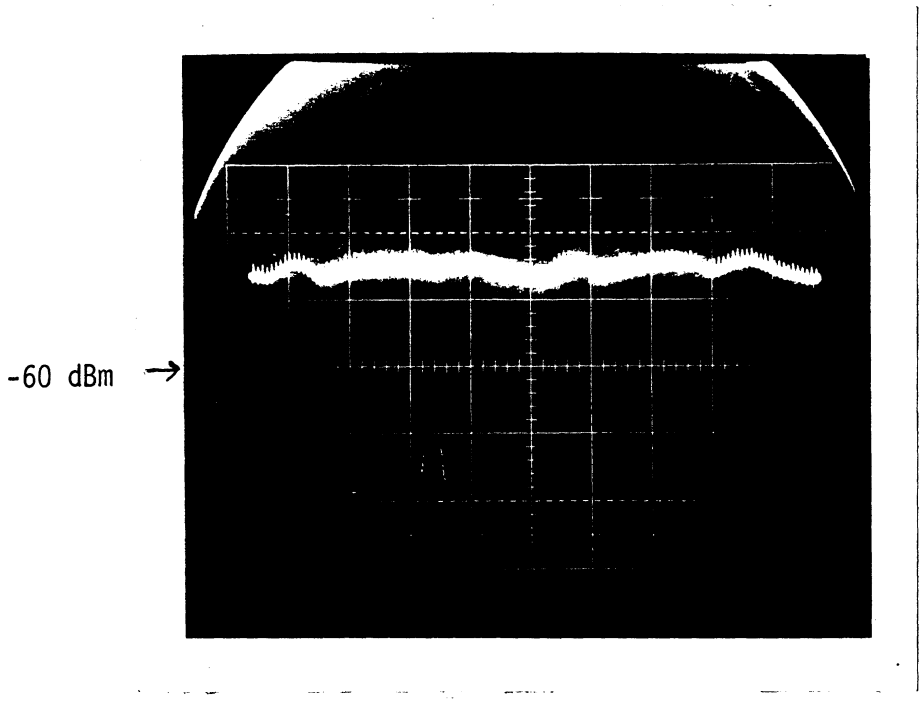

(a) R at (25 ft./90°, 75°)

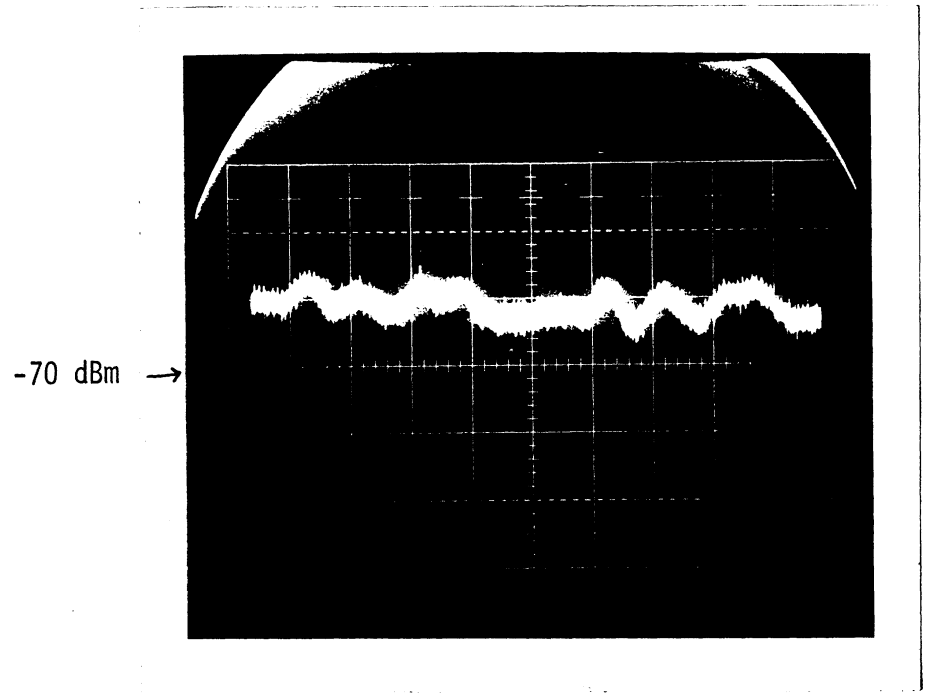

(b) R at (25 ft./90°, 80°)

Fig. 5-22: Video signal as a function of time received in the presence of the MOD-0 blades rotating at 40 rpm (Note: 5 dBm/vertical division and 0.2 sec/horizontal division).

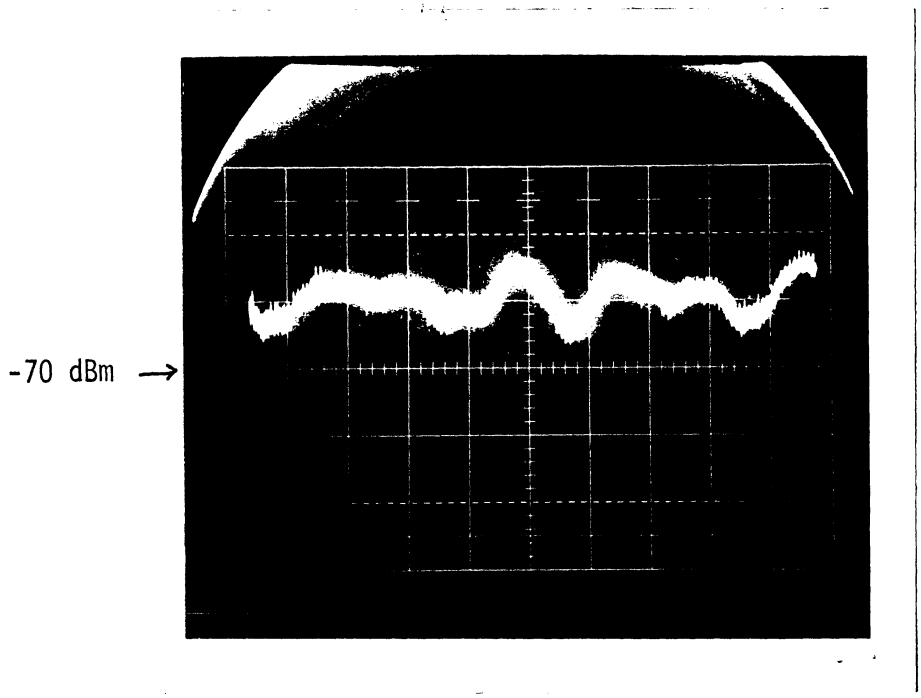

(c) R at (25 ft./90°, 90°)

Fig. 5-22 (continued).

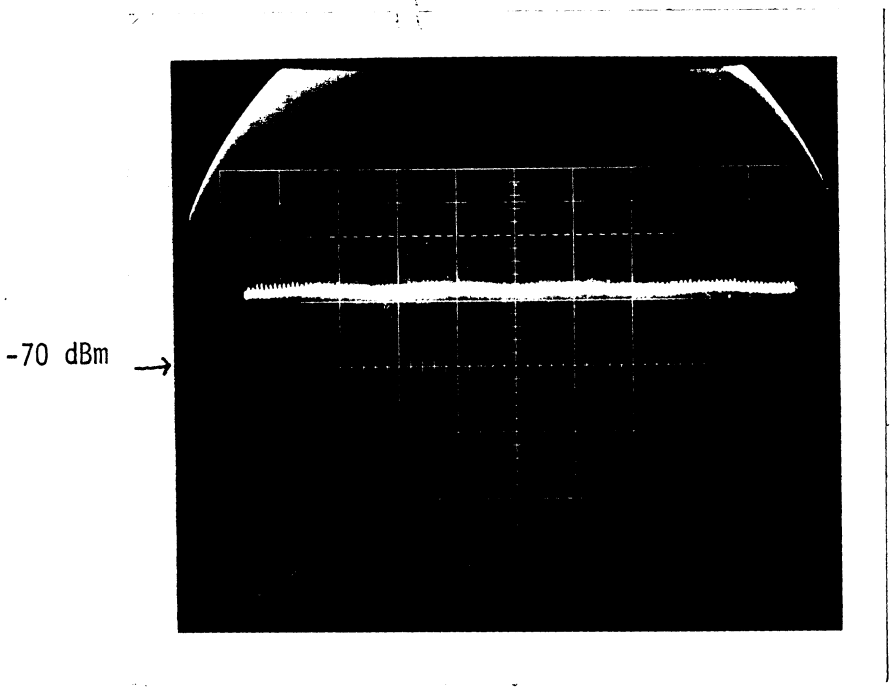

Fig. 5-23: Video signal as a function of time received in the presence of the MOD-0 blades rotating at 40 rpm: R at (50 ft./ 180°, 26°) (Note: 5 dBm/vertical division and 0.2 sec/ horizontal division).

The modulation and modulation waveform of the received signal and the nature and degree of video distortion due to interference by the rotating scale models of MOD-0 windmill blades have been found similar to those obtained during our on-site measurements with the full-scale MOD-0 windmill using commercial TV signals at approximately the TV Channel 6 frequency.

The Giromill and the Darrieus results show the interference at a frequency corresponding approximately to TV Channel 14. The most detailed results have been obtained with the Giromill which is found to cause observable interference out to a distance of about 600 wavelengths at the Channel 14 frequency. The threshold modulation with the Giromill was found to be about 27 percent. The interference effects caused by the Darrieus are generally less severe, and the interference distance is correspondingly smaller. Further study is needed to obtain more detailed results so that the effects may be quantitatively correlated with the various parameters involved.

5.6 Conclusions

A laboratory microwave TV system has been developed. It transmits and receives signals at 4.067 GHz ($\lambda \simeq 2.9$ in.), and the signal is compatible with the usual TV signal so that after suitable frequency conversion, it can be received by a conventional TV receiver. The use of a microwave frequency for signal transmission and reception makes it possible to investigate the electromagnetic interference effects of windmills on TV reception receiving the microwave signals in the presence of rotating scale models of the windmills. At the present time, with 1/10 and 1/39.5 scale model windmills, the system provides results corresponding to those produced by the full scale windmills on TV Channels 14 and 6 respectively. The system is capable of providing sufficient data for quantitative evaluation of the interference effects without

requiring further on-site measurements with full-scale windmills and laboratory simulation studies.

The system developed is still undergoing improvement. Currently, the signal is somewhat noisy due to one of the mixer stages which should be replaced. We hope also to expand the system capability to obtain results for upper UHF channel frequencies at which the interference effects may be more severe. One way to do this is to use larger scale models, but a more convenient approach is to increase the frequency range of the test equipment so that it can operate at frequencies up to 8 GHz.

CHAPTER 6

WINDMILL INTERFERENCE TO A LORAN-C SYSTEM

Loran-C (Long Range Navigation System: version C) is a hyperbolic navigation system [17-19] that enables the user to determine very precisely his position, anywhere within the designated coverage area, by measuring the times of arrival of the signals received from at least three known stations. Currently the coverage area encompasses more than 16 million square miles of the earth's surface; today there are eight Loran-C transmitting chains, with a total of twelve expected to be in operation by 1980 [20]. It is a pulse system with common carrier frequency (usually 100 KHz implying wavelength λ = 3 Km) in the band 90 - 110 KHz for all stations. A chain of transmitting stations consists of one master and two to four slaves, the master and a slave station being separated by 600 to 800 miles. The operating range of the system is in excess of 1000 miles with position errors of 50 - 200 feet at 250 to 600 miles, increasing to approximately 500 feet at a range in excess of 1000 miles [20].

Since the objective of a Loran-C system is to provide over-the-ocean coverage, its transmitting stations are often located on islands or in coastal regions where, with favorable wind conditions, future wind turbine generators (WTG) or windmills may also be sited. A WTG in the vicinity of a Loran-C transmitting station could affect the performance of the system in two ways. First, by mutual interaction between the Loran-C transmitting antenna and the windmill. Since this is an effect which could be corrected at the station by using proper impedance matching of the antenna input terminals, it is unlikely to have a major impact on the system performance.

Nevertheless, we shall discuss this problem briefly in a later section. The second is potentially more severe. A windmill near to a station could act as a parasitic transmitter radiating similar Loran-C signals delayed in time whose affect on the system performance is not obvious. In the following sections we investigate theoretically the possible electromagnetic interference to Loran-C system performance caused by a windmill located in the vicinity of a signal transmitting station. We begin with a brief description of the Loran-C system and its mode of operation.

6.1 The Loran-C System

Various aspects of the Loran-C system and the principles of its operation may be found in [17-25]. Here we shall describe the basic system, and discuss only those aspects of its operation which are relevant to the investigation of the windmill interference problem.

Loran-C differs from other hyperbolic navigation systems in that it uses pulses instead of near-continuous signals. The theory of hyperbolic navigation is well documented [17-19] and is based on the fact that the locus of a point, in a horizontal plane, whose distances from two fixed points in that plane differ by a constant amount is a hyperbola with the fixed points as its focii. Assuming two signal transmitters located at these points, each such hyperbola, henceforth called the Line of Position (LOP), identifies the Difference in the Times of Arrival (DTA) of the two signals at the receiver. A second pair of transmitters yields another LOP which, together with the first, specifies the position of the receiving point with respect to the known positions of the transmitting stations.

6.1.1 Parameters Associated with Transmitting Stations

Each Loran-C system uses a chain of ground-based transmitters

consisting of one master and 2 to 4 slaves. Peak power of up to 4 MW is generated by each transmitter, and is radiated by a single vertical monopole antenna as high as 410 m. For later discussion the following notations will be used to identify various quantities associated with the transmitting stations:

M: master station

S_n: slave station number n, n = 1, 2, 3, 4

R: receiver or observer

T_B = time of travel of signal from master to a slave or base-line electric length

T_{CD} = coding delay or the time by which a slave delays transmission of its signal after receiving the master's signal.

Since the slaves are located about 1000 Km from the master, the base-line electric length T_B is of the order of 4 msec [20]. The coding delay T_{CD} is varied in the range of 10 - 80 msec depending on the location of the transmitters, special operational requirements of the station sites, and other factors. Using the above notation, one can write the following formal relationships characterizing the difference in times of arrival (DTA) of the signals at R:

$$DTA = T_B + T_{CD} + t_{MR} - t_{SR} \quad , \tag{6.1}$$

$$T_{CD} \leq DTA \leq T_{CD} + 2\,T_B \quad , \tag{6.2}$$

where

t_{MR} = time taken by the signal to travel from the master to the receiver,

and t_{SR} = time taken by the signal to travel from the slave to the receiver.

Thus, $(t_{MR} - t_{SR})$ is the actual difference in the times of arrival of the signals at the receiver from the master and a slave station, and it is clear that each LOP has a unique DTA associated with it.

6.1.2 Transmitted Signals

The receiving system of a Loran-C is required to perform an accurate measurement of the DTA of signals from different pairs of transmitters. Accordingly, the transmitted signals are designed to facilitate the practical implementation of a receiver which performs the difficult task of unambiguous and precise measurement of DTA.

The Loran-C composite signal at the receiver consists of groups of pulses radiated psiodically at a specified group repetition interval (GRI) and is shown in Fig. 6-1.

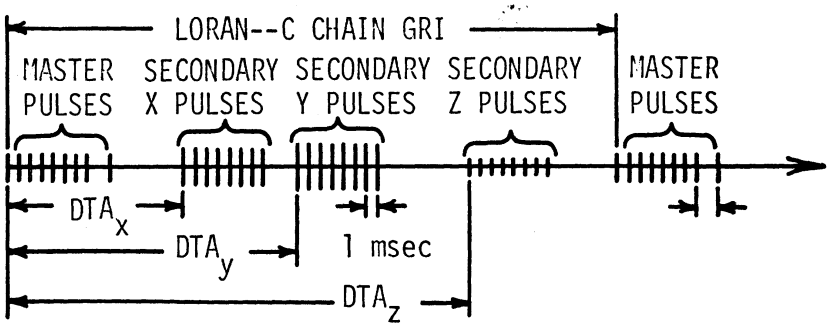

Fig. 6-1: Example of received Loran-C signal format. Each pulse is as in Fig. 6-2.

The group of the master contains 9 pulses per GRI and that of a slave 8. The first 8 pulses of the master group are spaced 1 msec apart, and the ninth pulse is separated from the eighth by 2 msec. All pulses of a slave group are separated by 1 msec. The minimum GRI is chosen to be of sufficient length so that there is enough time for the transmission of pulse groups from the master and slaves, and that there is no overlap between the various pulse groups. It is clear that this depends on the number of stations in a chain and their separation. With a Loran-C chain consisting of 4 slaves, the typical GRI is 100 msec [22]. The low duty cycle of pulses permits transmission of a group of pulses and, therefore, increased signal energy at the receiver, and this in turn provides higher signal-to-noise ratio (SNR) without having to increase the peak radiated power of the transmitter.

6.1.3 Loran-C Pulse

The carrier frequency for the Loran-C pulse is normally 100 KHz and is universal in the sense that all stations within different chains transmit at the same frequency; however, they may have different GRI if they belong to different chains. Atmospheric noise level, practical antenna structure considerations, signal propagation characteristics and ground conductivity are some of the factors which dictate the selection of the specific carrier frequency of the transmitted signals. As shown in Fig. 6-2, each Loran-C pulse is composed of cycles of 100 KHz carrier. Time synchronization at the receiver depends on the identification of a particular cycle and the comparison of a cross-over within the cycle with the reference clock [20]. In order to facilitate this cycle identification, the leading edge of the pulse envelope is carefully controlled at the transmitter to conform to the following expression [20,22]:

$$f(t) = At^2 \exp [- (2t)/65x10^{-6}] \sin(2\pi \times 10^5 t), \qquad (6.3)$$

where A is a constant, so that the relative amplitudes of the first few cycles are identical for every transmitter. The envelope of (6.3) reaches a maximum at the positive peak of the seventh cycle at 65 μsec (see Fig. 6-2), and this is

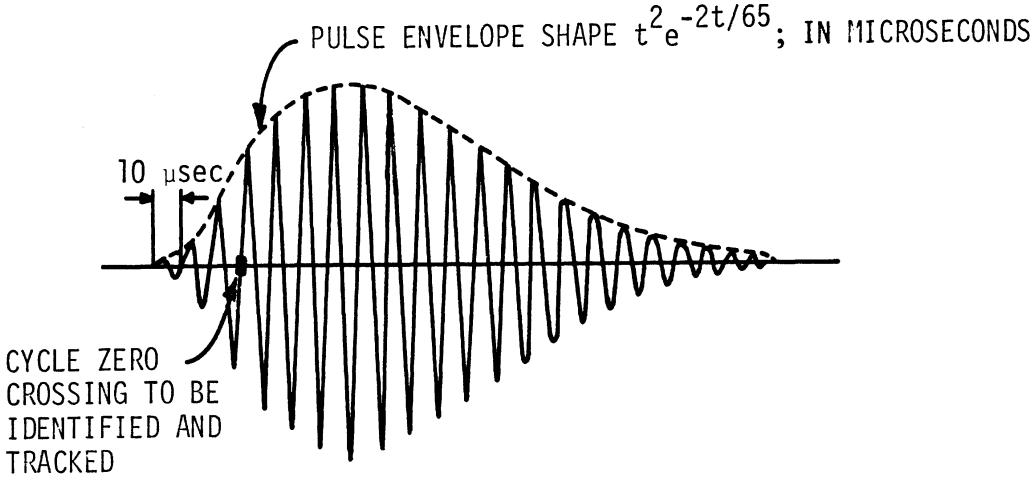

Fig. 6-2: Loran-C pulse.

one of the outstanding features of the Loran-C signal which enables the receiver to discriminate between signals received via ground and sky waves [22]. The latter signals are subject to random variations in the ionosphere and should be avoided by the receiver. At the Loran-C frequency of 100 KHz, the skywave signal appears at the receiver about 35 μs later than the ground wave signal. With the nature of the transmitter signal discussed above, it can be seen that the receiver avoids the skywave signal by processing the first 30 μs of the received ground wave signal which is free of any skywave contamination.

6.1.4 Receiving System

The Loran-C receiver is a fully automatic signal processing system which performs the following search-and-track operations: (i) searching for the master signal, identifying it by repetition rate and phase code; (ii) locking a local reference oscillator on to the master signal; and (iii) locking on to the two slave signals and determining their time differences from the master. The desired time differences are obtained from phase comparison of the corresponding pulses of the appropriate groups. The optimum place for phase measurement is chosen to be the 30 μs zero cross-over point (ZC) of a pulse in each group. The detailed procedure by which the receiver accomplishes this is described in [18, 23].

In the presence of atmospheric noise, modern receivers can provide very good performance up to a signal-to-noise ratio of -30 dB. CW or near CW interfering signals in the Loran-C band can cause serious degradation in the system performance [23]. With WTG in the vicinity of a Loran-C transmitter, the scattered signal will generally suffer a time delay relative to the ground wave signal before reaching the receiver. If this delay is larger than 30 μsec (or outside the range $30 + 100\nu$ with $\nu = 1, 2, \ldots, 9$) then the received scattered signal will act almost similar to the skywave signal, and therefore will have no effect on the receiver performance. However, if the delay is less than 30 μsec, then although the searching of the Loran-C signal by the receiver will not be affected, the scattered signal if sufficiently strong may degrade the receiver performance.

6.2 Received Signal in Presence of a Windmill

The effects of a windmill on the performance of a Loran-C system will be investigated by studying the changes in the amplitude and phase of the

received signals due to the scattering of signals by the windmill. The analysis is simplified by assuming that the Loran-C transmitting chain consists of a master and one slave station located in free space, and that the phase velocity of signal propagation is $c = 3 \times 10^5$ Km/sec. Since the DTA measurements by the Loran-C receiver depend on the relative phase and amplitude of the received signals, the present analysis will bring out the dominant effects of the scattered signal on the system performance in spite of the above idealized assumptions.

6.2.1 Phase Comparison of Direct and Scattered Signals

The geometry of the windmill (represented as a scatterer S), the receiver (R), the master station (M), and a slave station (S_n) (all located in free space) is as shown in Fig. 6-3. Let τ denote the DTA between the direct

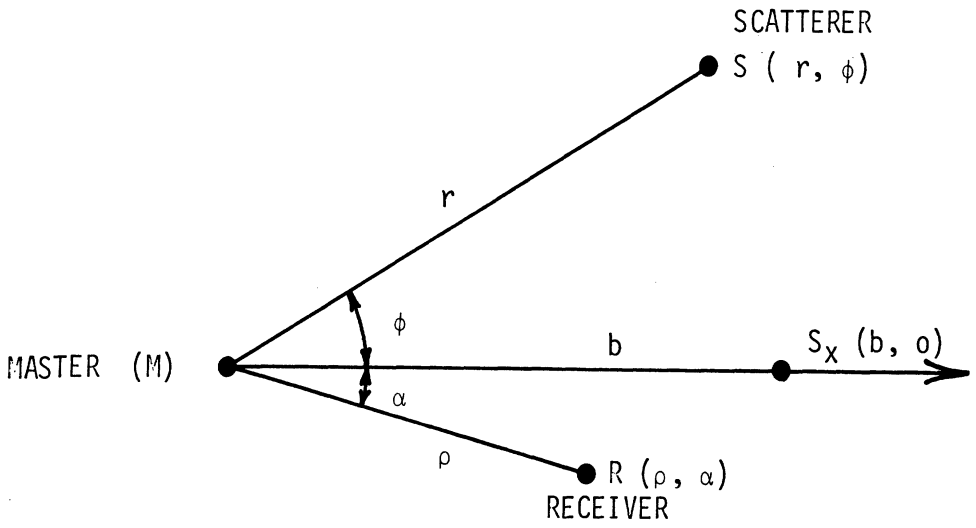

Fig. 6-3: Geometry of the windmill scattering center (S) and the Master (M), a slave (x) and the receiver of a Loran-C system.

and scattered master ground wave signals at R. For every fixed position of the receiver, we have (Fig. 6-3)

$$\overline{SM} + \overline{SR} - \overline{MR} = C\tau = \rho_0, \tag{6.4}$$

i.e., $$\overline{SM} + \overline{SR} = \rho + \rho_0, \tag{6.5}$$

where ρ_0 is the distance travelled by the signal in time τ and it is assumed that the scatterer does not introduce any time delay. The latter assumption is not necessary, and is made here for simplicity. From (6.5) it can be seen that, for given ρ_0 (i.e., τ), the locus of S is an ellipse having foci at M and R and eccentricity

$$\varepsilon = \frac{\rho}{\rho_0 + \rho} \quad . \tag{6.6}$$

As the angle α (Fig. 6-3) changes, the receiving point R traces a circle of radius ρ centered at M, and correspondingly, for constant time delay τ the point S traces a family of ellipses whose envelope is another circle of radius $\rho + \rho_0/2$ and centered at M. Therefore, for any receiving point R (ρ,α) there exists a point $P(r,\phi)$ in the circular region of radius ρ, denoted by S_ρ, such that $0 \leq r \leq \rho + \rho_0/2$ with $\overline{PM} + \overline{PR} = \rho + \rho_0$. Mathematically, we write this as

$$\left.\begin{aligned} P \in S_\rho &= \{(r,\phi): 0 \leq r \leq \rho + \rho_0/2\} \\ \overline{PM} + \overline{PR} &= \rho + \rho_0 \end{aligned}\right\} \tag{6.7}$$

It follows from the discussion in Section 6.1 that if the scattered signal suffers a time delay similar to that of the skywave signal, it would not have any effect on the receiver performance, since the scattered signal

would not then appear within the 30 μs time interval during which the receiver processes the received direct signal. As indicated previously, an improper interference affecting the receiver's functions may take place whenever the following relationship is satisfied

$$1000\ \nu \ < \tau \ < 1000\ \nu + 30\ \mu\text{sec} \quad , \tag{6.8}$$

with $\nu \in \Gamma$ such that

$$\Gamma = \{0, 1, 2, \ldots 7, 9\} \tag{6.9}$$

where it is recalled that the master pulse group consists of 9 pulses with the last (ninth) one having a separation of 2 msec instead of 1 msec from the adjacent pulse.

The task now is to transform the condition (6.8) on τ into restrictions on the distance parameter r, i.e., on the position of the windmill. This will determine the regions where the placement of a windmill would lead to a value of τ satisfying (6-8). We shall refer to these as "forbidden regions" in the sense that a windmill located there could degrade the receiver performance. Let us rewrite (6-8) as

$$300\ \nu < \rho_0 = c\tau < 300\ \nu + 9\ \text{Km} \tag{6.10}$$

with ν given by (6.9). Eq. (6.10) indicates that the received direct pulse corresponding to a given $\nu \in \Gamma$ may be corrupted by the scattered pulse from the windmill if the windmill is located inside the regions defined by

$$S_\rho^\nu = \{(r,\phi): 0 \leq r \leq \rho + \frac{\rho_0}{2} < \rho + 150\ \nu + 4.5\ \text{Km}\} \quad . \tag{6.11}$$

If $\nu > 1$, the regions corresponding to

$$\left.\begin{aligned} &1000\ (\nu\text{-}1) + 30 < \tau < 1000\ \nu\ \mu\text{sec} \\ \text{or}\quad &300\ (\nu\text{-}1) + 9 < \rho_0 < 300\ \nu\ \text{Km} \end{aligned}\right\} \tag{6.12}$$

should be excluded from S_ρ^ν. Let the regions defined by (6.12) be denoted by

$$G_\rho^\nu = \{(r,\phi):\ 150\ (\nu\text{-}1) + 4.5 + \rho < r < 150\ \nu + \rho\ \text{Km}\} \tag{6.13}$$

The forbidden zones around the master station, defined as F_ρ^ν, are therefore given by

$$F_\rho^0 = S_\rho^0 = \{(r,\phi):\ 0 \leq r < \rho + 4.5\ \text{Km}\},\ \nu = 0 \tag{6.14}$$

$$F_\rho^\nu = S_\rho^\nu - G_\rho^\nu\ ,\quad \nu \in \Gamma\ ,\quad \nu \neq 0\ . \tag{6.15}$$

The complete set of such forbidden zones is

$$F_\rho = \bigcup_{\nu\in\Gamma} F_\rho^\nu = \bigcup_{\nu\in\Gamma} S_\rho^\nu - \bigcup_{\substack{\nu\in\Gamma \\ \nu\neq 0}} G_\rho^\nu \tag{6.16}$$

where U denotes the union operator. Observe that $US_\rho^\nu = S_\rho^9$, so that

$$F_\rho = \bigcup_{\nu\in\Gamma} F_\rho^\nu = S_\rho^9 - \bigcup_{\substack{\nu\in\Gamma \\ \nu\neq 0}} G_\rho^\nu \tag{6.17}$$

The outer boundary of the overall forbidden zone is now a circle of radius

$$r = 150 \times 9 + 4.5 + \rho = 1354.5 + \rho\ \text{Km}\ .$$

This outer radius is very large because it has been obtained purely on the basis of the DTA without any consideration of the amplitude of the scattered signal relative to the direct signal. However, the results obtained here are instructive in that they indicate the general shape and arrangement of the forbidden regions. Forbidden regions obtained from (6.17) are shown in Fig. 6-4, where the master station is located at the center of the diagram

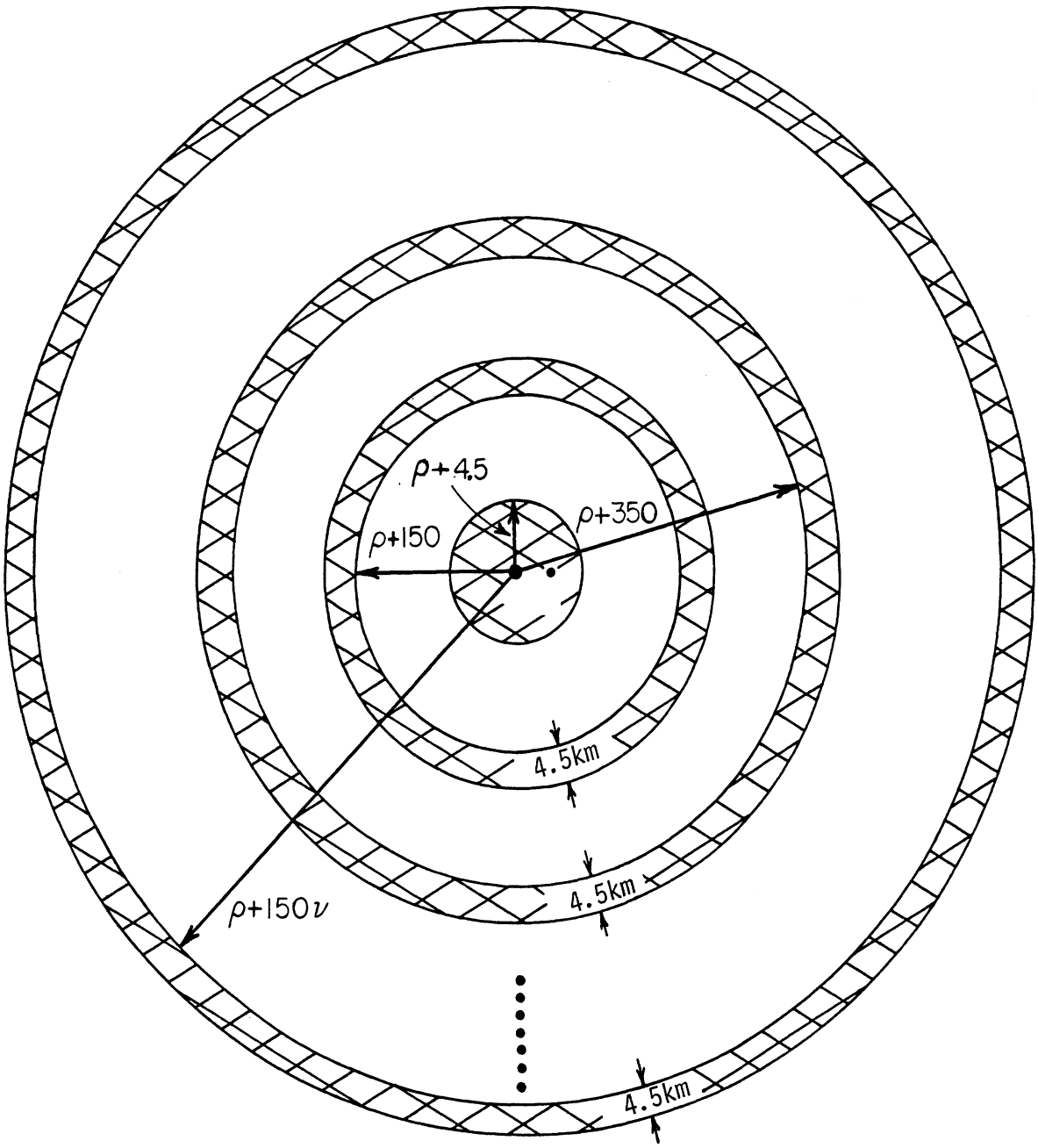

Fig. 6-4: Forbidden regions (shaded) around the master M for a given location ρ of the receiver. Each region with ν>0 is 4.5 Km wide.

and ρ denotes the receiver distance from the master. Note that the central forbidden region, i.e., for $\nu = 0$ is a complete circle of radius $r = \rho + 4.5$ Km; all the other forbidden regions (for $\nu \neq 0$) are annular in shape with width equal to 4.5 Km. For a receiver located a distance ρ from the main transmitter, various forbidden regions are the annulae

$$\left.\begin{aligned} &0 \leq r_0 \leq \rho + 4.5 \quad \text{Km} \\ &\rho + 150 \leq r_1 \leq \rho + 104.5 \quad \text{Km} \\ &\rho + 150\,\nu \leq r \leq \rho + 150\,\nu + 4.5 \quad \text{Km}.\ \nu = 1, 2, \ldots 7, 9 \end{aligned}\right\} \quad (6.18)$$

The forbidden regions around a slave station S_n may be obtained in a similar manner by assuming S_n in Fig. 6-1 to be the origin and referring ρ,r etc. with respect to S_n and re-defining Γ in (6-9) by

$$\Gamma = \{0, 1, 2, \ldots, 7\} \quad . \qquad (6.19)$$

With this modification, the forbidden regions around S_n are now given by (6.17) with the new definitions of ρ, r, and Γ given by (6.19).

6.3 Amplitude Comparison of Direct and Scattered Signals

In obtaining the forbidden regions discussed in the previous section it was assumed that the direct and scattered signals at the receiver are of the same order of magnitude. However, in a real situation the scattered signal is generally small compared with the direct one. In the present section we modify the regions obtained purely on DTA basis, and study their potential impact on the system performance by taking into account the amplitude of the scattered signal at the receiver relative to that of the direct signal.

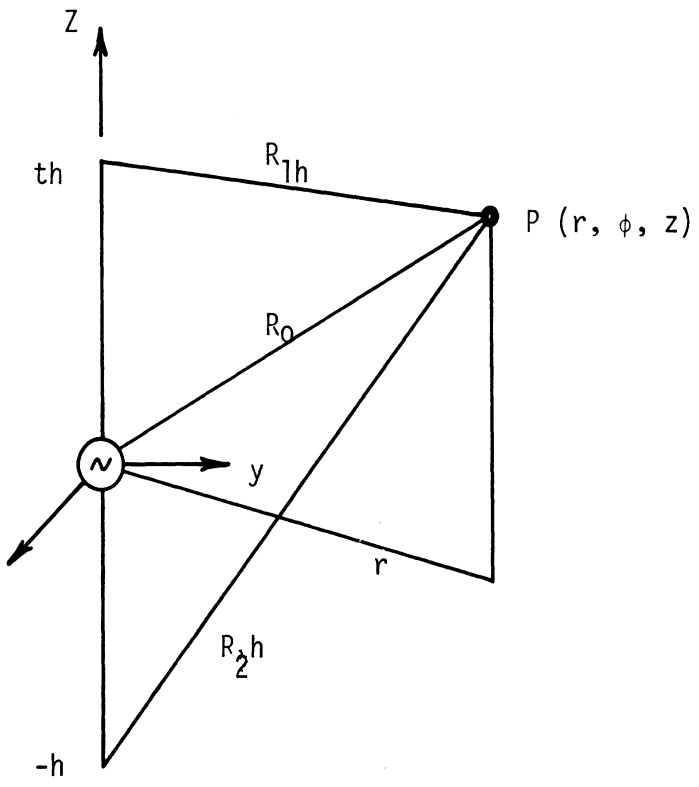

Fig. 6-5: Distances from center-driven antenna to an arbitrary point ρ (r, ϕ, z). r, ϕ, z are cylindrical coordinates of ρ.

6.3.1 Direct Signal

Let a linear antenna of length $2h$ be oriented along the z-axis of a rectangular coordinate system with origin 0 located at the center of the antenna, as shown in Fig. 6-5. An arbitrary field point P is represented by its cylindrical coordinates (r,ϕ,z). By invoking the image principle, the field produced by the antenna at a point P such that $z \geq 0$ may be identified with that produced by a Loran-C monopole antenna of height h located on a perfectly conducting ground plane placed at $z = 0$.

For simplicity, it is assumed that the antenna in Fig. 6-5 carries a sinusoidal current distribution

$$I(z) = I_m \sin k(h - |z|), \qquad |z| \leq h \leq \lambda/\mu \quad , \tag{6.20}$$

where I_m is a real constant and $k = 2\pi/\lambda$, λ being the wavelength in free space.

The complete electric field produced at all points in space is found to be [26]

$$E_r(P) = \frac{i I_m \eta_o}{4\pi r} \left[\frac{z-h}{R_{1h}} \exp(-ik R_{1h}) + \frac{z+h}{R_{2h}} \exp(-ik R_{2h}) - \frac{2z}{R_o} \cos(kh) \exp(-ik R_o) \right], \quad (6.21)$$

$$E_\phi(P) = 0 \quad (6.22)$$

$$E_z(P) = -\frac{i I_m \eta_o}{4\pi} \left[\frac{\exp(-ik R_{1h})}{R_{1h}} + \frac{\exp(-ik R_{2h})}{R_{2h}} - \frac{2}{R_o} \cos(kh) \exp(-ik R_o) \right], \quad (6.23)$$

where the assumed time dependence $\exp(i\omega t)$ is suppressed, and

$$\left.\begin{aligned} \eta_o &= \sqrt{\mu_o/\varepsilon_o} = 120\pi \text{ ohms} \\ R_o &= \left[z^2 + r^2\right]^{1/2} \\ R_{1h} &= \left[(z-h)^2 + r^2\right]^{1/2} \\ R_{2h} &= \left[(z+h)^2 + r^2\right]^{1/2} \end{aligned}\right\} \quad (6.24)$$

The quantities R_o, R_{1h} and R_{2h} are also shown in Fig. 6-5. For a field point located in the plane $z = 0$ or such that $z \ll h$, (6.24) reduces to

$$R_{1h} \simeq R_{2h} \simeq (h^2 + r^2)^{1/2} \quad (6.25)$$

Note that (6.21) - (6.23) give the cylindrical components of the complete field at P produced by the antennas. It is convenient to use the field expression in this form when P is located in the near zone of the antenna.

Later we shall modify (6.21) - (6.23) to obtain appropriate expressions for the spherical components of the field when P is located in the far zone.

Assuming $h = \lambda/4$ and $z \ll r$, (6.21) - (6.23) give

$$E_r(P) \simeq \frac{i\, I_m \eta_o}{4\pi r} \frac{2z \exp\left[-ik(r^2+h^2)^{1/2}\right]}{(r^2+h^2)^{1/2}} , \tag{6.26}$$

$$E_\phi(P) = 0 \tag{6.27}$$

$$E_z(P) \simeq \frac{-i\, I_m \eta_o}{4\pi} \frac{2 \exp[-ik(r^2+h^2)1/2]}{(r^2+h^2)^{1/2}} . \tag{6.28}$$

The amplitude of the complete electric field at P is therefore

$$|E(P)| = 60\, I_m \frac{(1+z^2/r^2)^{1/2}}{(r^2+h^2)^{1/2}} \tag{6.29}$$

We use (6.29) to obtain the amplitude of the direct signal at a receiving point located in the near zone of the antenna. For a receiving point R located such that its polar coordinates are $r = \rho$, $\phi = \alpha$ (see Fig. 6-1) we identify R with P, and obtain the following for the amplitude of the direct signal from the Loran-C transmitter to the receiver:

$$|E^T(R)| = 60\, I_m \frac{1}{(\rho^2+h^2)^{1/2}} . \tag{6.30}$$

Let us assume that a windmill having a tower height h_s is located at a distance r from the antenna. The scattering center of the WTG blades may now be assumed to be located at a point S having the coordinates $r = r$, ϕ and $z = h_s$ (see also Fig. 6-1). Under these conditions we obtain from (6.29) the following expression for the amplitude of the incident (or direct) signal at S arriving from the transmitter:

$$|E^T(S)| = 60\, I_m \frac{(1 + h_s^2/r^2)^{1/2}}{(r^2 + h^2)^{1/2}} \tag{6.31}$$

6.3.2 Scattered Signal

To obtain the amplitude of the scattered signal $|E^S(R)|$ at S, it is sufficient to regard the windmill blades as stationary, and to model each blade as a rectangular metal plate having a scattering cross-section σ. This concept was found useful in our previous study [1,2]. It is also assumed that the blades are so oriented as to direct the maximum scattered signal to the receiver. Under these conditions it can be shown [2] that the amplitude of the scattered field at R is

$$|E^S(R)| = \sqrt{\frac{\sigma}{4\pi}}\ \frac{|E^T(S)|}{d(S,R)}\ , \tag{6.32}$$

where d(S,R) is the distance between the windmill blade scattering center S and the receiving point P:

$$d(S,R) = \left[\rho^2 + r^2 - 2\rho r \cos\beta\right]^{1/2} \tag{6.33}$$

with $\beta = \alpha + \phi$ (see Fig. 6-3).

In (6.32) the scattering cross-section σ of the blade is still unknown. To obtain σ we observe that all the dimensions of the blade are much less than the Loran-C wavelength (λ = 3 Km) so that Rayleigh scattering is applicable. An adequate model of a blade is a very thin prolate spheroid for which the Rayleigh scattering cross-section is known. Given a prolate spheroid of semi-major axis a aligned along the z-axis, semi-minor axis b ($<< a$) and interfocal distance 2 ℓ, the Rayleigh scattering cross-section is [27]

$$\sigma = \frac{k^4}{r\pi} \quad |P_{33}(\hat{a} \cdot \hat{z})\hat{r} \cdot (\hat{r} \cdot \hat{z})|^2 \quad , \tag{6.34}$$

where

$$P_{33} = \frac{4\pi\ell^3}{3} \quad \frac{1}{\ell n \left(\frac{2a}{eb}\right)} \tag{6.35}$$

$k = 2\pi/\lambda$, $= 2.71828 \ldots$.

$\hat{r}$ is a unit vector the direction of observation,

$\hat{z}$ is the unit vector along the z-axis (axis of revolution direction) and

$\hat{a}$ is the unit vector in the directions of the incident electric field.

For a blade of (equivalent) area A_e and length L, it is clear that

$$\ell \simeq a = L/2$$

and the most logical identification of A is with the area πab of the ellipse. Hence,

$$b = \frac{2A}{\pi L}$$

giving

$$P_{33} = \frac{\pi L^3}{6}\left[\ell n\left(\frac{\pi L^2}{2eA_e}\right)\right]^{-1} \tag{6.36}$$

In the present problem we are interested in the maximum value that the scattered signal can have, and from (6.34) this maximum is

$$\sigma_{max} = \frac{k^4}{4\pi} P_{33}^2 \tag{6.37}$$

From now on we shall identify the scattering cross-section σ with σ_{max}, and hence

$$\sigma = \frac{\pi^5 L^6}{9\lambda^4}\left[\ell n\left(\frac{\pi L^2}{2eA_e}\right)\right]^{-2} \tag{6.38}$$

In the case of a MOD-1 blade, A = 40 m^2 and L = 28 m, giving σ = 3.43 x 10^{-5} m^2 at λ = 3 Km.

Introducing (6.38) into (6.32), the scattered signal amplitude at R is found to be

$$|E^S(R)| = \frac{\pi^2 L^3}{6\lambda^2} \left[\ell n \left(\frac{\pi L^2}{2eA}\right)\right]^{-1} \frac{|E^T(S)|}{d(S,R)} \tag{6.39}$$

6.3.3 Ratio of the Scattered and Direct Signals

We now define m as the ratio of the amplitudes of the scattered and direct signals at R, and using (6.30), (6.31), and (6.39), we obtain the following:

$$m = \frac{|E^S(R)|}{|E^T(R)|}$$

$$= \frac{\pi^2 L^3}{6\lambda^2 r} \left[\ell n \frac{\pi L^2}{2eA}\right]^{-1} \frac{(\rho^2 + h^2)^{1/2}}{d(S,R)} \cdot \left(\frac{1 + h_s^2/r^2}{1 + h^2/r^2}\right)^{1/2} \tag{6.40}$$

For given locations of the transmitter and the windmill (i.e., r fixed), the scattered field at R and hence 'm', decreases inversely as the distance from the windmill (see (6.32)). Note that (6.32) and (6.40) are valid for $kd \geq 1$, with $d \simeq \lambda/2\pi$ being the approximate distance of the beginning of the far zone of the point scatter located at S. However, from the 2 D^2/λ criterion of the blade, (6.32) and (6.40) can be used to estimate the scattered field and the field ratio for smaller values of d. In fact, we shall use (6.40) to estimate m for d as small as $d \simeq h_s$.

A study of (6.40) reveals that for a given windmill and a receiver located at a constant distance from the transmitter such that $\rho > r$, m assumes its largest value (m_F) when R is located in the forward direction, i.e., when

$\rho = r + d$, (see (6.33)) with respect to the scattering from the blade. Similar considerations indicate that for $\rho < r$, the largest field ratio (m_B) occurs when R is located in the backscattering direction, i.e., when $\rho = r - d$. In both cases the transmitter, the receiver and the blade scattering center are colinear. Under these conditions, the maximum signal ratio at R is

$$m = \frac{\pi^2 L^3}{6\lambda^2 r}\left[\ell n\left(\frac{\pi L^2}{2eA}\right)\right]^{-1}\frac{(\rho^2 + h^2)^{1/2}}{d}\left(\frac{1 + h_s^2/r^2}{1 + h^2/r^2}\right)^{1/2}, \qquad (6.41)$$

which yields $m = m_F$ when $\rho = r + d$, and $m = m_B$ when $\rho = r - d$, for $d < r$. Generally, $m_F > m_B$.

If the locations of the windmill and the receiver are such that $d >> r,h$, (6.41) gives the following approximate relationship:

$$m_F \simeq \frac{\pi^2 L^3}{6\lambda^2 r}\left[\ell n\left(\frac{\pi L^2}{2eA}\right)\right]^{-1}\left(\frac{1 + h_s^2/r^2}{1 + h^2/r^2}\right)^{1/2}, \qquad (6.42)$$

which can be used to determine the signal ratio at a distant receiver as a function of the windmill-to-transmitter distance. In the other extreme, when $r >> d, h_s$ we obtain from (6.41)

$$m_F \simeq \frac{\pi^2 L^3}{6\lambda^2 d}\left[\ell n\left(\frac{\pi L^2}{2eA}\right)\right]^{-1} \qquad (6.43)$$

which can be used to estimate the signal ratio at a receiver as a function of its distance from the windmill when both the windmill and the receiver are located far from the transmitter.

6.3.4 Numerical Results: Forbidden Regions

By numerically computing the expressions derived in the previous section, we discuss here the variation of the signal ratio at a receiver when a windmill is located in the vicinity of a Loran-C master transmitting station. The results are then used to judge the practical implications of the forbidden regions, derived in Section 6.2 based on phase comparison of the direct and scattered signals at the receiver.

Let us consider a MOD-1 windmill (L = 28 m, A = 40 m^2, and h_s = 45 m) located at a distance 0.5 Km from the Loran-C transmitter. With a receiver-to-windmill distance of 0.1 Km, the forward and backward direction signal ratios at the receiver can now be determined from (6.41), and are: m_F = - 95.1 dB and m_B = - 96.4 dB, obtained with the receiver-to-transmitter distance ρ = 0.6 and 0.4 Km, respectively. With the receiver located at ρ = 0.6 Km, if the WTG is removed to a distance of r = ρ + 150 = 150·6 Km, it is found that $m_B \simeq$ - 203.1 dB which is 108 dB less than the maximum signal ratio obtained with r = 0.5 Km. Note that with ρ = 0.6 Km, the windmill is located in the first forbidden region, defined as $0 < r \leq \rho + 4.5$ Km, when r = 0.5 Km, and in the second forbidden region, defined as $\rho + 150 \leq r \leq \rho + 154.5$ Km, when r = 150.6 Km. If the receiver is located at the same distance ρ = 0.6 Km, the signal ratio obtained with the WTG located within each of the successive forbodden regions is found to be about 40 $\log_{10} \nu$ dB, ν = 2, 3, ..., 9, less than the previous case. From these considerations it is concluded that a MOD-1 windmill located within a higher order forbidden region ($\nu > 0$) will not cause any adverse receiver performance because in each case the received signal ratio would be < - 108 dB compared to that when the windmill is located in the first (ν = 0) forbidden

region. From now on, we shall ignore the effects of a windmill located in the higher order forbidden regions.

Fig. 6-6 shows the signal ratio in the forward direction, obtained from (6.41), as a function of the distance of the receiver from the transmitter and for selected values of the windmill-to-transmitter distance. Observe that the final and initial values of the curves in Fig. 6-6 are given approximately by (6.42) and (6.43), respectively. The results of Fig. 6-6 indicate that even for a windmill-to-transmitter distance of 100 m, the scattered signal level at a receiver, located as close as 100 m to the windmill, is of the order of 95 dB down from the direct signal. Assuming that a Loran-C receiver is unaffected by an interfering (scattered) signal whose level is 95 dB down (or more) less than that of the desired (or direct) signal, it may be concluded that a MOD-1 WTG located at a distance $\gtrsim \lambda/30$ from the transmitter will not cause any significant change in the performance of a Loran-C receiver. However, at a distance of $\frac{\lambda}{30}$, the WTG would be located well within the near zone of the transmitting antenna (note: $2\,D^2/\lambda$ for the transmitting antenna of height $\lambda/4$ is $= \lambda/8$). Therefore, it seems that the minimum siting distance of a WTG from the transmitter would be determined mainly from a consideration of the mutual interaction between the windmill and the transmitting antenna. This is investigated in the next section.

6.4 Mutual Interaction Between a Windmill and Loran-C Transmitting Antenna

The effect of a windmill on the performance of a Loran-C transmitting antenna can be investigated using the known [28] results for the mutual impedance between vertical antenna of unequal heights, located above a perfectly conducting ground. Let the Loran-C transmitting antenna of height $h = \lambda/4$

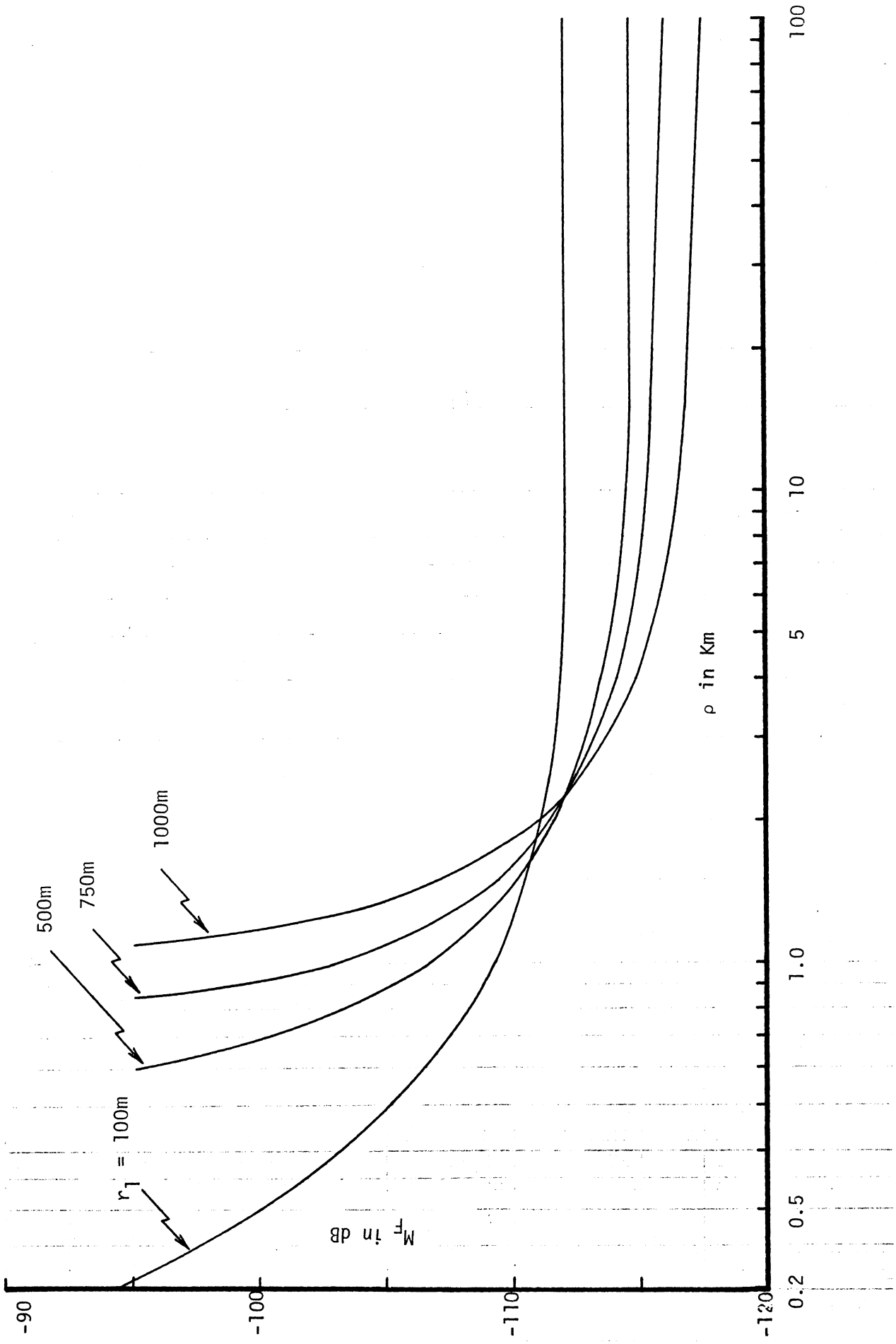

Fig. 6-6: Signal ratio in the forward direction as a function of the transmitter to receiver distance for variable location of the windmill.

and the windmill acting as a parasitic antenna of height h_s, located at a distance r from the transmitter, be vertically oriented above a perfectly conducting horizontal ground. It is assumed that both h and h_s carry sinusoidal distributions of current. Under these conditions, the resistive and reactive components of the mutual impedance (defined as $Z_{21} = R_{21} + jX_{21}$) between the two antennas are [28]:

$$R_{21} = 15\{Ci(u^+) + Ci(u^-) - Ci(v^+) - Ci(v^-) + \cot(kh_s)[Si(u^+) - Si(u^-) + Si(v^+) - Si(v^-) - 2\,Si(w^+) + 2\,Si(w^-)]\}\ \text{ohms}, \tag{6.44}$$

$$X_{21} = 15\{Si(v^+) + Si(v^-) - Si(u^+) - Si(u^-) + \cot(kh_s)[Ci(u^+) - Ci(u^-) + Ci(v^+) - Ci(v^-) - 2\,Ci(w^+) + 2\,Ci(w^-)]\}\ \text{ohms}, \tag{6.45}$$

where
$$Ci(u) = \int_{\infty}^{u} \frac{\cos t}{t}\, dt, \tag{6.46}$$

$$Si(u) = \int_{0}^{u} \frac{\sin t}{t}\, dt, \tag{6.47}$$

and

$$\left.\begin{aligned} u^{\pm} &= k\,[(r^2 + h^2)^{1/2} \pm h\,] \\ v^{\pm} &= k\,[(r^2 + h_{+}^{2})^{1/2} \pm h] \\ w^{\pm} &= k\,[(r^2 + h^2)^{1/2} \pm h] \end{aligned}\right\} \tag{6.48}$$

with
$$h_{\pm} = h \pm h_s\ . \tag{6.49}$$

For a quarter wave transmitting antenna having $h = \lambda/4 = 750$ m, the mutual impedance between the antenna and a parasitic element of height h_s = 45 m, 75 m and 100 m, has been computed from (6.44) and (6.45) for selected

values of the separation distance r. The results are shown in Table 6.1 .

Table 6.1: Mutual impedance between the transmitting antenna and windmill.

r	h_s = 45 m		h_s = 75 m		h_s = 100 m	
	R_{21}(ohms)	X_{21}(ohms)	R_{21}(ohms)	X_{21}(ohms)	R_{21}(ohms)	X_{21}(ohms)
$\frac{\lambda}{12}$ = 250 m	-10.74	-4.78	-8.16	-3.43	-10.74	-4.78
$\frac{\lambda}{6}$ = 500 m	-8.42	-4.51	-5.97	-2.18	-8.42	-4.51
$\frac{\lambda}{4}$ = 750 m	-6.34	-6.25	-4.92	-6.85	-6.34	-6.25

The self-impedance of the transmitting antenna is [26] Z_{11} = (1/2) (73.1 + j 42.5) = 36.55 + j 21.25 ohms. The change in the input impedance of the transmitting antenna due to the presence of the windmill is $\Delta Z_{in} = - Z_{21}^2/Z_{22}$, where $Z_{in} = Z_{11} - \frac{Z_{21}^2}{Z_{22}}$ and Z_{22} is the self-impedance of the parasitic element of height h_s simulating the windmill. For the values of h_s used in Table 6.1, the self-impedance Z_{22} is predominantly capacitive. Under the thin wire approximation (i.e., $\frac{h_s}{a} \simeq 40$), [29] $Z_{22} \simeq$ - j 550 ohms for h_s = 45 m = 0.015 λ; and for the other values of h_s in Table 6.1, $|Z_{22}| >$ 550 ohms. Thus, using the values of Z_{21} shown in Table 6.1, it is found that $|\Delta Z_{in}| << Z_{11}$, showing that the input impedance of the transmitting antenna is not significantly affected by the windmill for the cases in Table 6.1 .

6.5 Conclusions

The performance of a Loran-C system in the presence of a windmill has been theoretically investigated. Since the physical dimensions of the largest existing windmill (MOD-1) are very small compared to the extremely large wavelength ($\lambda = 3 \times 10^3$ m) of Loran-C signals, the scattered signals from the windmill are found to be about 100 dB lower than the direct signals at the receiver even when the windmill is located as close as 100 m to the transmitter or the receiver. It is unlikely that the Loran-C receiver performance would be degraded by such low level interfering signals. The mutual interaction effects of the WTG on the performance of the transmitting antenna are found to be insignificant for a windmill located as close as $\lambda/12$ (= 250 m) to the transmitter. From the results discussed it appears that a windmill located at a distance $\geq \lambda/12$ (= 250 m) from any transmitter (a receiver) will not have any significant effect on the Loran-C system performance.

REFERENCES

1. Senior, T.B.A., Sengupta, D.L., and Ferris, J.E., "TV and FM Interference by Windmills," Final Report No. 1 on Contract No. E(11-1)-2846, Energy Research and Development Administration, Washington, D.C., February 1977.

2. Sengupta, D.L. and Senior, T.B.A., "Electromagnetic Interference by Windmills," Final Report No. 2 on Contract EY-76-S-02-2846, A001, Department of Energy Wind Systems Branch, Division of Solar Technology, Washington, D.C., March 1978.

3. Senior, T.B.A. and Sengupta, D.L., "Wind Turbine Generator Siting and TV Reception Handbook," Technical Report No. 1, on Contract EY-76-S-02-2846.A001, Department of Energy, Wind Systems Branch, Division of Solar Technology, Washington, D.C., January 1978.

4. LaHaie, I.J. and Sengupta, D.L., "Scattering of Electromagnetic Waves by a Slowly Rotating Rectangular Metal Plate," IEEE Trans., Vol. AP-27, No. 1, pp. 40-46, January 1979.

5. IRE Standards on Radio Wave Propagation (definition of terms), Supplement to Proc. IRE, Vol. 30, No. 7, Part III, p. 2, 1942.

6. Kraus, J.D., Antennas, McGraw-Hill Book Co., Inc., NY., pp. 464-478, 1950.

7. Rumsey, V.H., Deschamps, G.A., Kales, M.L., and Bohnert, J.I., "Techniques for Handling Eliptically Polarized Waves with Special Reference to Antennas," Proc. IRE, Vol. 39, No. 5, pp. 538-556, May 1951.

8. Schelkunoff, S.A. and Friis, H.T., Antennas -- Theory and Practice, John Wiley and Sons, Inc., NY, pp. 390-393, 1952.

9. Sinclair, G., "The Transmission and Reception of Elliptically Polarized Waves," Proc. IRE, Vol. 38, No. 2, pp. 148-515, February 1950.

10. Collin, R.E. and Zucker, F.J., Antenna Theory, Part I, McGraw-Hill Book Co., NY, pp. 103-109, 1969.

11. "Candidate Wind Turbine Generator Site Meteorological Monitoring Program Final Data Analysis Report," prepared for NASA-Lewis Research Center Feb. 14, 1979 by Western Scientific Services, Inc., 328 Airpark Drive, Fort Collins, CO 80521 (report no. F1-975-130).

12. Renne, D., Personal Communication, April 1979.

13. Bolle, D.M., Personal Communication, April 1979.

14. Sengupta, D.L. and Senior, T.B.A., "Electromagnetic Interference to Television Reception Caused by Horizontal Axis Windmills," Proc. IEEE, Vol. 67, No. 8, pp. 1133-1142, August 1979.

15. Walts, R.E., "Innovative Vertical Axis Klind Machines," Wind Workshop, Proc. of the Second Workshop on Wind Energy Conversion Systems, Washington, D.C., June 9-11, 1975, The Mitre Corporation, pp. 443-451.

16. Carter, Joe, "VAWT Research at Sandia Labs," Wind Power Digest, No. 9, Summer 1977, pp. 42-45.

17. Pierce, J.A., McKenzie, A.A., and Woodward, R.H., LORAN -- Long Range Navigation, MIT Radiation Laboratory Series, Book 4, McGraw-Hill Book Co., NY, 1948.

18. Beck, G.E., Navigation Systems, Van Nostrand Reinhold, London, pp. 99-116, 1971.

19. Kayton, M. and Fried, W.R., Avionics Navigation Systems, John Wiley and Sons, Inc., NY, pp. 192-197, 1969.

20. "Lorand C User Handbook" Department of Transportation, U.S. Coast Guard, CG-462, August 1974.

21. Doherty, R.H., Hefley, G., and Linfield, R.F., "Timing Potentials of Loran-C," Proc. IRE, Vol. 49, No. 11, pp. 1659-1673, 1961.

22. Shapiro, L.D., "Time Synchronization from Loran-C," IEEE Spectrum, Vol. 5, No. 8, pp. 46-55, August 1968.

23. Vander Wal, P.W. and Van Willigen, D., "Hard Limiting and Sequential Detection Applied to Loran-C," IEEE Trans. on Aerospace and Electronic Systems, Vol. AES-14, No. 4, pp. 649-660, July 1978.

24. Van Etten, J.P., Medium Accuracy Low Cost Navigation: Loran C Versus the Alternatives," AGARD Conference Proceedings, No. 176, pp. 25/1-12, 1976.

25. DeLorane, J.F. and Tuppen, A.R., "Low Cost Navigation Processing for Loran-C and OMEGA," AGARD Conference Proceedings, No. 176, pp. 8/1-17, 1976.

26. King, R.W.P., Linear Antennas, Harvard University Press, Cambridge, Mass., pp. 526-528, 1956.

27. Kleinman, R.E. and Senior, T.B.A., Rayleigh Scattering Cross-Sections," Radio Science, Vol. 7, No. 10, pp. 937-942, 1972.

28. Cox, R.P., "Mutual Impedance Between Vertical Antennas of Unequal Heights," Proc. IRE -- Waves and Electronics Section, Vol. 35, No. 11, pp. 1367-1370, 1947.

29. Jordan, E.C. and Balmain, K.G., Electromagnetic Waves and Radiating Systems, Prentice-Hall, Inc., NJ, pp. 548, 1968.